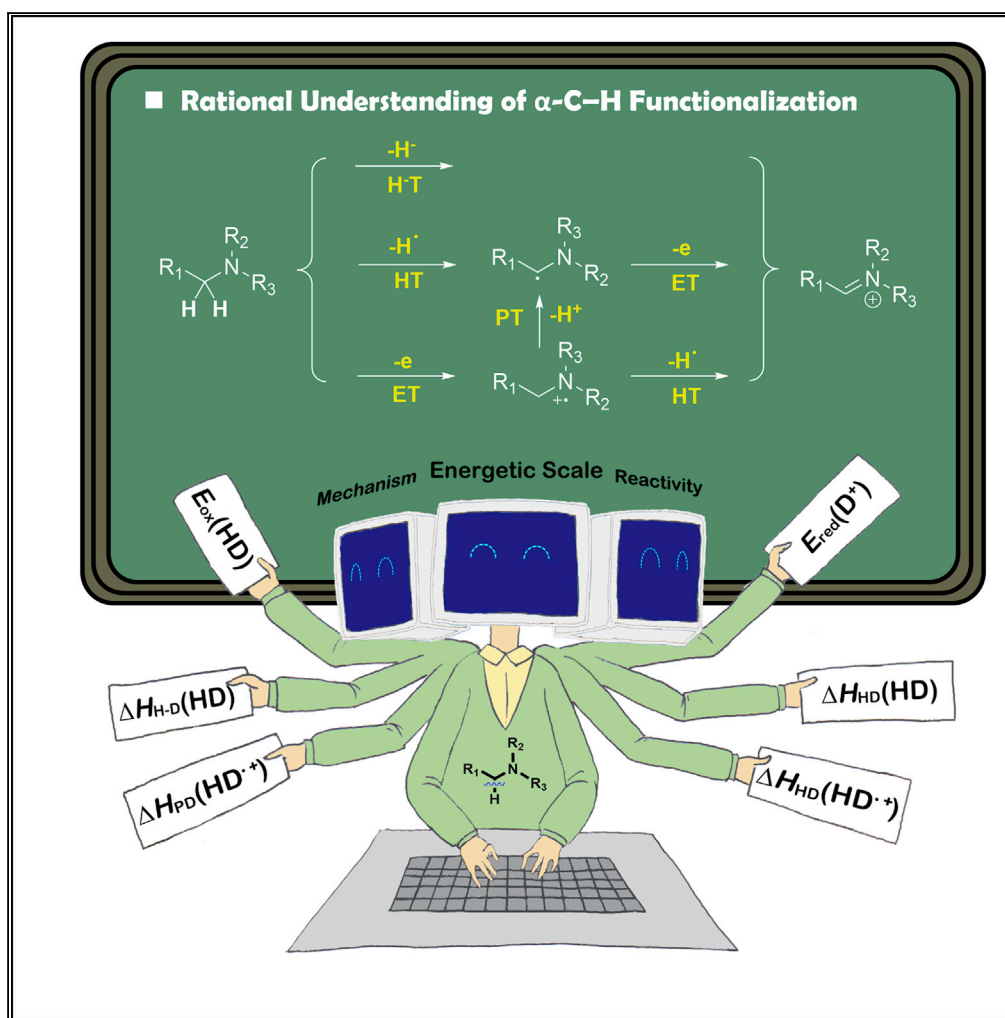**Article**

Toward Rational Understandings of α-C–H Functionalization: Energetic Studies of Representative Tertiary Amines

Wenzhi Luo, Jin-Dong Yang, Jin-Pei Cheng

jdyang@mail.tsinghua.edu.cn (J.-D.Y.)
jinpei_cheng@mail.tsinghua.edu.cn (J.-P.C.)

HIGHLIGHTS

A unique hydricity-based methodology for bond energy determination

The first integrated α-C–H bond energy scale of tertiary amines

Thermodynamics-based diagnosis of the feasibility/mechanism of amine oxidation

Article

Toward Rational Understandings of α-C–H Functionalization: Energetic Studies of Representative Tertiary Amines

Wenzhi Luo,[1] Jin-Dong Yang,[1,3,*] and Jin-Pei Cheng[1,2,*]

SUMMARY

Functionalization of α-C–H bonds of tertiary amines to build various α-C–X bonds has become a mainstream in synthetic chemistry nowadays. However, due to lack of fundamental knowledge on α-C–H bond strength as an energetic guideline, rational exploration of new synthetic methodologies remains a far-reaching anticipation. Herein, we report a unique hydricity-based approach to establish the first integrated energetic scale covering both the homolytic and heterolytic energies of α-C–H bonds for 45 representative tertiary amines and their radical cations. As showcased from the studies on tetrahydroisoquinolines (THIQs) by virtue of their thermodynamic criteria, the feasibility and mechanisms of THIQ oxidation were deduced, which, indeed, were found to correspond well with experimental observations. This integrated scale provides a good example to relate bond energetics with mechanisms and thermodynamic reactivity of amine α-C–H functionalization and hence, may be referenced for analyzing similar structure-property problems for various substrates.

INTRODUCTION

Because of a high efficiency and atom economy, direct C–H functionalization has become a prevalent strategy for converting readily accessible starting materials into potentially bioactive scaffolds (Blakemore et al., 2018; Qin et al., 2017; Saint-Denis et al., 2018). However, most C–H bonds are comparatively inactive, therefore substrates with a C–H bond at the α-position of some heteroatom-centered entities, such as an N-containing moiety, have attracted much attention, as a consequence of the latent stabilizing effect of the neighboring electron pair on the incipient α-radical or α-cation upon α-C–H bond scission (Campos, 2007; Chen, W. J. et al., 2018; Nakajima et al., 2016; Shi et al., 2012; Zhang et al., 2019). Among this category of Y-C–H (Y = N, O, S, P, etc.) type compounds, tertiary amines are the most popular due especially to the widespread presence of their structural motif in many natural alkaloids and bioactive molecules (Beatty et al., 2015; Rommelspacher et al., 1985; Shamma, 2012). As a result, numerous oxidative cross-dehydrogenative couplings (CDC) have been developed for functionalization of tertiary amines via α-C–H bond dissociation (Chi et al., 2019; Girard et al., 2014; Szatmári et al., 2016; Yoo et al., 2010) (Scheme 1).

In these CDC processes, the tertiary amine is first oxidized, via different modes of α-C–H bond rupture (Scheme 1), to α-amino radical or iminium ion either by transition metals (Cheng et al., 2017; Murahashi et al., 2003; Shao et al., 2015), organic oxidants (Allen et al., 2011; Damico et al., 1966; Sundberg et al., 1991), or by electro- (Basle et al., 2010; Fu et al., 2017; Yoshida et al., 2002) or photo-oxidants (Condie et al., 2010; McNally et al., 2011; Ravelli et al., 2016; Thullen et al., 2017). The α-amino intermediate is then intercepted by an appropriate reagent to furnish a new α-C–R bond (Scheme 1). It may need to mention that among the two primary modes of α-C-H bond rupture via CDC, the iminium route, rather than the radical route(McNally et al., 2011; Thullen et al., 2017), would be more emphasized in the context, due mainly to a higher degree of complexity of the former (vide infra). Some typical reaction trends observed experimentally are represented in Scheme 2. As shown in 2a, substitution change at the N atom substantially varied the tetrahydroisoquinoline (THIQ) reaction yield from 0% to 100%. Similar impact on the coupling yields could also be dominated by the choice of oxidants (Scheme 2B) (Wan et al., 2014; Xie et al., 2014). Moreover, Scheme 2C shows an example of a varying mechanism for two similar Cu-catalyzed CDCs, that is, an electron-hydrogen transfer (ET-HT) is followed with the CuCl2/O2 pair, whereas a hydrogen-electron transfer (HT-ET) is favored with a CuBr/tBuOOH pair. Although the relevance of α-C–H bond cleavage in affecting the reaction pattern and outcomes was well demonstrated (Oss et al., 2018; Zhang et al., 2012), till now, no practical guideline could be found in literature for reasonably

[1]Center of Basic Molecular Science (CBMS), Department of Chemistry, Tsinghua University, Beijing 100084, China
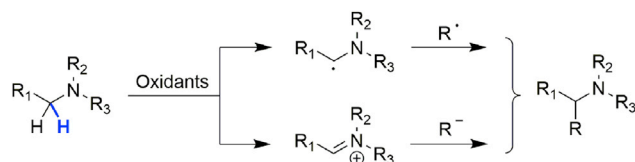
[2]State Key Laboratory of Elemento-organic Chemistry, College of Chemistry, Nankai University, Tianjin 300071, China

[3]Lead Contact

*Correspondence: jdyang@mail.tsinghua.edu.cn (J.-D.Y.), jinpei_cheng@mail.tsinghua.edu.cn (J.-P.C.)

https://doi.org/10.1016/j.isci.2020.100851

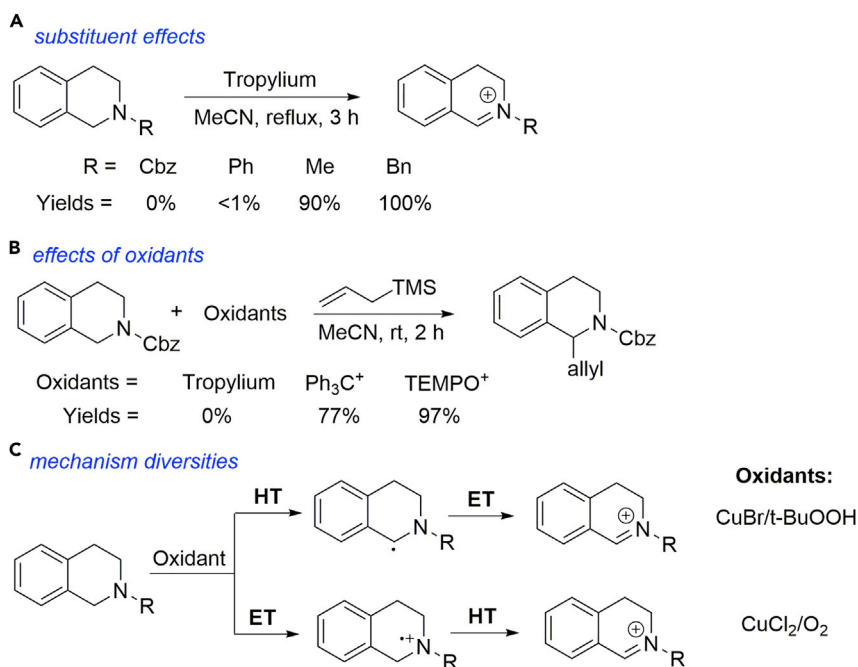**Scheme 1. CDC Process of Tertiary Amines in Organic Synthesis**

elucidating these puzzling observations exemplified. This actually points out a keen demand for a rational understanding of the diversified CDC reactivity and mechanisms.

As generally known, there are basically three mechanisms for amine oxidation (Scheme 3). Actually, direct hydride transfer (H$^-$T, pathway **a**) is quite frequently seen when organic cations (e.g., Ph$_3$C$^+$) are used as the acceptors (Richter and GarcíaMancheño, 2010; Xie et al., 2014). Alternatively, when a latent radical species [e.g., peroxides (Zhang et al., 2017) and azo compounds (Liu et al., 2017a)] is used as the initiator, the reaction may proceed through C–H bond homolysis to yield α-amino radicals (pathway **b**), which are then oxidized to iminium ions via fast electron transfer. On the other hand, if amine is to react with a single-electron oxidant [e.g., radical cations (Huo et al., 2014), transition metal (Brzozowski et al., 2015), photo-oxidant (Hariand König, 2011; McManus et al., 2018), or an anode (Franckeand Little, 2014)], formation of radical cation would be expected (pathway **c**), which can subsequently decompose through either hydrogen-atom transfer (HT) or stepwise proton-electron transfer (PT-ET). This rule of thumb provides a hint for one to assess which mechanism, a particular amine oxidation, is more likely to follow, but with no indication on reactivity issue in relation to the thermodynamic driving force of bond cleavage.

Although syntheses via oxidative cleavage of the α-C–H bonds of tertiary amines have advanced greatly, till present, investigations on the oxidation mechanisms are sparse, however (Liu et al., 2017b; Morgante et al., 2019), and, some are even subject to debates. For instance, Klussmann et al. and Doyle et al. both conducted serious investigations on Cu-catalyzed oxidative coupling mechanisms of THIQs with tBuO$^•$, but ended up in different conclusions on mechanisms (HT vs. ET), based on each other's sound experimental evidences (Boess et al., 2012, 2016; Ratnikovand Doyle, 2013). The controversy has lasted several years and seems still not fully settled down. This, in our view, is due to the fact that only the conventional measures, such as kinetic study, intermediate and product analysis, etc., are often not sufficient to describe a reaction mechanism. In this regard, establishment of an integrated energetic scale embracing all the possible elementary steps in Scheme 3 should be helpful for mechanistic judgment because of the inherent relationship between bond energy and reactivity.

Despite the definite need of thermodynamic data related to the α-C–H bonds of tertiary amines (Xue et al., 2017; Yang et al., 2018), they have seldom been determined. In fact, almost all the currently known bond energies of organic molecules that cannot be directly measured by the gas-phase techniques were derived from measurement of corresponding pK_a values in solution through the properly designed thermochemical cycles of Bordwell (Bordwell et al., 1988). However, this method would not be applicable to the present substrates, because the acidity of the C–H bond adjacent to nitrogen is too weak to allow a deprotonation by any strong base present in solution.

In the present work, we developed a unique hydride-transfer-based methodology to construct an integrated α-C–H bond energy scale of tertiary amines. The scale is composed of four fundamental quantities required for diagnosing the C–H functionalization mechanisms, including (1) the hydricity ΔH_{H^-D} (hydride-releasing ability) of tertiary amines (where D denotes donor), (2) the α-C–H bond homolytic energy ΔH_{HD}, (3) the deprotonation energy of amine radical cations $\Delta H_{PD}(HD^{•+})$, and (4) the hydrogen-atom-donating ability of radical cations $\Delta H_{HD}(HD^{•+})$. Direct measurement or derivation of these energetic parameters was described in the following section. This energetic scale (with 4 × 45 new bond energies), together with the redox data of relevant species, was then used to analyze the possible mechanisms and their corresponding structure–property relationships. Particularly, in order to help synthetic chemists to get more acquainted with this bond-energy-based mechanistic analysis, the feasibility and mechanisms of the well-studied THIQ oxidations by various oxidants were investigated in more details, perhaps with a sacrifice of some synthetically more favored cases, to showcase the plausible applicability of bond-energetic

A substituent effects

R =	Cbz	Ph	Me	Bn
Yields =	0%	<1%	90%	100%

B effects of oxidants

Oxidants =	Tropylium	Ph_3C^+	$TEMPO^+$
Yields =	0%	77%	97%

C mechanism diversities

Scheme 2. Representative Reactivity Trends for THIQ-Involved Processes in Organic Synthesis
(A) Substituent effects; (B) Effects of oxidants; (C) Mechanism diversities.

diagnosis of reaction feasibility/mechanism issues. Experimental confirmations of this line of rational analyses were also exemplified and discussed. Although only representative tertiary amines were chosen in this first systematic study on the Y-C–H type bond energy scale and its application, we believe the insights derived herewith could provide useful hints for analyzing other Y-C–H systems as well.

RESULTS

In a CDC process, the tertiary amine actually acts as a reductant to transfer its α-C–H to a suitable acceptor. In order to assess the trend of this bond to deliver its hydrogen, we explored an alternative approach, rather than by using the method of Bordwell that requires the knowledge of pK_a (Bordwell et al., 1988), to measure the hydride-releasing ability instead, i.e., hydricity ΔH_{H^-D} of this α-C–H bond. As mentioned above, this is because the α-C–H bond of amines is too weak to allow deprotonation, but it is feasible to deliver a hydride. As expected, THIQ analogs could quantitatively exchange their α-C–H hydride with 4-acetamido-2,2,6,6-tetramethyloxopiperidinium perchlorate ($AcNH\text{-}TEMPO^+ClO_4^-$) (Equation 1) whose hydride affinity ΔH_{H^-A} (where A denotes acceptor) in acetonitrile was well established (Table S1 in Supplemental Information). Thus, determination of the THIQ hydricity ΔH_{H^-D} becomes a matter of measuring the heat ΔH_{rxn} of the hydride exchange reaction (by isothermal titration calorimetry, see Supplemental Information for details). The hydricity ΔH_{H^-D}(HD) can then be evaluated from Equation 2 using the known $\Delta H_{H^-A}(AcNH\text{-}TEMPO^+)$ of -105.6 kcal mol^{-1} (Zhu et al., 2011). For acyclic amines, another reduction process (Equation 3) was employed to avoid the possible coupling of amines with hydride acceptors. Their hydricity was derived from the known hydricity of the dihydropyridine ($\Delta H_{H^-D}(PyH_2) = 48.0$ kcal mol^{-1}) and ΔH_{rxn} (Equation 4).
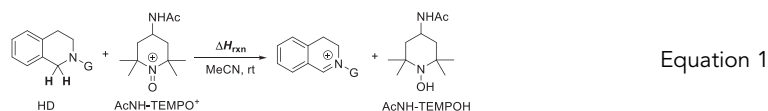
Equation 1

$$\Delta H_{H^-D}(HD) = \Delta H_{rxn} - \Delta H_{H^-A}(AcNH\text{-}TEMPO^+)$$

Equation 2
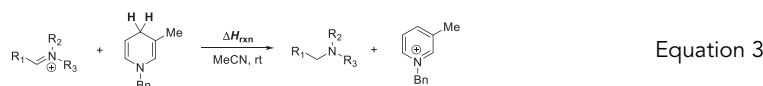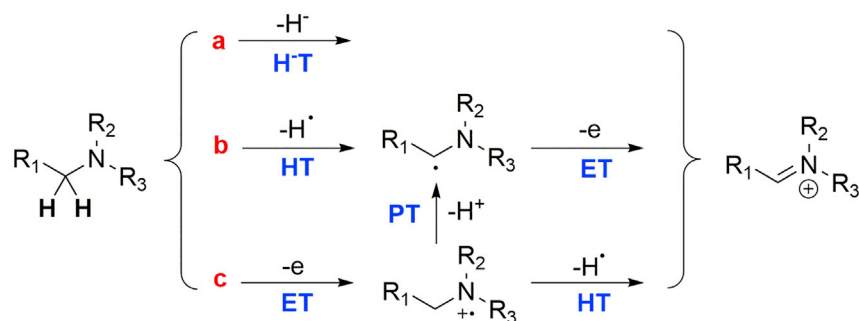
Equation 3

Scheme 3. Possible Pathways for Generation of Iminium Ions from Tertiary Amines

$$\Delta H_{\text{H}^-\text{D}}(\text{HD}) = \Delta H_{\text{H}^-\text{D}}(\text{PyH}_2) - \Delta H_{\text{rxn}}$$

Equation 4

Next, a thermochemical cycle was established according to the Hess's Law to derive other thermodynamic quantities on the basis of the available $\Delta H_{\text{H}^-\text{D}}(\text{HD})$ (Scheme 4). As shown, the hydrogen-atom donability of tertiary amines, i.e. the homolytic α-C–H bond dissociation energy $\Delta H_{\text{HD}}(\text{HD})$, can be obtained from the experimentally measurable hydricity $\Delta H_{\text{H}^-\text{D}}(\text{HD})$ and the reduction potential of its corresponding iminium ion, $E_{\text{red}}(\text{D}^+)$ (Equation 5). The respective cycles for evaluating the α-C–H homolytic ($\Delta H_{\text{HD}}(\text{HD}^{\bullet+})$) and heterolytic energies ($\Delta H_{\text{PD}}(\text{HD}^{\bullet+})$) of amine radical cations were also designed (Equations 6 and 7), where the energy required for converting amines (HD) to its radical cations (HD$^{\bullet+}$) is described by their oxidation potentials $E_{\text{ox}}(\text{HD})$ (see Supplemental Information for details). These bond parameters, together with the relevant redox potentials determined in this work, are summarized in Table 1.

DISCUSSION

Structural Effects and Energetic Criteria of Amine α-C–H Bond Scission

As shown in Scheme 3, generation of iminium ion is the key step in α-C–H functionalization of tertiary amines, which could be initiated by either hydride (H$^-$T), hydrogen (HT), or electron transfer (ET), corresponding respectively to the energetic terms of $\Delta H_{\text{H}^-\text{D}}$, ΔH_{HD}, or $E_{\text{ox}}(\text{HD})$. The effects of amine structural variations on the corresponding energies as well as on understanding of amine α-transformations are addressed below, jointly with experimental verification, wherever applicable.

On Hydride Removal

As known from the hydricity data ($\Delta H_{\text{H}^-\text{D}}$) of amines in Table 1, series **2**, **6**, and **9** mimic the general trend as seen in other hydridic systems (e.g. NADH models (Zhu and Wang, 2010)), that is, remote electron-donating groups (EDGs) at N atom facilitate C–H bond scission by stabilizing the nascent iminium ion, whereas electron-withdrawing groups (EWGs) do the opposite. Although such trend basically remains also for series **7** with adjacent substitution at N atom, the structural effect is notably more pronounced and likely also complicated by factors other than the electronic effect. For example, steric effect should at least be partially responsible for the derived hydricity order of **7a** (R = CH$_3$: 72.7) <**7e** (CH$_2$Ph: 75.1) <**7f** (CHPh$_2$: 76.6) and **7i** (2-Naph: 76.1) <**6e** (Ph: 77.9) <**7h** (1-Naph: 82.2). Also, it is worth noting that the effects of changing the ring size (**6e** vs. **11** and **12**) or aromaticity (**7a** vs. **14**) are quite significant. One can find that the hydricity of serial **6** determined here correlates well with the previously observed kinetic trend of THIQ oxidation by DDQ (Tsang et al., 2017). Besides, the gradual increase of $\Delta H_{\text{H}^-\text{D}}$ for N-Ph (**6e**), N-(1-Naph) (**7h**), and N-Cbz (**7g**) is also found to agree with the descending reaction rates of their oxidation by DDQ (Tsang et al., 2017).

To help people to more easily apply these energetic data in analyzing/predicting the trend of hydride exchange reactions, the hydricity ($\Delta H_{\text{H}^-\text{D}}$) of amines derived in this work are depicted in Figure 1, along with the known hydride affinity ($\Delta H_{\text{H}^-\text{A}}$) data of common hydride acceptors for comparison. The combined scale reveals that amines (colored bars, ranging 60–92 kcal mol^{-1}) are generally weaker hydride donors than biomimetic donors such as 1,3-dimethyl-2,3-dihydro-1H-benzimidazole (DMBI, 54.1 kcal mol^{-1}), 1-benzyl-1,4-dihydropyridine-3-car-boxamide (BNAH, 64.2 kcal mol^{-1}), and diethyl 2,6-dimethyl-1,4-dihydropyridine-3,5-dicarboxylate (HEH, 69.3 kcal mol^{-1}). Indeed, strong oxidants with $-\Delta H_{\text{H}^-\text{A}}$ values greater than 100 kcal mol^{-1} (e.g., DDQ, Ph$_3$C$^+$,
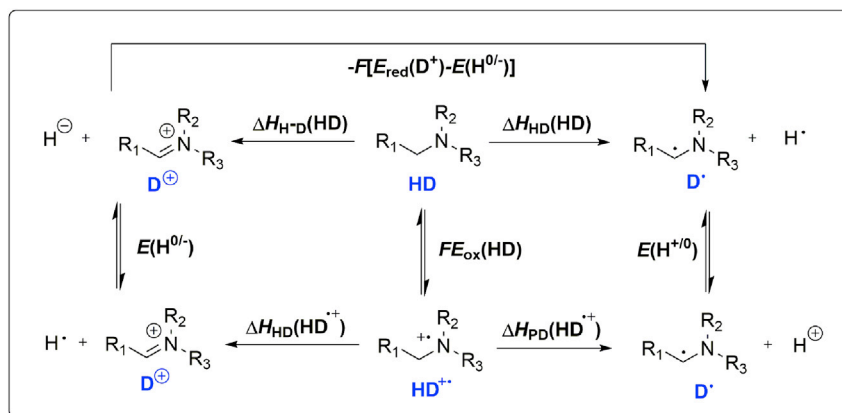
$$\Delta H_{HD}(HD) = \Delta H_{H^-D}(HD) - F[E_{red}(D^+) - E(H^{0/-})] \qquad \text{eq. 5}$$

$$\Delta H_{PD}(HD^{\cdot+}) = \Delta H_{HD}(HD) - F[E_{ox}(HD) - E(H^{+/0})] \qquad \text{eq. 6}$$

$$\Delta H_{HD}(HD^{\cdot+}) = \Delta H_{H^-D}(HD) - F[E_{ox}(HD) - E(H^{0/-})] \qquad \text{eq. 7}$$

Scheme 4. Thermodynamic Cycles for Derivation of $\Delta H_{HD}(H)$, $\Delta H_{HD}(HD^{\bullet+})$, and $\Delta H_{PD}(HD^{\bullet+})$

AcNH-TEMPO$^+$) were experimentally observed to be capable of splitting the α-C–H bonds of all N-alkyl/aryl-THIQs in a few minutes at room temperature (de Costa et al., 1992; Tsang et al., 2017). This also explains the need of a longer reaction time (2h) reported for N-Cbz-THIQ (Yan et al., 2015) and the loss of its reactivity with a weaker oxidant, tropylium (T$^+$,–ΔH_{H^-A} = 85 kcal mol^{-1}) (Oss et al., 2018). It was also found that only the more reactive N-alkyl-THIQs (ΔH_{H^-D}: 72–76 kcal mol^{-1}) could be oxidized by T$^+$ (Oss et al., 2018). These examples demonstrated that the energetic data here derived can actually well rationalize the previously observed reactivity trend in the oxidation of various THIQs by different oxidants as represented in Scheme 2A and 2B. Based on energetic criteria, if a weak oxidant such as AcrH$^+$, p-BQ, or B(C$_6$F$_5$)$_3$ (Heiden et al., 2015) with a –ΔH_{H^-A} close to the ΔH_{H^-D} of the amines is employed, no complete reaction would be expected. Under this circumstance, only an equilibrium may be realized. Recently, such reversible H$^-$T between tertiary amines and B(C$_6$F$_5$)$_3$ was indeed observed in a double-acid catalyzed amine α-C–H functionalization (Shang et al., 2018).

On Hydrogen Removal

The amine α-C–H bond may also be cleaved through HT (i.e., HAT) when there exist radical initiators. In such cases, hydrogen-donating ability of the C–H bond (ΔH_{HD}, i.e., BDE) is the key factor governing amines' reactivity. As seen in Table 1, the ΔH_{HD} (88.1 kcal mol^{-1}) of tribenzylamine **1** obtained here agrees well with the gas-phase value 89.1 kcal mol^{-1} in literature (Dombrowski et al., 1999). On the other hand, the newly derived ΔH_{HD} of 79.4 kcal mol^{-1} for **2e** may suggest a need for reexamining the previously reported value of 88.6 kcal mol^{-1} (Denisov et al., 2005), because it is well known that replacing a hydrogen from trimethylamine (ΔH_{HD} = 87 kcal mol^{-1}) (Grela et al., 1984) with a phenyl group could not be expected to largely increase ΔH_{HD} due to a better delocalization of spin (Cheng et al., 2016). Generally, the ΔH_{HD} values of the amine α-C–H bonds in the absence of a strong EWG or steric disturbance are found to be around 80 kcal mol^{-1} or below, which are significantly lower than the regular C(sp^3)–H bonds (Cheng et al., 2016) without a so-called "two-center-three-electron" (3 in 2) radical stabilization (Griller et al., 1981; Lalevée et al., 2002; Wayner et al., 1997). As realized, the effect of structural variations on the ΔH_{HD} (i.e., BDE) of amines is more complicated than on hydricities; this situation was also commonly observed in other studies on radical stability in the literature (Hioe et al., 2010; Johnny et al., 2012; Zipse, 2006). Nevertheless, the effect of structural variation in these radicals still could be reasonably understood by considering the interplays between the electronic and steric factors, with special attention paid on the differences between the remote and adjacent substitution and on their electron density between the "3 in 2" radicals and the normal carbon radicals.
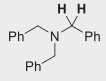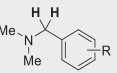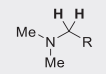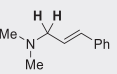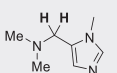
Substrates	R		$\Delta H_{H-D}(HD)^a$	$\Delta H_{HD}(HD)^a$	$\Delta H_{HD}(HD\bullet+)^a$	$\Delta H_{PD}(HD\bullet+)^a$	$E_{ox}(HD)^b$	$E_{red}(D^+)^b$
	1		76.6	88.1	34.9	19.4	0.67	−1.64
	2a	p-CN	81.4	79.3	40.1	12.9	0.65	−1.05
	2b	p-Br	77.0	80.0	37.3	15.2	0.58	−1.27
	2c	p-Cl	75.7	79.2	36.3	14.6	0.57	−1.29
	2d	p-F	76.0	81.3	36.6	16.7	0.57	−1.37
	2e	H	73.9	79.4	35.2	15.5	0.54	−1.38
	2f	p-Me	70.2	76.7	31.7	13.0	0.53	−1.42
	2g	p-OMe	63.1	71.4	24.8	8.0	0.52	−1.50
	2h	p-NMe$_2$	60.9	73.4	27.5	14.8	0.31	−1.68
	2i	o,o'-Me$_2$	62.9	72.1	24.2	8.2	0.54	−1.54
	3a	1-Naph	76.2	79.7	37.5	15.8	0.54	−1.29
	3b	2-Naph	75.2	78.4	36.7	14.8	0.53	−1.28
	4		69.8	71.0	31.8	7.7	0.51	−1.19
	5		61.9	70.0	18.5	1.5	0.74	−1.49

Table 1. Integrated α-C−H Bond Homolytic Energy [ΔH_{HD}(HD)] and Hydricity [ΔH_{H-D}(HD)] Scale of Tertiary Amines, Homolytic/Heterolytic Energy Scales of Amine Radical Cations [ΔH_{HD}(HD•+)/ΔH_{PD}(HD•+)], and the Relevant Redox Data in Acetonitrile at 298 K
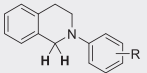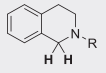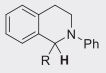
Substrates	R		$\Delta H_{\text{H-D}}(\text{HD})$[a]	$\Delta H_{\text{HD}}(\text{HD})$[a]	$\Delta H_{\text{HD}}(\text{HD}\bullet+)$[a]	$\Delta H_{\text{PD}}(\text{HD}\bullet+)$[a]	$E_{\text{ox}}(\text{HD})$[b]	$E_{\text{red}}(\text{D}^+)$[b]
	6a	p-NO$_2$	82.1[c]	74.7	36.7	2.3	0.83	−0.82
	6b	p-CN	80.7	74.5	36.9	3.7	0.76	−0.87
	6c	p-CF$_3$	79.7	75.0	37.2	5.6	0.70	−0.94
	6d	p-Cl	78.9	75.7	41.3	11.1	0.49	−1.00
	6e	H	77.9	76.5	41.7	13.4	0.43	−1.08
	6f	p-Me	77.6	76.3	42.9	15.0	0.35	−1.10
	6g	p-OMe	75.4	74.9	43.8	16.4	0.23	−1.12
	6h	o-OMe	77.6	78.7	42.3	16.4	0.39	−1.19
	6i	m-OMe	79.0	77.6	43.5	15.1	0.40	−1.08
	7a	Me	72.7	78.0	34.9	13.2	0.50	−1.37
	7b	Et	72.2	77.7	35.5	14.1	0.45	−1.38
	7c	CH$_2$CO$_2$Et	79.4	81.2	37.6	12.5	0.67	−1.22
	7d	CH$_2$CHCH$_2$	73.1	77.5	33.4	10.8	0.58	−1.33
	7e	CH$_2$Ph	75.1	79.0	35.2	12.1	0.59	−1.31
	7f	CHPh$_2$	76.6	79.8	34.8	11.1	0.67	−1.28
	7g	Cbz	92.5[c]	80.5	32.5	−6.4	1.46	−0.62
	7h	1-Naph	82.2	83.5	47.5	21.8	0.43	−1.13
	7i	2-Naph	76.1	73.5	42.2	12.7	0.33	−1.03
	8a	Me	75.8	84.1	39.8	21.1	0.42	−1.50
	8b	Ph	74.3	80.5	36.2	15.4	0.51	−1.41

Table 1. Continued

iScience
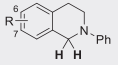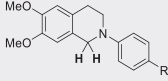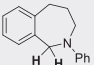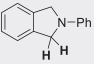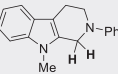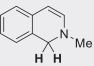
Substrates	R		$\Delta H_{H\text{-}D}(HD)^a$	$\Delta H_{HD}(HD)^a$	$\Delta H_{HD}(HD\bullet+)^a$	$\Delta H_{PD}(HD\bullet+)^a$	$E_{ox}(HD)^b$	$E_{red}(D^+)^b$
(structure)	9a	7-NO$_2$	81.4	75.4	43.6	10.6	0.50	−0.88
	9b	6-CN	82.0	74.1	44.4	9.5	0.49	−0.80
	9c	6-Br	80.3	77.1	43.4	13.2	0.46	−1.00
	9d	6-OMe	76.9	79.2	41.3	16.7	0.40	−1.24
(structure)	10a	Cl	77.5	77.5	40.6	13.6	0.46	−1.14
	10b	H	75.7	77.3	40.2	14.8	0.40	−1.21
	10c	OMe	72.0	75.2	41.1	17.3	0.20	−1.28
(structure)	11		80.0^c	78.1	44.0	15.2	0.42	−1.06
(structure)	12		71.1	70.2	34.4	6.5	0.45	−1.10
(structure)	13		77.9	77.4	41.0	13.5	0.46	−1.12
(structure)	14		66.7	74.5	42.0	22.8	−0.07	−1.48

Table 1. Continued

Note: The hydricity [$\Delta H_{H\text{-}D}(HD)$] of **6e** (77.9 kcal mol^{-1}) is consistent well with the values of 77.0 and 78.6 kcal mol^{-1} derived independently from other acceptors (phenothiazinium perchlorate and Ph$_3$C$^+$ClO$_4^-$).

[a]In units of kcal mol^{-1}, obtained from Scheme 4 within experimental error of ±0.5 kcal mol^{-1}, taking $E(H^{0/+}) = -2.31$ V and $E(H^{-/0}) = -1.14$ V (Parker, 1992).

[b]In units of V vs Fc$^{0/+}$, obtained from CV experiments within experimental error of ±30 mV.

[c]Measured by Ph$_3$C$^+$ClO$_4^-$ with $\Delta H_{H\text{-}A}(Ph_3C^+) = -104.3$ kcal mol^{-1}.
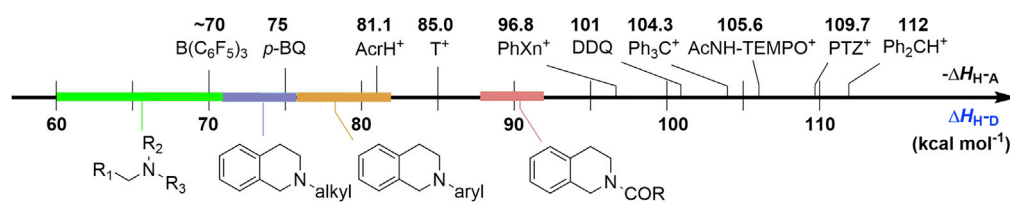
Figure 1. Hydricity Scale ($\Delta H_{H\text{-}D}$) of Amines (Colored Bars) and Hydride Affinity ($\Delta H_{H\text{-}A}$) for Common Hydride Acceptors in Acetonitrile (Data on Top)

Note: p-BQ: p-benzoquinone; AcrH$^+$: acridinium; T$^+$: tropylium; PhXn$^+$: 9-phenylxanthylium, also see Table S1 (Zhu et al., 2008a, 2008b; Zhu et al., 2007).

Figure 2 shows the ΔH_{HD} range for amines (blue bar), together with hydrogen affinities (ΔH_{HA}) of some common hydrogen acceptors (Cheng et al., 2016; Pedley, 2012; Ruscic et al., 2013) for the convenience of energetic comparison that would benefit rational selection of reaction partners in synthesis. As implied in Figure 2, very reactive radicals with $-\Delta H_{HA} > 90$ kcal mol^{-1} (e.g., triethylenediamine radical cation, phenyl, alkoxy, and hydroxyl radicals), which can only be generated in situ from precursors, would be able to cleave the amine α-C–H bonds via HT (i.e., HAT). This anticipation has actually been experimentally confirmed, as will be exemplified below. In the oxidative α-C–H functionalization of tertiary amines, both the Cl$_3$C$^\bullet$ ($-\Delta H_{HA} = 93.8$ kcal mol^{-1}) and Br$^\bullet$ ($-\Delta H_{HA} = 88$ kcal mol^{-1}) radicals were observed to be able to abstract the hydrogen atom from amines (Yan et al., 2015). And, the in-situ-generated triethylenediamine radical cation ($-\Delta H_{HA} = 107$ kcal mol^{-1}) was found to be feasible in hydrogen atom abstraction to selectively functionalize α-C–H bonds of trialkylamines (Barham et al., 2016). Moreover, hydrogen transfers from THIQs to various oxygen-centered radicals (e.g., HO$^\bullet$, tBuO$^\bullet$, tBuOO$^\bullet$, isobutyronitrile-derived alkoxyl radical) (Chu and Qing, 2010; Ghobrial et al., 2010; Tang et al., 2011) were also reported as the initiated step to trigger CDCs. By the same line, moderate oxidants ($-\Delta H_{HA}$: 80–90 kcal mol^{-1}) would be expected to react with amines reversibly, and they may possibly be used as catalysts to deliver hydrogen atom between amines and other substrates. Indeed, thiyl radical Ph$_3$Si-S$^\bullet$ ($-\Delta H_{HA} \approx 90$ kcal mol^{-1}) was found to be a good catalyst for homolysis of α-C–H bonds of N-Acyl-THIQ (Yan et al., 2016). For some commercially available oxidants with $-\Delta H_{HA}$ values of 50–80 kcal mol^{-1} [e.g., O$_2$, 1,1-diphenyl-2-picrylhydrazyl (DPPH), tert-Butyl hydroperoxide (TBHP), butylatedhydroxytoluene (BHT), and 2,2,6,6-tetramethylpiperidine-1-oxyl (TEMPO)], their relatively low hydrogen-accepting capacities should actually be the cause to prevent them from triggering homolysis of amine C–H bonds. However, if an amine radical cation is generated in advance, they should be able to easily abstract a hydrogen atom from this radical intermediate (vide infra).

On Electron-Coupled C–H Bond Cleavage of Amine Radical Cations

Removal of an electron from organic molecules is a very efficient way to activate inert C–H bond for inducing C–H functionalization (McManus et al., 2018; Ueda et al., 2014). Understanding of the mechanisms of degradation paths for radical cations generated by ET would require the energetic knowledge of their bond homolysis and heterolysis (cf. Scheme 3, path **c**). As presented herewith, the ΔH_{HD}(HD$^{\bullet+}$) (releasing an H$^\bullet$) covers a range of 29–46 kcal mol^{-1}, which is roughly 40 kcal mol^{-1} lower than the ΔH_{HD} values of the parent amines, indicating a tremendous C-H bond activation. On the other hand, the ΔH_{PD}(HD$^{\bullet+}$) (donating a proton) shows an energy range from -6.4 to 21.8 kcal mol^{-1} (Table 1). Here an even greater activation effect is demonstrated, although the pK_a values of the parent amine α-C–H bonds are too high to measure in any solution.

Applications of Energetic Scale for Understanding THIQ Oxidation Mechanisms

Considering the inherent relationship between the bond energy and reactivity, further exploration of its predictive value would be beneficial for understanding amine chemistry, especially for those who are not too much familiar with the ways to use the available bond energy data in their synthetic methodology investigation. In the following subsections, we present examples to demonstrate the good potential of the bond energetic data in elucidating amine oxidation mechanisms. To make this line of energetic analysis easier to follow, here we have intended to choose some better-studied cases (rather than synthetically maybe more "useful" ones) to show the effectiveness of the energy data in mechanistic analysis. This is because the well-studied cases would allow the predictive value of the derived bond energy data to be directly backed up with existing experimental observations.
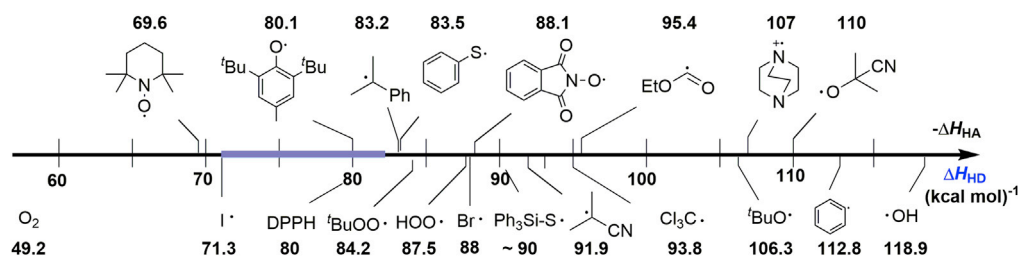
Figure 2. Hydrogen-Atom-Donating Abilities (ΔH_{HD}) of Amines (Blue Bar) and Hydrogen Atom Affinities (ΔH_{HA}) of Common Acceptors

Also see Table S1 (Cheng et al., 2016).

Generally, there are two types of oxidants used in the CDCs of amines: single-component hydride acceptors and dual-component oxidants (electron and hydrogen acceptors). We will start with the former, which were more extensively developed.

Oxidation by Hydride Acceptors

When a hydride acceptor serves as the oxidant, it was found that cleavage of the amine α-C–H bond could possibly be initiated either by hydride, hydrogen, or by electron transfer. Among them, the intrinsic barrier of electron transfer is known to be much lower than those of atom/group transfers (Brinkley et al., 2005; Fukuzumi, 2003; Gust et al., 1993; Li and Zhu, 2018). Therefore, even an uphill ET can be expected to occur if the energetic barrier is not much greater than 0.5 eV (1 eV = 23.1 kcal mol^{-1}), because the deficiency of driving forces could be easily compensated by exothermic follow-up processes (Cheng et al., 1998; Eberson, 1982). This energetic feature makes ET the preferential pathway for initiating C–H bond cleavage.

As known, DDQ, Ph$_3$C$^+$, and TEMPO$^+$ are popular oxidants used in CDC of amines (Richter and GarcíaMancheño, 2011; Song et al., 2018; Wendlandtand Stahl, 2015; Zhang and Li, 2006). Their E_{red}, ΔH_{H^-A}, and ΔH_{HA} values in acetonitrile were reported (Table S1) (Heiden and Lathem 2015; Zhu et al., 2007, 2010, Zhu and Wang, 2010). This allowed the thermodynamics of the elementary steps of their reactions with THIQs to be evaluated by jointly using the corresponding data in Table 1. The so-derived energetic data are presented in Table 2. Taking the oxidation of N-Ph-THIQ with DDQ as an example, all its elementary steps are illustrated in Scheme 5.

Based on thermodynamic criteria, a comparison of the energies of paths *a*, *b*, and *c* in Scheme 5 immediately excludes the HT path, because it is 16.5 kcal mol^{-1} uphill. At first, one may guess that the H$^-$T (path *b*:−26.1 kcal mol^{-1}) must be a favorable process because of the exothermicity of the overall H$^-$T. However, many previous studies indicated that this is most likely not the case especially when competing with an ET (path *c*: 6.8 kcal mol^{-1}) in the reaction system, due to the extremely higher intrinsic barrier for H$^-$T (Brinkley and Roth, 2005; Eberson, 1982; Gust et al., 1993; Li and Zhu, 2018). The energy requirement for ET to occur in N-Ph-THIQ oxidation by DDQ ($\Delta G_{ET} = 6.8$ kcal mol^{-1}) can be well filled up by the highly exothermic follow-up hydrogen release from its radical cation (step *d*, $\Delta H_{HT} = -31.8$ kcal mol^{-1}). Therefore, the ET-HT process would be most favorable. On the other side, the PT-ET path for N-Ph-THIQ$^{·+}$ decay should be unlikely to follow, because the PT (step *e*) is endothermic ($\Delta H_{PT} = 9.7$ kcal mol^{-1}). This bond-energy-based analysis of oxidation mechanism can, indeed, be backed up by experiments and calculations (Chen et al., 2015). The oxidation mechanisms of other THIQ analogs by DDQ may be identified as well by similar thermodynamic analysis. For example, one could expect that the oxidation of N-(1-Naph)-THIQ may also go through an ET-HT path mechanism, because its ΔG_{ET} of 6.8 kcal mol^{-1} satisfies the empirical ET criterion (<0.5 eV, see above), whereas for oxidation of N-Cbz-THIQ, a direct H$^-$T pathway would be preferred (Chen et al., 2015), because its ET is well above Eberson's maximum energetic criterion of 1 eV for electron transfer to take place (Cheng et al., 1998; Eberson, 1982). These energetic diagnoses exemplified, despite yet only on a thermodynamic basis, have already showed their good potential in accounting for the diversified observations of the CDCs of THIQs. This is most likely because, for this type of chemical transformation, the reaction can be largely driven by the inherent energetic factor featuring an enhanced reactivity of the C-H bond adjacent to an electron pair at nitrogen.

THIQ	Oxidant	Step aΔH_{H-T}	Step bΔH_{HT}	Step cΔG_{ET}	Step dΔH_{HT}	Step eΔH_{PT}	Step fΔG_{ET}	Mechanism
N-Cbz	DDQ	−11.5	20.5	30.5	−41.0	−10.0	−32.0	H$^-$T
N-Ph	DDQ	−26.1	16.5	6.8	−31.8	9.7	−42.6	ET–HT
N-(1-Naph)	DDQ	−21.8	23.5	6.8	−26.0	16.7	−45.3	ET–HT
N-Cbz	Ph$_3$C$^+$	−11.8	37.1	37.6	−51.0	−0.5	−48.9	H$^-$T
N-(4-MeO-Ar)	Ph$_3$C$^+$	−28.9	31.5	9.2	−39.7	22.3	−60.4	ET–HT

Table 2. Thermodynamics for Each Elementary Step in the Oxidation of THIQs by Hydride Acceptors in Acetonitrile at 298 K (kcal Mol^{-1})
Also see Table S1.

As for reactions with other oxidants, Ph$_3$C$^+$ and TEMPO$^+$, there are some discussions in literature regarding their mechanisms (Richter et al., 2012; Xie et al., 2014), but further clarification is needed. By the same line of argument, we have also made predictions for them. The results are presented in Table 2 as examples, along with the relevant energetic data required for the mechanism elucidation. Additional experiments were also carried out for this purpose to further verify our thermodynamic prediction, and the results can be found in the Supplemental Information (see Figures S2 and S3 for details) to save space.

Oxidation by Dual-Component Oxidants

In the cases where dual-component oxidants [e.g., FeCl$_2$/O$_2$ (Brzozowski et al., 2015), I$_2$/H$_2$O$_2$ (Nobuta et al., 2013), CuCl$_2$/O$_2$ (Boess et al., 2011), and CuBr/^{t}BuOOH (Li and Li, 2004)] are used cooperatively in CDCs, it is known that the amine oxidation can be initiated either by HT to radical scavengers such as I$_2$ (Dhineshkumar et al., 2013) and TBHP (Li and Li, 2004) or by ET to single-electron oxidants, e.g., Cu^{2+} (Boess et al., 2011), Fe^{3+} (Brzozowski et al., 2015), I$_2$ (Dhineshkumar et al., 2013), photo-oxidants (Condie et al., 2010), and anodes (Fu et al., 2017). The resulting amine radical or radical cation would then collapse to an iminium ion through ET or HT. As the above, these oxidation mechanisms can also be differentially elucidated based on the thermodynamics of amines and the particular oxidant pairs. A representative example is given below.

As briefly touched in the Introduction, Klussmann et al. (Boess et al., 2012) investigated the mechanistic differences between the CuCl$_2$·H$_2$O/O$_2$- and CuBr/TBHP-catalyzed CDCs of THIQs with nucleophiles. They found that the key intermediate with the aerobic method was an iminium ion formed via oxidation by Cu(II). However, in the CuBr/TBHP system, the precursor α-amino peroxide was formed from amine and TBHP via a radical pathway (Scheme 6). Now these two mechanisms can be reasonably differentiated using the thermodynamic data obtained here and elsewhere (see Table S2). The energetics for each possible step is shown in Scheme 6. For the CuCl$_2$/O$_2$ system (Scheme 6A), it is obvious that an ET from THIQ to Cu^{2+} is
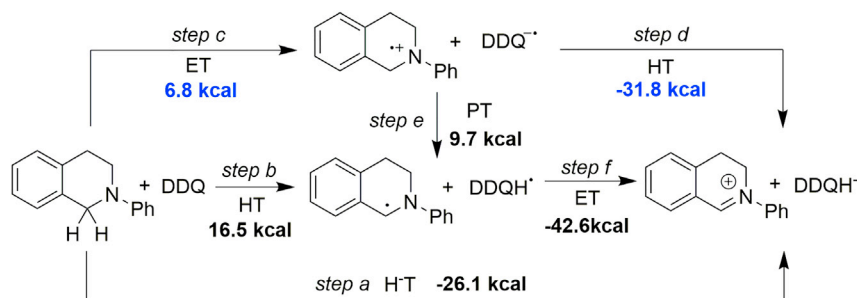
Scheme 5. Thermodynamic Analysis of Possible Pathways in the Oxidation of N-Ph-THIQ by DDQ (kcal mol^{-1})
Also see Table S1.
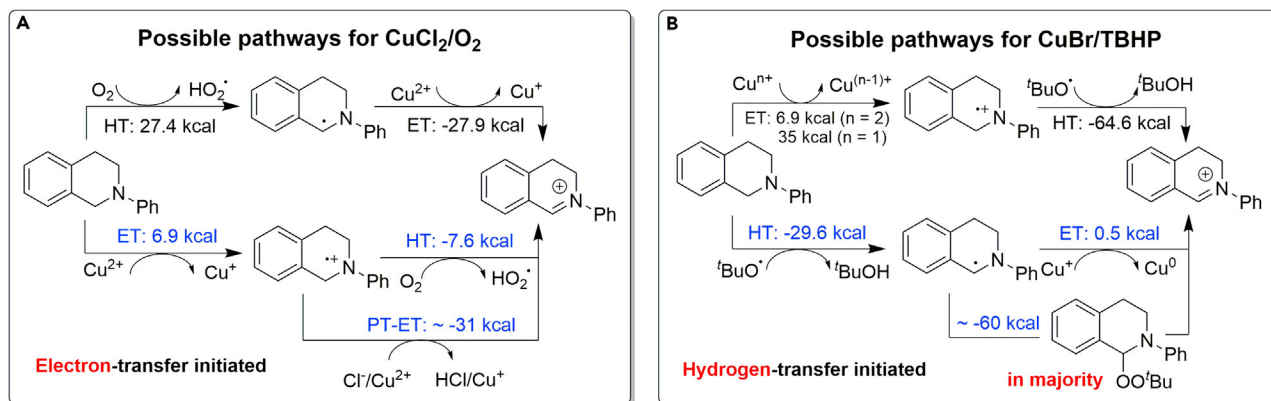
Scheme 6. Thermodynamic Rationalization of Possible Pathways for Oxidization of *N*-Ph-THIQ by Dual-Component Oxidants
(A) the oxidatants are CuCl$_2$/O$_2$; (B) the oxidatants are CuBr/TBHP.
Also see Table S2.

feasible, because its thermodynamic driving force is only 6.9 kcal mol^{-1}; but an HT between THIQ and O$_2$ would be unlikely to occur, because it is extremely endothermic (27.4 kcal mol^{-1}). Consequently, the resulted THIQ$^{\cdot+}$ then rapidly degenerates to iminium ion by either HT (−7.6 kcal mol^{-1}) to O$_2$ or a PT-ET sequence to Cl$^-$/Cu^{2+} (ca.−31 kcal mol^{-1}). On the other hand, in the CuBr/TBHP system (Scheme 6B), HT should be the feasible initiating step for THIQ oxidation, because it is downhill by 29.6 kcal mol^{-1}, whereas ET is, however, endothermic. As for the subsequent processes of HT, coupling of the THIQ$^\cdot$ radical with ^{t}BuOO$^\cdot$ or ^{t}BuO$^\cdot$ (ca.−60 kcal mol^{-1}) is much more favorable than the ET path (0.5 kcal mol^{-1}). This actually explains why α-amino peroxide was observed as the major intermediate.

Conclusion

Due to the inherent difficulties in measuring the pK_a of α-C−H bond of tertiary amines, the Bordwell's method for solution BDEs is unfortunately not applicable for the target system of this work. For this reason, we have developed a new approach for the present bond energy study by taking advantage of our expertise in hydricity measurement. The first integrated α-C−H bond energy scale for representative tertiary amines were hereby established via a series of different cycles based on experimentally determined hydricities. Four major types of α-C−H bond energies including the hydricity [$\Delta H_{\text{H-D}}$(HD)] and BDE [ΔH_{HD}(HD)] values for 45 parent tertiary amines and the BDEs [ΔH_{HD}(HD$^{\cdot+}$)] and acidities [ΔH_{PD}(HD$^{\cdot+}$)] for their radical cations in acetonitrile were determined. General utility of this integrated bond energetic scale for elucidating experimental observations were demonstrated, verifying its predictive value and reliability of the bond energetic analysis for understanding bond transformations via CDC process. The success of this type of rational analyses represented here would encourage more general practices along this line in the future and eventually promotes it to become a mainstream logic in reaction analysis and design.

Limitations of the Study

Present strategy is applicable for the tertiary amine with at least one benzyl substituent at the nitrogen atom. We are currently working on improving the methodology to accommodate broader range of substrates such as aliphatic cyclic amine, etc.

METHODS

All methods can be found in the accompanying Transparent Methods supplemental file.

DATA AND CODE AVAILABILITY

The related figures and data in this article can be found at the database: https://data.mendeley.com/datasets/r8ynb4s6s4/draft?a=16da539e-259c-45a1-9e05-7e4a2a79a6ae.

SUPPLEMENTAL INFORMATION

Supplemental Information can be found online at https://doi.org/10.1016/j.isci.2020.100851.

REFERENCES

Allen, J.M., and Lambert, T.H. (2011). Tropylium ion mediated α-cyanation of amines. J. Am. Chem. Soc. *133*, 1260–1262.

Barham, J.P., John, M.P., and Murphy, J.A. (2016). Contra-thermodynamic hydrogen atom abstraction in the selective C–H functionalization of trialkylamine N-CH₃ groups. J. Am. Chem. Soc. *138*, 15482–15487.

Basle, O., Borduas, N., Dubois, P., Chapuzet, J.M., Chan, T.H., Lessard, J., and Li, C.J. (2010). Aerobic and electrochemical oxidative cross-dehydrogenative-coupling (CDC) reaction in an imidazolium-based ionic liquid. Chem. Eur. J. *16*, 8162–8166.

Beatty, J.W., and Stephenson, C.R.J. (2015). Amine functionalization via oxidative photoredoxcatalysis: methodology development and complex molecule synthesis. Acc. Chem. Res. *48*, 1474–1484.

Blakemore, D.C., Castro, L., Churcher, I., Rees, D.C., Thomas, A.W., Wilson, D.M., and Wood, A. (2018). Organic synthesis provides opportunities to transform drug discovery. Nat. Chem. *10*, 383–394.

Boess, E., Sureshkumar, D., Sud, A., Wirtz, C., Farès, C., and Klussmann, M. (2011). Mechanistic studies on a Cu-catalyzed aerobic oxidative coupling reaction with N-phenyl tetrahydroisoquinoline: structure of intermediates and the role of methanol as a solvent. J. Am. Chem. Soc. *133*, 8106–8109.

Boess, E., Schmitz, C., and Klussmann, M. (2012). A comparative mechanistic study of Cu-catalyzed oxidative coupling reactions with N-phenyltetrahydroisoquinoline. J. Am. Chem. Soc. *134*, 5317–5325.

Boess, E., Wolf, L.M., Malakar, S., Salamone, M., Bietti, M., Thiel, W., and Klussmann, M. (2016). Competitive hydrogen atom transfer to oxyl- and peroxyl radicals in the Cu-catalyzed oxidative coupling of N-aryl tetrahydroisoquinolines using tert-butyl hydroperoxide. ACS Catal. *6*, 3253–3261.

Bordwell, F.G., Cheng, J.P., and Harrelson, J.A. (1988). Homolytic bond dissociation energies in solution from equilibrium acidity and electrochemical data. J. Am. Chem. Soc. *110*, 1229–1231.

Brinkley, D.W., and Roth, J.P. (2005). Determination of a large reorganization energy barrier for hydride abstraction by glucose oxidase. J. Am. Chem. Soc. *127*, 15720–15721.

Brzozowski, M., Forni, J.A., Paul Savage, G., and Polyzos, A. (2015). The direct α-C(sp³)–H functionalisation of N-aryl tetrahydroisoquinolines via an iron-catalysed aerobic nitro-mannich reaction and continuous flow processing. Chem. Commun. *51*, 334–337.

Campos, K.R. (2007). Direct sp³ C–H bond activation adjacent to nitrogen in heterocycles. Chem. Soc. Rev. *36*, 1069–1084.

Chen, Q., Zhou, J., Wang, Y., Wang, C., Liu, X., Xu, Z., Lin, L., and Wang, R. (2015). Transition-metal-free dehydrosilylativedifluoroamidation of tetrahydroisoquinolines under mild conditions. Org. Lett. *17*, 4212–4215.

Chen, W.J., Ma, L.L., Paul, A., and Seidel, D. (2018). Direct α-C-H bond functionalization of unprotected cyclic amines. Nat. Chem. *10*, 165–169.

Cheng, J.-P., Lu, Y., Zhu, X., and Mu, L. (1998). Energetics of multistep versus one-step hydride transfer reactions of reduced nicotinamideadenine dinucleotide (NADH) models with organic cations and p-quinones. J. Org. Chem. *63*, 6108–6114.

Cheng, J.-P., et al. (2016). Internet bond-energy databank (pKₐ and BDE)-iBonD. http://ibond.nankai.edu.cn.

Cheng, Z., Yu, Z., Yang, S., Shen, H.C., Zhao, W., and Zhong, S. (2017). C–H bond functionalization of tetrahydropyridopyrimidines and other related hetereocycles. J. Org. Chem. *82*, 13678–13685.

Chi, H., Li, H., Liu, B., Ye, R., Wang, H., Guo, Y.-L., Tan, Q., and Xu, B. (2019). From isocyanides to iminonitriles via silver-mediated sequential insertion of C(sp³)–H bond. iScience *21*, 650–663.

Chu, L., and Qing, F.-L. (2010). Benzoyl peroxide (BPO)-Promoted oxidative trifluoromethylation of tertiary amines with trimethyl(trifluoromethyl) silane. Chem. Commun. *46*, 6285–6287.

Condie, A.G., González-Gómez, J.C., and Stephenson, C.R.J. (2010). Visible-light photoredoxcatalysis: aza-henry reactions via C–H functionalization. J. Am. Chem. Soc. *132*, 1464–1465.

de Costa, B.R., and Radesca, L. (1992). A practical triphenylcarbeniumtetrafluoroborate mediated one-pot synthesis of 1-substituted N-Alkyl-1,2,3,4-tetrahydroisoquinolines. Synthesis *1992*, 887–890.

Damico, R., and Broaddus, C.D. (1966). Hydride transfer. Reactions of triphenylcarboniumfluoroborate and triphenylmethylbromide with tertiary amines. J. Org. Chem. *31*, 1607–1612.

Denisov, E.T., and Tumanov, V.E. (2005). Estimation of the bond dissociation energies from the kinetic characteristics of liquid-phase radical reactions. Russ. Chem. Rev. *74*, 825–858.

Dhineshkumar, J., Lamani, M., Alagiri, K., and Prabhu, K.R. (2013). A versatile C–H functionalization of tetrahydroisoquinolines catalyzed by iodine at aerobic conditions. Org. Lett. *15*, 1092–1095.

Dombrowski, G.W., Dinnocenzo, J.P., Farid, S., Goodman, J.L., and Gould, I.R. (1999). α-C–H bond dissociation energies of some tertiary amines. J. Org. Chem. *64*, 427–431.

Eberson, L. (1982). Electron-transfer reactions in organic chemistry. In Advances in Physical Organic Chemistry, *18*, V. Gold and D. Bethell, eds (Academic Press), pp. 79–185.

Francke, R., and Little, R.D. (2014). Redox catalysis in organic electrosynthesis: basic principles and recent developments. Chem. Soc. Rev. 43, 2492–2521.

Fu, N., Li, L., Yang, Q., and Luo, S. (2017). Catalytic asymmetric electrochemical oxidative coupling of tertiary amines with simple ketones. Org. Lett. 19, 2122–2125.

Fukuzumi, S. (2003). New perspective of electron transfer chemistry. Org. Biomol. Chem. 1, 609–620.

Ghobrial, M., Harhammer, K., Mihovilovic, M.D., and Schnürch, M. (2010). Facile, solvent and ligand free iron catalyzed direct functionalization of N-protected tetrahydroisoquinolines and isochroman. Chem. Commun. 46, 8836–8838.

Girard, S.A., Knauber, T., and Li, C.-J. (2014). The cross-dehydrogenative coupling of $C_{sp3}H$ bonds: a versatile strategy for C-C bond formations. Angew. Chem. Int. Ed. 53, 74–100.

Grela, M.A., and Colussi, A.J. (1984). Pyrolysis of ethylenediamines. The stabilization energies of aminomethyl and N,N-dimethylaminomethyl radicals. J. Phys. Chem. 88, 5995–5998.

Griller, D., and Lossing, F.P. (1981). Thermochemistry of α-aminoalkyl radicals. J. Am. Chem. Soc. 103, 1586–1587.

Gust, D., Moore, T.A., and Moore, A.L. (1993). Molecular mimicry of photosynthetic energy and electron transfer. Acc. Chem. Res. 26, 198–205.

Hari, D.P., and König, B. (2011). Eosin Y catalyzed visible light oxidative C–C and C–P bond formation. Org. Lett. 13, 3852–3855.

Heiden, Z.M., and Lathem, A.P. (2015). Establishing the hydride donor abilities of main group hydrides. Organometallics 34, 1818–1827.

Hioe, J., and Zipse, H. (2010). Radical stability and its role in synthesis and catalysis. Org. Biomol. Chem. 8, 3609–3617.

Huo, C., Wu, M., Jia, X., Xie, H., Yuan, Y., and Tang, J. (2014). Aerobic oxidative mannich reaction promoted by catalytic amounts of stable radical cation salt. J. Org. Chem. 79, 9860–9864.

Johnny, H., and Hendrik, Z. (2012). Radical Stability—Thermochemical Aspects.In Encyclopedia of Radicals in Chemistry, Biology and Materials (John Wiley & Sons, Ltd).

Lalevée, J., Allonas, X., and Fouassier, J.-P. (2002). N−H and α(C−H) bond dissociation enthalpies of aliphatic amines. J. Am. Chem. Soc. 124, 9613–9621.

Li, Z., and Li, C.-J. (2004). CuBr-catalyzed efficient alkynylation of sp^3 C−H bonds adjacent to a nitrogen atom. J. Am. Chem. Soc. 126, 11810–11811.

Li, Y., and Zhu, X.-Q. (2018). Theoretical predictiong of activation free energies of various hydride self-exchange reactions in acetonitrile at 298 K. ACS Omega 3, 872–885.

Liu, P.-Y., Zhang, C., Zhao, S.-C., Yu, F., Li, F., and He, Y.-P. (2017a). Metal-free aerobic oxidative cyanation of tertiary amines:

azobis(isobutyronitrile) (AIBN) as a sole cyanide source. J. Org. Chem. 82, 12786–12790.

Liu, Y., Wang, C., Xue, D., Xiao, M., Li, C., and Xiao, J. (2017b). Reactions catalysed by a binuclear copper complex: aerobic cross dehydrogenative coupling of N-aryl tetrahydroisoquinolines. Chem. Eur. J. 23, 3051–3061.

McManus, J.B., Onuska, N.P.R., and Nicewicz, D.A. (2018). Generation and alkylation of α-carbamyl radicals via organic photoredoxcatalysis. J. Am. Chem. Soc. 140, 9056–9060.

McNally, A., Prier, C.K., and MacMillan, D.W.C. (2011). Discovery of anα-amino C–H arylation reaction using the strategy of accelerated serendipity. Science 334, 1114.

Morgante, P., Dughera, S., and Ghigo, G. (2019). Aerobic CuCl2-catalyzed dehydrogenative cross-coupling of tertiary amines.A combined computational and experimental study. J. Phys. Chem. A 123, 2796–2814.

Murahashi, S.-I., Komiya, N., Terai, H., and Nakae, T. (2003). Aerobic ruthenium-catalyzed oxidative cyanation of tertiary amines with sodium cyanide. J. Am. Chem. Soc. 125, 15312–15313.

Nakajima, K., Miyake, Y., and Nishibayashi, Y. (2016). Synthetic utilization of α-aminoalkyl radicals and related species in visible light photoredoxcatalysis. Acc. Chem. Res. 49, 1946–1956.

Nobuta, T., Tada, N., Fujiya, A., Kariya, A., Miura, T., and Itoh, A. (2013). Molecular iodine catalyzed cross-dehydrogenative coupling reaction between two sp^3 C–H bonds using hydrogen peroxide. Org. Lett. 15, 574–577.

Oss, G., de Vos, S.D., Luc, K.N.H., Harper, J.B., and Nguyen, T.V. (2018). Tropylium-promoted oxidative functionalization of tetrahydroisoquinolines. J. Org. Chem. 83, 1000–1010.

Parker, V.D. (1992). Homolytic bond (H-A) dissociation free energies in solution.Applications of the standard potential of the (H^+/H·) Couple. J. Am. Chem. Soc. 114, 7458–7462.

Pedley, J.B. (2012). Thermochemical Data of Organic Compounds (Springer Science & Business Media).

Qin, Y., Zhu, L., and Luo, S. (2017). Organocatalysis in inert C–H bond functionalization. Chem. Rev. 117, 9433–9520.

Ratnikov, M.O., and Doyle, M.P. (2013). Mechanistic investigation of oxidative Mannich reaction with tert-butyl hydroperoxide.The role of transition metal salt. J. Am. Chem. Soc. 135, 1549–1557.

Ravelli, D., Protti, S., and Fagnoni, M. (2016). Carbon–carbon bond forming reactions via photogenerated intermediates. Chem. Rev. 116, 9850–9913.

Richter, H., Fröhlich, R., Daniliuc, C.G., and Mancheño, O.G. (2012). Mild metal-free tandem α-alkylation/cyclization of N-benzyl carbamates

with simple olefins. Angew. Chem. Int. Ed. 51, 8656–8660.

Richter, H., and GarcíaMancheño, O. (2010). Dehydrogenative functionalization of C(sp^3)–H bonds adjacent to a heteroatom mediated by oxoammoniumsalts. Eur. J. Org. Chem. 2010, 4460–4467.

Richter, H., and GarcíaMancheño, O. (2011). TEMPO oxoammonium salt-mediated dehydrogenativepovarov/oxidation tandem reaction of N-alkyl anilines. Org. Lett. 13, 6066–6069.

Rommelspacher, H., and Susilo, R. (1985). Tetrahydroisoquinolines and β-carbolines: putative natural substances in plants and mammals. In Progress in Drug Research, E. Jucker, ed. (Birkhäuser Basel), pp. 415–459.

Ruscic, B., Feller, D., and Peterson, K.A. (2013). Active thermochemicaltables: dissociation energies of several homonuclear first-row diatomics and related thermochemical values. Theor. Chem. Acc. 133, 1415.

Saint-Denis, T.G., Zhu, R.Y., Chen, G., Wu, Q.F., and Yu, J.Q. (2018). EnantioselectiveC(sp^3)-H bond activation by chiral transition metal catalysts. Science 359, 759.

Shamma, M. (2012). TheIsoquinoline Alkaloids Chemistry and Pharmacology (Elsevier).

Shang, M., Chan, J.Z., Cao, M., Chang, Y., Wang, Q., Cook, B., Torker, S., and Wasa, M. (2018). C–H functionalization of amines via alkene-derived nucleophiles through cooperative action of chiral and achiral lewis acid catalysts: applications in enantioselective synthesis. J. Am. Chem. Soc. 140, 10593–10601.

Shao, G., He, Y., Xu, Y., Chen, J., Yu, H., and Cao, R. (2015). Three-component C1 alkynylation of tetrahydroisoquinolines catalyzed by silver acetate. Eur. J. Org. Chem. 2015, 4615–4619.

Shi, L., and Xia, W. (2012). Photoredox functionalization of C–H bonds adjacent to a nitrogen atom. Chem. Soc. Rev. 41, 7687–7697.

Song, C., Dong, X., Yi, H., Chiang, C.-W., and Lei, A. (2018). DDQ-catalyzed direct C(sp^3)–H amination of alkylheteroarenes: synthesis of biheteroarenes under aerobic and metal-free conditions. ACS Catal. 8, 2195–2199.

Sundberg, R.J., Hunt, P.J., Desos, P., and Gadamasetti, K.G. (1991). Oxidative fragmentation of catharanthine by dichlorodicyanoquinone. J. Org. Chem. 56, 1689–1692.

Szatmári, I., Sas, J., and Fülöp, F. (2016). C-3 functionalization of indole derivatives with isoquinolines. Curr. Org. Chem. 20, 2038–2054.

Tang, R.-Y., Xie, Y.-X., Xie, Y.-L., Xiang, J.-N., and Li, J.-H. (2011). TBHP-mediated oxidative thiolation of an sp^3 C–H bond adjacent to a nitrogen atom in an amide. Chem. Commun. 47, 12867–12869.

Thullen, S.M., and Rovis, T. (2017). A mild hydroaminoalkylation of conjugated dienes using a unified cobalt and photoredoxcatalytic system. J. Am. Chem. Soc. 139, 15504–15508.

Tsang, A.S.K., Hashmi, A.S.K., Comba, P., Kerscher, M., Chan, B., and Todd, M.H. (2017). N-aryl groups are ubiquitous in cross-dehydrogenative couplings because they stabilize reactive intermediates. Chem. Eur. J. 23, 9313–9318.

Ueda, H., Yoshida, K., and Tokuyama, H. (2014). Acetic acid promoted metal-free aerobic carbon–carbon bond forming reactions at α-position of tertiary amines. Org. Lett. 16, 4194–4197.

Wan, M., Meng, Z., Lou, H., and Liu, L. (2014). Practical and highly selective C-H functionalization of structurally diverse ethers. Angew. Chem. Int. Ed. 53, 13845–13849.

Wayner, D.D.M., Clark, K.B., Rauk, A., Yu, D., and Armstrong, D.A. (1997). C−H bond dissociation energies of alkyl Amines: radical structures and stabilization energies. J. Am. Chem. Soc. 119, 8925–8932.

Wendlandt, A.E., and Stahl, S.S. (2015). Quinone-catalyzed selective oxidation of organic molecules. Angew. Chem. Int. Ed. 54, 14638–14658.

Xie, Z., Liu, L., Chen, W., Zheng, H., Xu, Q., Yuan, H., and Lou, H. (2014). Practical metal-free C(sp³)-H functionalization: construction of structurally diverse α-substituted N-benzyl and N-allylcarbamates. Angew. Chem. Int. Ed. 53, 3904–3908.

Xue, X.-S., Ji, P., Zhou, B., and Cheng, J.-P. (2017). Theessential role of bond energetics in C-H activation/functionalization. Chem. Rev. 117, 8622–8648.

Yan, C., Liu, Y., and Wang, Q. (2015). Direct C–H allylation of N-Acyl/Sulfonyltetrahydroisoquinolines and analogues. Org. Lett. 17, 5714–5717.

Yan, C., Li, L., Liu, Y., and Wang, Q. (2016). Direct and oxidant-free electron-deficient arylation of N-Acyl-Protected tetrahydroisoquinolines. Org. Lett. 18, 4686–4689.

Yang, J.-D., Ji, P., Xue, X.-S., and Cheng, J.-P. (2018). Recent advances and advisable applications of bond energetics in organic chemistry. J. Am. Chem. Soc. 140, 8611–8623.

Yoo, W.J., and Li, C.J. (2010). Cross-dehydrogenative coupling reactions of sp³-hybridized C-H bonds. In C-H Activation, J.Q. Yu and Z. Shi, eds. (Springer-Verlag Berlin), pp. 281–302.

Yoshida, J.-i., and Suga, S. (2002). Basic concepts of "cationpool" and "cationflow" methods and their applications in conventional and combinatorial organic synthesis. Chem. Eur. J. 8, 2650–2658.

Zhang, Y., and Li, C.-J. (2006). DDQ-mediated direct cross-dehydrogenative-coupling (CDC) between benzyl ethers and simple ketones. J. Am. Chem. Soc. 128, 4242–4243.

Zhang, G., Ma, Y., Wang, S., Zhang, Y., and Wang, R. (2012). Enantioselective metal/organo-catalyzed aerobic oxidative sp3C–H olefination of tertiary amines using molecular oxygen as the sole oxidant. J. Am. Chem. Soc. 134, 12334–12337.

Zhang, Z., Gu, K., Bao, Z., Xing, H., Yang, Q., and Ren, Q. (2017). Mechanistic studies of thiourea-catalyzed cross-dehydrogenative C-P and C-C coupling reactions and their further applications. Tetrahedron 73, 3118–3124.

Zhang, J., Liu, D., Liu, S., Ge, Y., Lan, Y., and Chen, Y. (2019). Visible-light-induced alkoxyl radicals enable α-C(sp³)-H bond allylation. iScience 23, 100755.

Zhu, X.-Q., Wang, C.-H., Liang, H., and Cheng, J.-P. (2007). Theoretical prediction of the hydride affinities of various p- and o-quinones in DMSO. J. Org. Chem. 72, 945–956.

Zhu, X.-Q., Dai, Z., Yu, A., Wu, S., and Cheng, J.-P. (2008a). Driving forces for the mutual conversions between phenothiazines and their various reaction intermediates in acetonitrile. J. Phys. Chem. B 112, 11694–11707.

Zhu, X.-Q., Liang, H., Zhu, Y., and Cheng, J.-P. (2008b). Hydride affinities of cumulated, isolated, and conjugated dienes in acetonitrile. J. Org. Chem. 73, 8403–8410.

Zhu, X.-Q., and Wang, C.-H. (2010). Accurate estimation of the one-electron reduction potentials of various substituted quinones in DMSO and CH₃CN. J. Org. Chem. 75, 5037–5047.

Zhu, X.-Q., Tan, Y., and Cao, C.-T. (2010). Thermodynamic diagnosis of the properties and mechanism of dihydropyridine-type compounds as hydride source in acetonitrile with "molecule ID card". J. Phys. Chem. B 114, 2058–2075.

Zhu, X.-Q., Chen, X., and Mei, L.-R. (2011). Determination of hydride affinities of various aldehydes and ketones in acetonitrile. Org. Lett. 13, 2456–2459.

Zipse, H. (2006). Radical stability—a theoretical perspective. In Radicals in Synthesis I, A. Gansäuer, ed. (Springer Berlin Heidelberg), pp. 163–189.

Supplemental Information

Toward Rational Understandings

of α-C–H Functionalization: Energetic Studies

of Representative Tertiary Amines

Wenzhi Luo, Jin-Dong Yang, and Jin-Pei Cheng

Supplemental Information

Supplemental tables, schemes, figures and experimental graghs

Table S1. Thermodynamic parameters of hydride acceptors (V or kcal mol^{-1})[a], related to Figure 1, Figure 2, Table 2 and Scheme 5.

A^+	$E_{red}(A^+)$	$H_{H-A}(A^+)$	$H_{HA}(A^+)$	$H_{HA}(A^\cdot)$
DDQ	0.137 (Huynh et al., 2016)	-104 (Zhu et al., 2007)	-60	-73.5
T^+	-0.56	-85.0	-35.4	-71.6
AcNH-TEMPO$^+$	0.32 (Zhu et al., 2007)	-105.6 (Zhu et al., 2007)	-62.4	-73.5
TP$^+$	-0.17	-104.3	-43.4	-83.5
PhXn$^+$	-0.39 (Grüning et al., 2001)	-96.8 (Grüning et al., 2001)	-43.2	-79.9

[a] Obtained from the PhD dissertation of Nankai University in 2010 and 2011, unless otherwise indicated. DDQ: 4,5-Dichloro-3,6-dioxo-1,4-cyclohexadiene-1,2-carbonitrile; T$^+$: tropylium; AcNH-TEMPO$^+$: 4-acetamido-2,2,6,6-tetramethyl-1-oxopiperidin-1-ium; TP$^+$: trityl cation; PhXn$^+$: 9-phenyl-9H-xanthen-9-ylium.

Table S2. Thermodynamic parameters of related species used in mechanistic diagnosis, related to Scheme 6.

Energetics	Cu^{2+}/Cu$^+$	Cu$^+$/Cu^0		
E_{redox}/V *vs* Fc	0.13 (Della Pergola et al., 2010)	-1.1 (Della Pergola et al., 2010)		
	HO$_2^\bullet$	*t*-BuOH	*t*-BuOOH	H$_2$
BDE/kcal mol^{-1}	49.1 (Cheng, 2016)	106.3 (Cheng, 2016)	84.2 (Cheng, 2016)	104.1 (Cheng, 2016)
	HCl			
pK_a/in acetonitrile	10.3 (Cheng, 2016)			
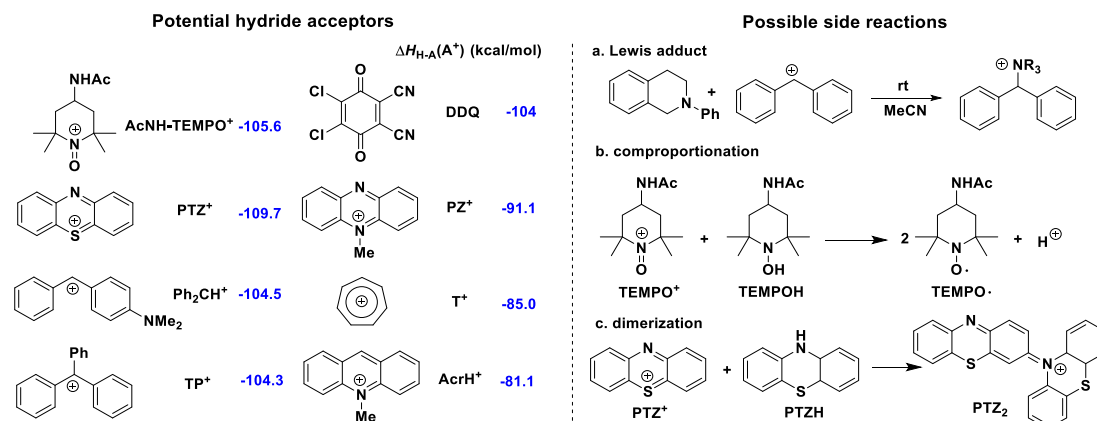
Scheme S1. Potential hydride acceptors and their hydride affinity; side reaction probably existing in the reactions of related hydride acceptors (Grüning et al., 2001; Hanson et al., 1973; Semmelhack et al., 1984), related to Scheme 4 and Table 1.
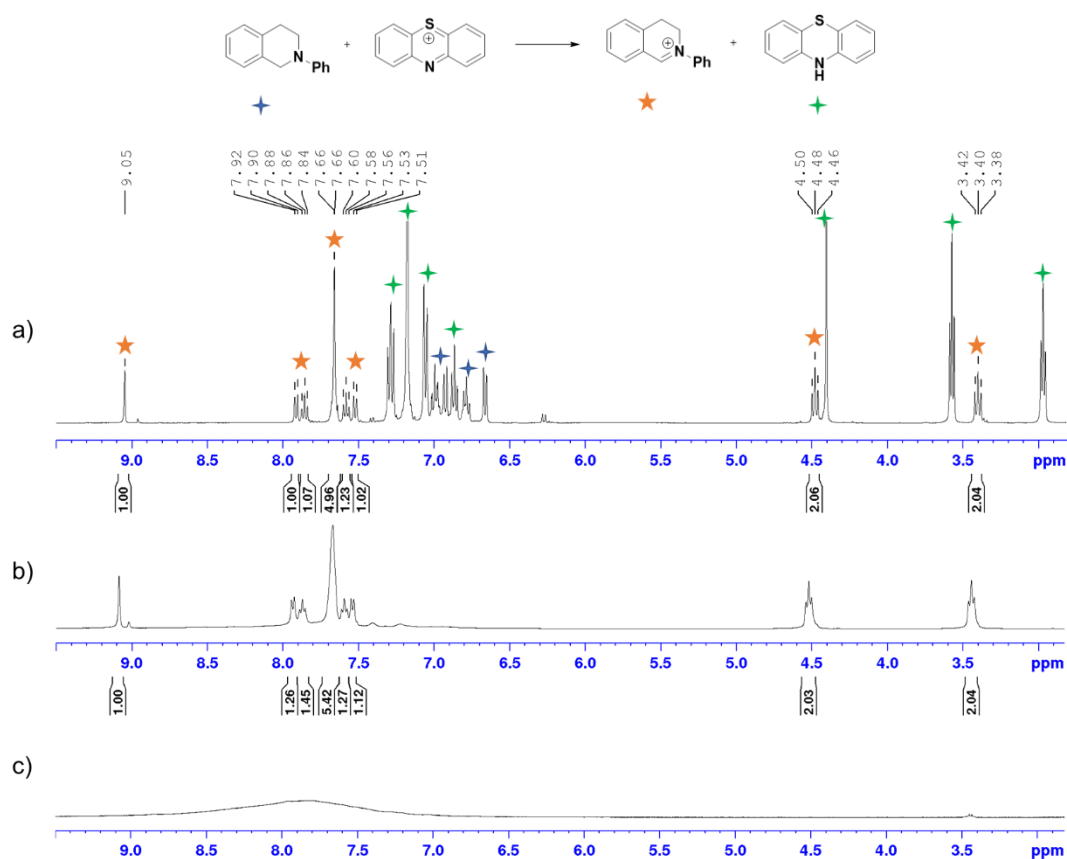
Fig. S1. The dimerization of PTZH with residual PTZ⁺. NMR spectra of **a)** N-Ph-THIQ (2 eq.) and PTZ⁺ (1 eq.); **b)** N-Ph-THIQ (1 eq.) and PTZ⁺ (2 eq.); **c)** PTZH (1 eq.) and PTZ⁺ (1 eq.), related to Table 1.
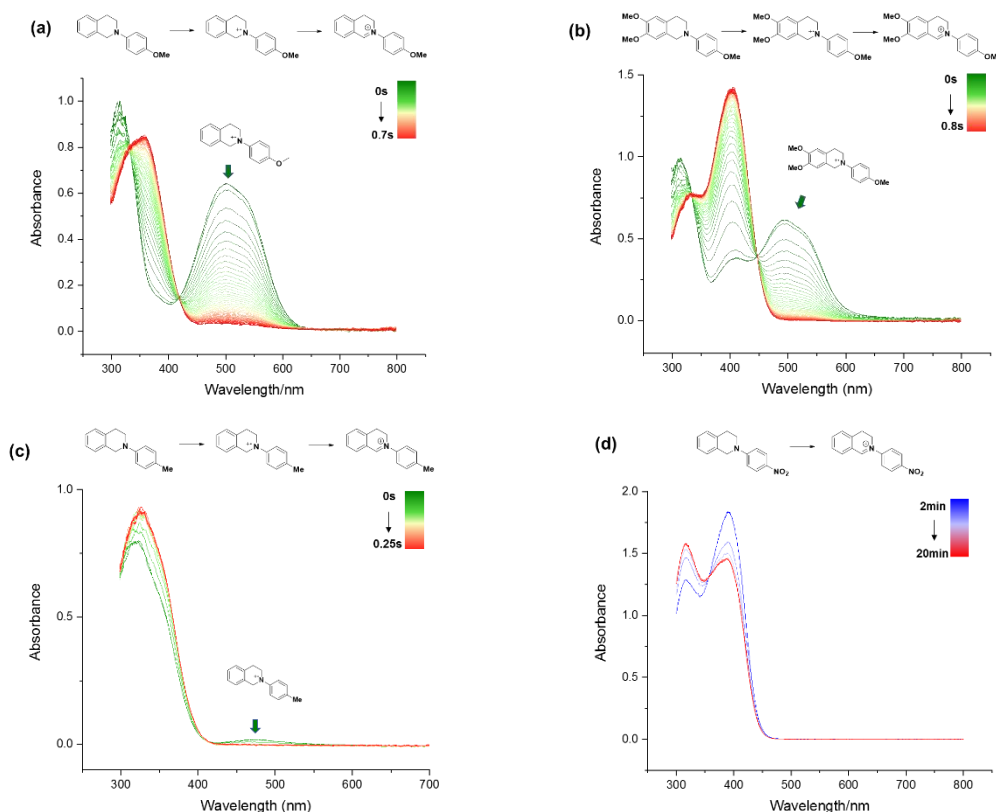
Fig. S2. Intermediate detection by UV/Vis spectra in acetonitrile at 298 K for the reaction of a) 0.30 mM **6g** was mixed with 0.25 mM AcNH-TEMPO$^+$, corresponding THIQ radical cation was intermediately generated with characteristic UV-Vis absorption at 502 nm and then degenerated rapidly within 0.7s; b) 0.30 mM **10c** was mixed with 0.25 mM AcNH-TEMPO$^+$, corresponding THIQ radical cation was intermediately generated with characteristic UV-Vis absorption at 490 nm and then degenerated rapidly within 0.8 s; c) 0.5 mM **6f** was mixed with 0.25 mM AcNH-TEMPO$^+$, corresponding THIQ radical cation was intermediately generated with characteristic UV-Vis absorption at 480 nm and then degenerated rapidly within 0.25 s; d) 1.50 mM **6a** was mixed with 1.49 mM AcNH-TEMPO$^+$ and no intermediate was detected in 20 min, related to Table 2.
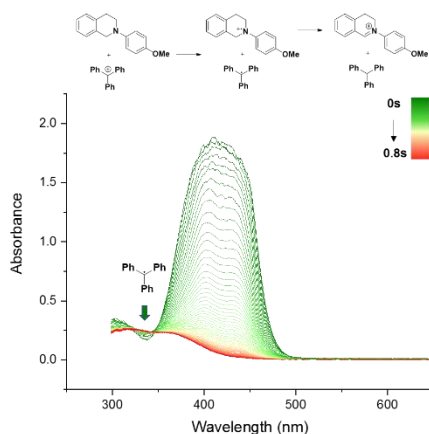
Fig. S3. UV/Vis spectra in acetonitrile for the reaction of 0.2 mM **7g** and 0.4 mM Ph$_3$C$^+$ in 0.8 s, the formation of steady-state Ph$_3$C$^\bullet$ was generated with characteristic UV-Vis absorption at 335 nm, related to Table 2. (Braïda et al., 1998)

Representative NMR spectra of hydride transfer reaction

Data S1. NMR spectra of Substrate 6g and hydride acceptor AcNH-TEMPO$^+$ClO$_4^-$, related to Table 1.
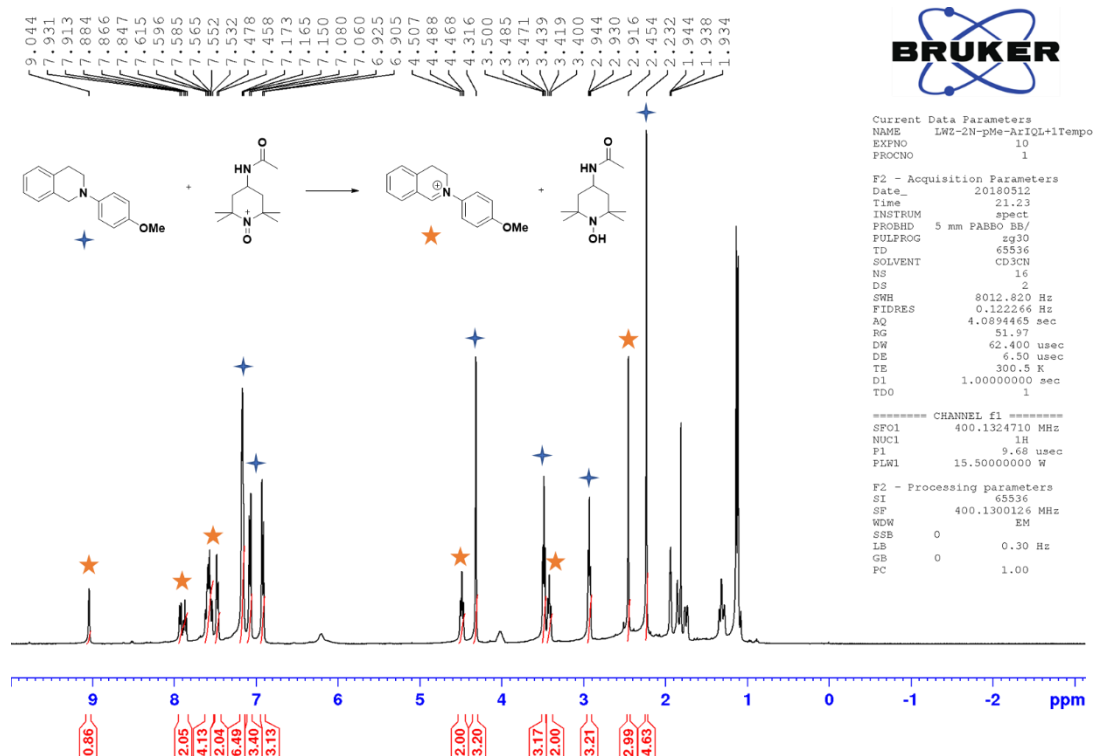
Data S2. NMR spectra of Substrate 6b and hydride acceptor AcNH-TEMPO$^+$ClO$_4^-$, related to Table 1.
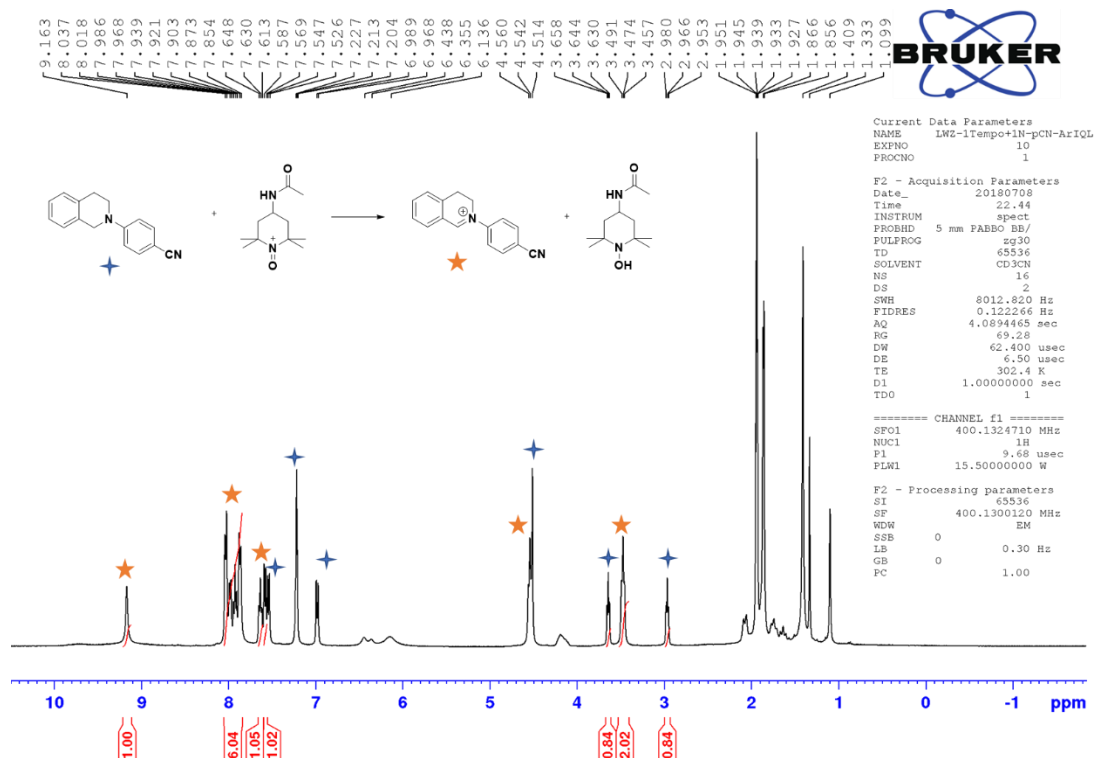
Data S3. NMR spectra of Substrate 7g and hydride acceptor Ph₃C⁺ClO₄⁻, related to Table 1.
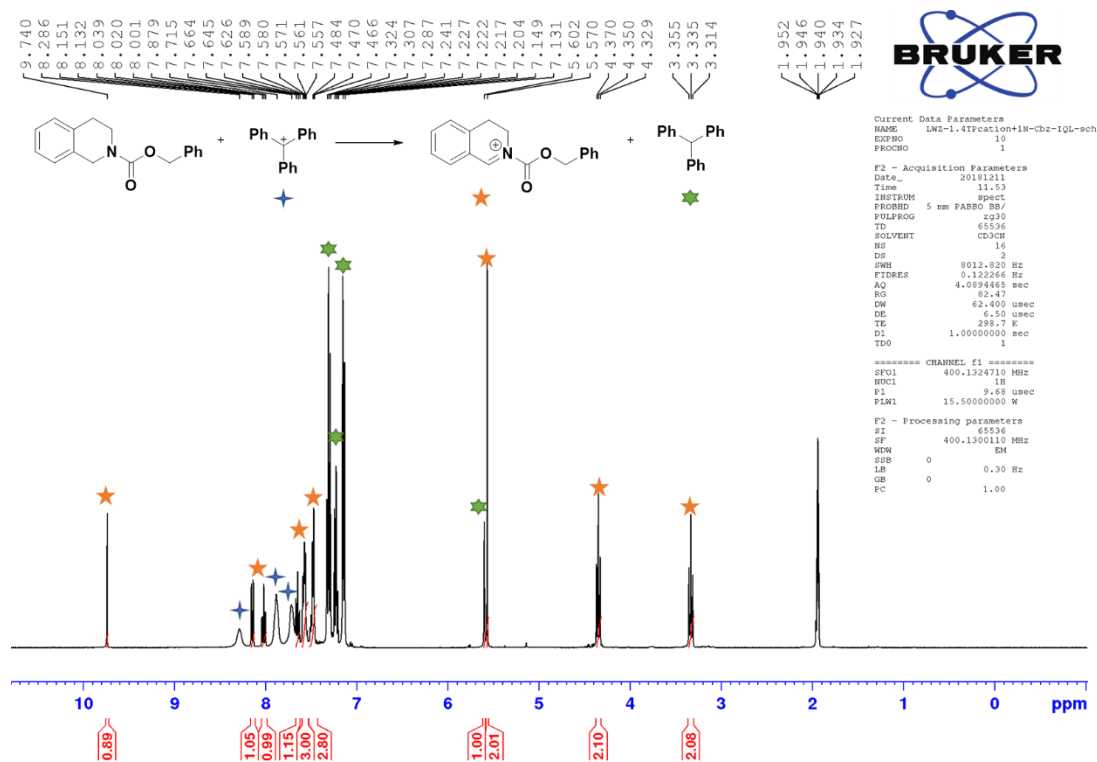
Data S4. NMR spectra of Substrate 6a and hydride acceptor Ph₃C⁺ClO₄⁻, related to Table 1.
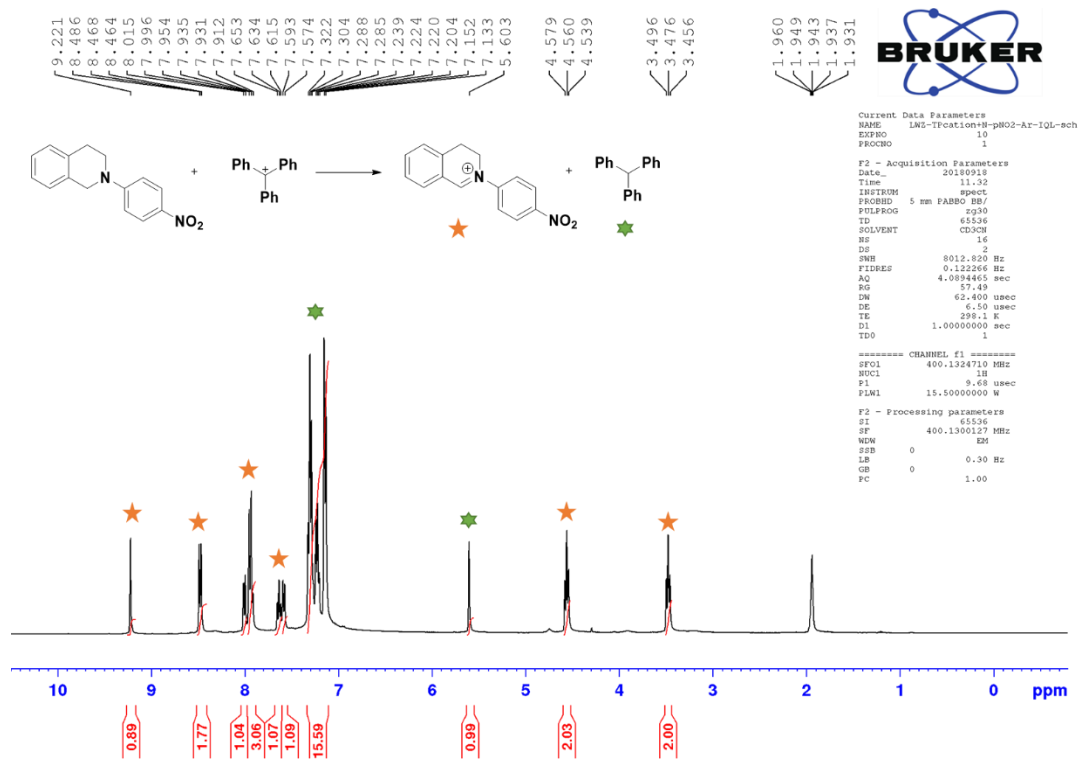
ΔH_{rxn}-titration graphs

Data S5. Titration graph of hydride transfer reaction between Substrate 1 and hydride acceptor AcNH-TEMPO$^+$ClO$_4^-$, related to Table 1.
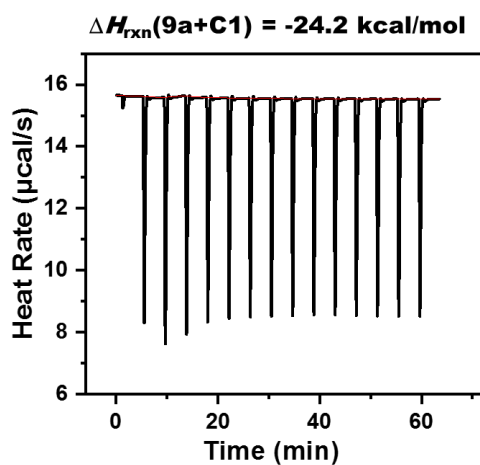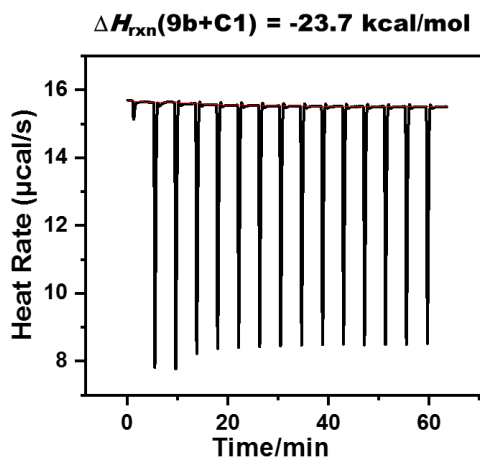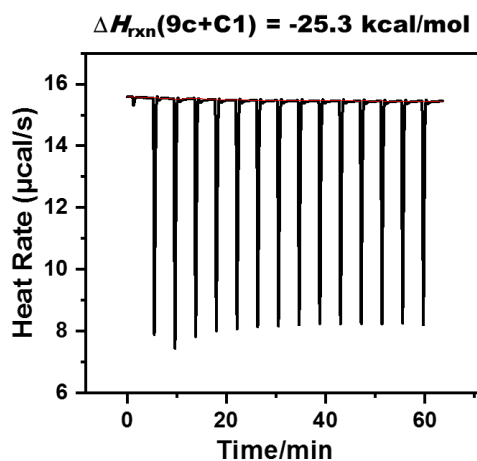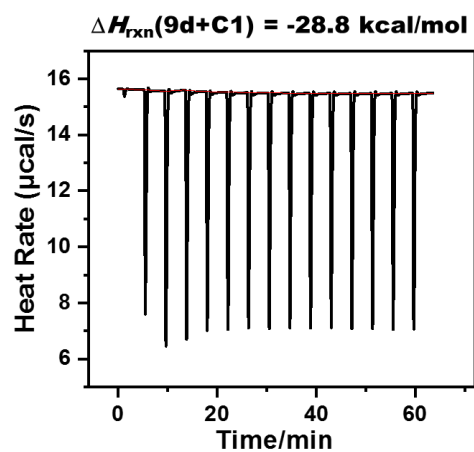
$$\Delta H_{rxn}(1+C1) = -33.4 \text{ kcal/mol}$$
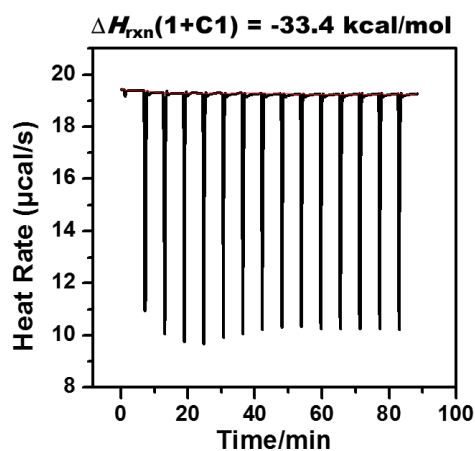
Data S6. Titration graph of hydride transfer reaction between Substrate 2a$^+$ and hydride donor 3-methylpyridine, related to Table 1.

$$\Delta H_{rxn}(2a^+ + H) = -33.4 \text{ kcal/mol}$$
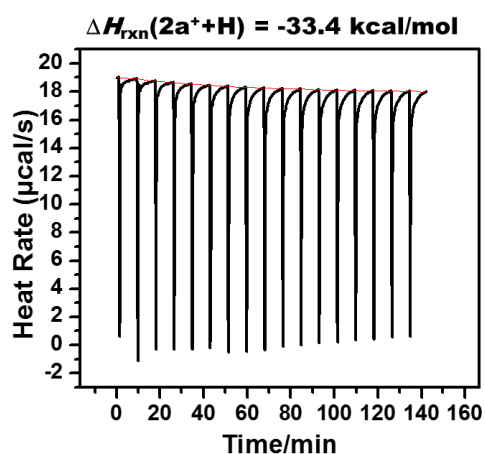
Data S7. Titration graph of hydride transfer reaction between between Substrate 2a$^+$ and hydride donor 3-methylpyridine, related to Table 1.

$$\Delta H_{rxn}(2b^+ + H) = -29.0 \text{ kcal/mol}$$
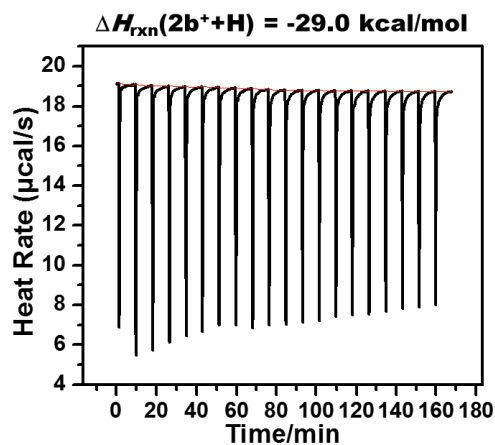
Data S8. Titration graph of hydride transfer reaction between Substrate 2c$^+$ and hydride donor 3-methylpyridine, related to Table 1.

$$\Delta H_{rxn}(2c^+ + H) = -27.7 \text{ kcal/mol}$$
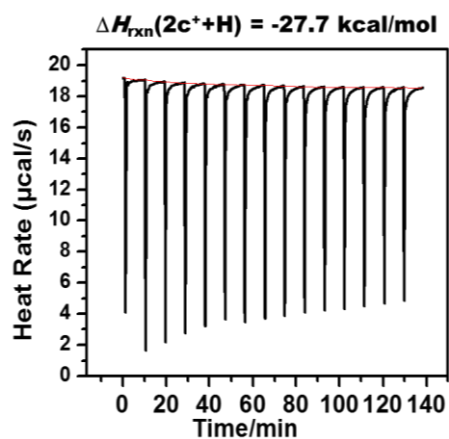
Data S9. Titration graph of hydride transfer reaction between Substrate 2d$^+$ and hydride donor 3-methylpyridine, related to Table 1.

$$\Delta H_{rxn}(2d^+ + H) = -26.3 \text{ kcal/mol}$$
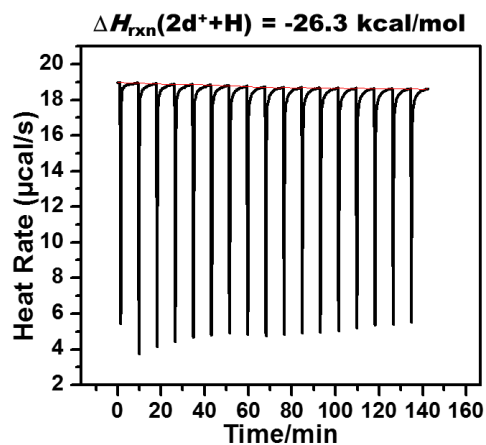
Data S10. Titration graph of hydride transfer reaction between Substrate 2e$^+$ and hydride donor 3-methylpyridine, related to Table 1.

$$\Delta H_{rxn}(2e^+ + H) = -25.9 \text{ kcal/mol}$$
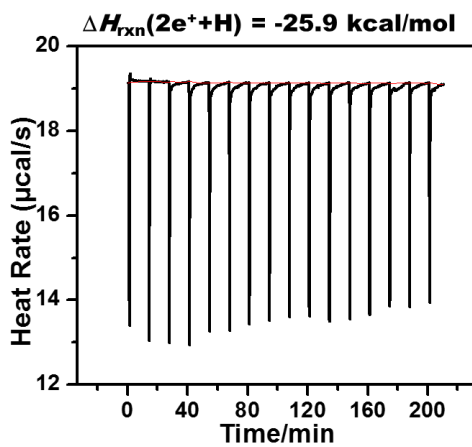
Data S11. Titration graph of hydride transfer reaction between Substrate 2g$^+$ and hydride donor 3-methylpyridine, related to Table 1.

$\Delta H_{rxn}(2g^+ + H) = -15.1$ kcal/mol
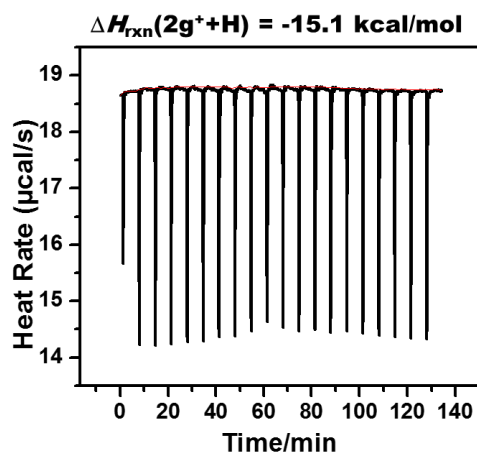
Data S12. Titration graph of hydride transfer reaction between Substrate 2i$^+$ and hydride donor 3-methylpyridine, related to Table 1.

$\Delta H_{rxn}(2i^+ + H) = -14.9$ kcal/mol
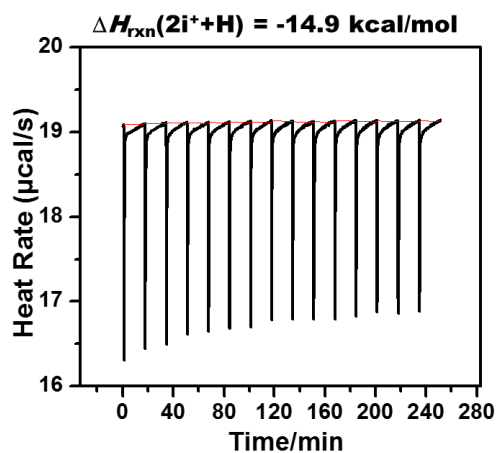
Data S13. Titration graph of hydride transfer reaction between Substrate 3a$^+$ and hydride donor 3-methylpyridine, related to Table 1.

$\Delta H_{rxn}(3a^+ + H) = -28.2$ kcal/mol
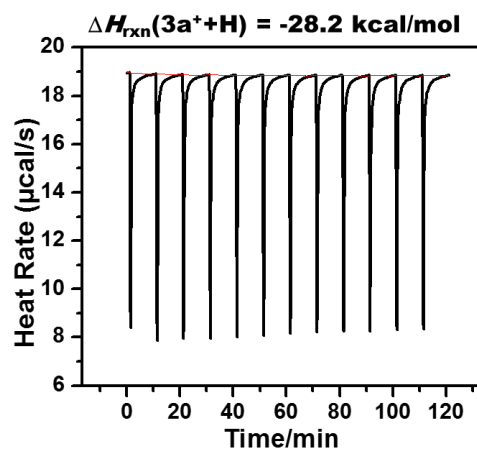
Data S14. Titration graph of hydride transfer reaction between Substrate 3b+ and hydride donor 3-methylpyridine, related to Table 1.

$\Delta H_{rxn}(3b^+ + H) = -27.2$ kcal/mol
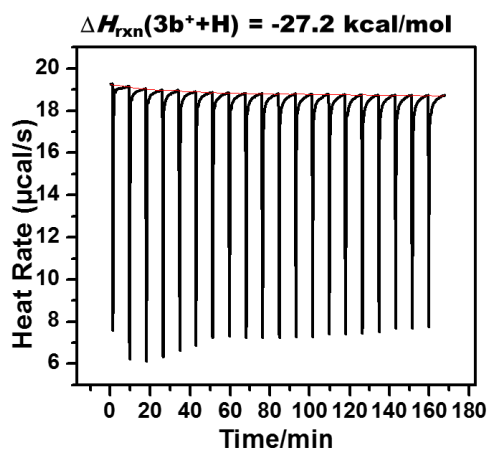
Data S15. Titration graph of hydride transfer reaction between Substrate 4+ and hydride donor 3-methylpyridine, related to Table 1.

$\Delta H_{rxn}(4^+ + H) = -21.8$ kcal/mol
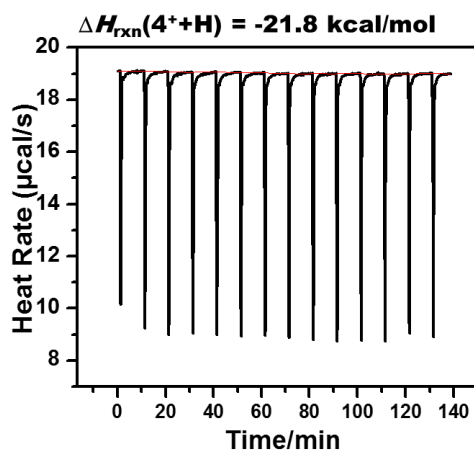
Data S16. Titration graph of hydride transfer reaction between Substrate 5+ and hydride donor 3-methylpyridine, related to Table 1.

$\Delta H_{rxn}(5^+ + H) = -13.9$ kcal/mol
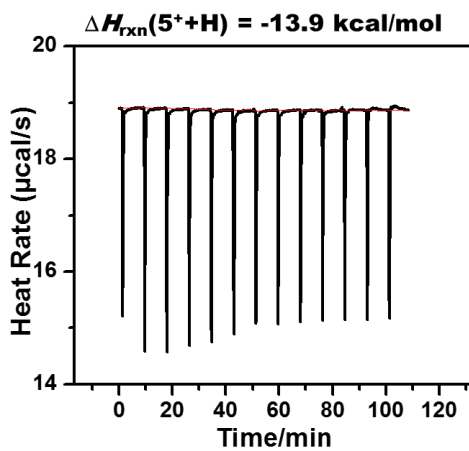
Data S17. Titration graph of hydride transfer reaction between Substrate 6a and hydride acceptor $Ph_3C^+ClO_4^-$, related to Table 1.

$\Delta H_{rxn}(6a+C2) = -22.2$ kcal/mol
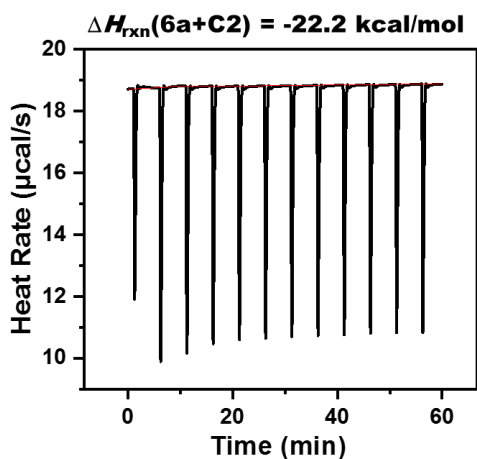
Data S18. Titration graph of hydride transfer reaction between Substrate 6b and hydride acceptor $AcNH\text{-}TEMPO^+ClO_4^-$, related to Table 1.
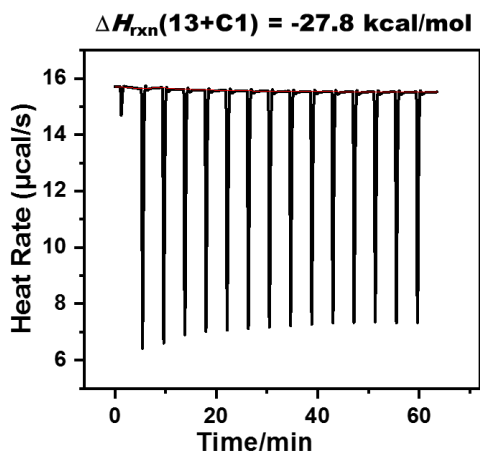

$\Delta H_{rxn}(6b+C1) = -24.9$ kcal/mol
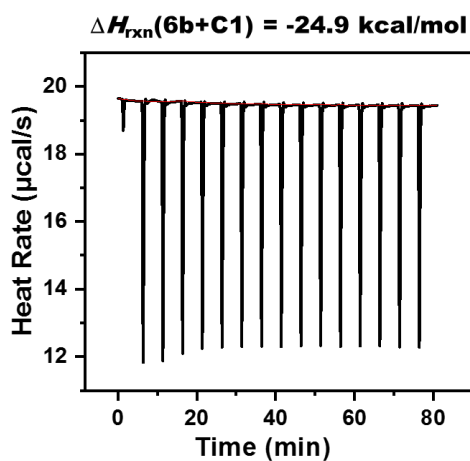
Data S19. Titration graph of hydride transfer reaction between Substrate 6c and hydride acceptor $AcNH\text{-}TEMPO^+ClO_4^-$, related to Table 1.

$\Delta H_{rxn}(6c+C1) = -26.0$ kcal/mol
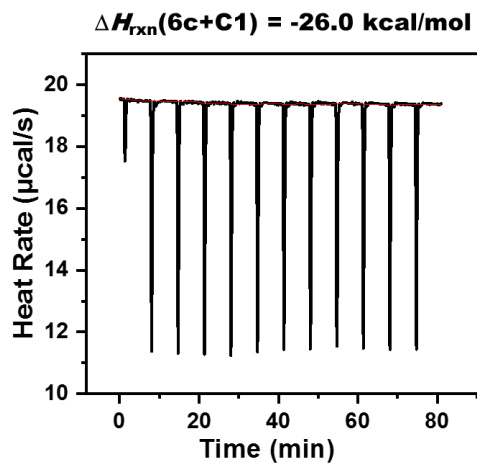
Data S20. Titration graph of hydride transfer reaction between Substrate 6d and hydride acceptor AcNH-TEMPO$^+$ClO$_4^-$, related to Table 1.


ΔH_{rxn}(6d+C1) = -26.7 kcal/mol
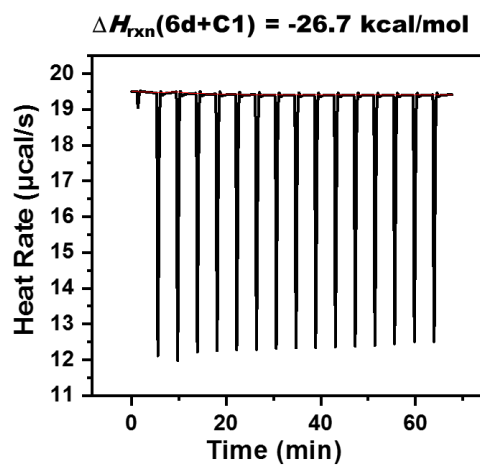
Data S21. Titration graph of hydride transfer reaction between Substrate 6e and hydride acceptor AcNH-TEMPO$^+$ClO$_4^-$, related to Table 1.

ΔH_{rxn}(6e+C1) = -27.7 kcal/mol
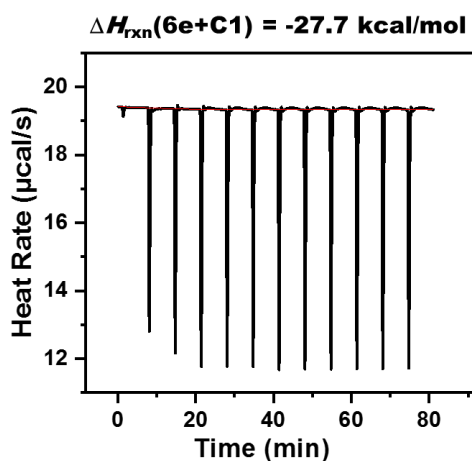
Data S22. Titration graph of hydride transfer reaction between Substrate 6f and hydride acceptor AcNH-TEMPO$^+$ClO$_4^-$, related to Table 1.

ΔH_{rxn}(6f+C1) = -28.4 kcal/mol
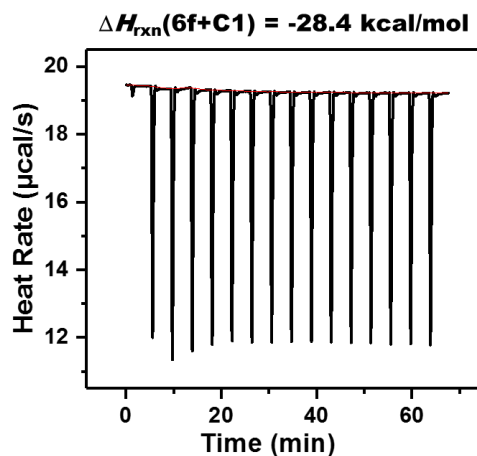
Data S23. Titration graph of hydride transfer reaction between Substrate 6g and hydride acceptor AcNH-TEMPO$^+$ClO$_4^-$, related to Table 1.

ΔH_{rxn}(6g+C1) = -30.2 kcal/mol
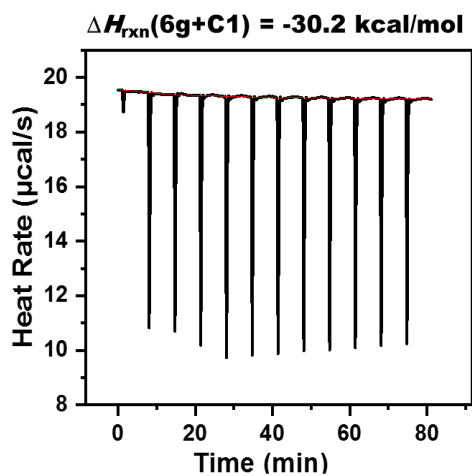
Data S24. Titration graph of hydride transfer reaction between Substrate 6h and hydride acceptor AcNH-TEMPO$^+$ClO$_4^-$, related to Table 1.

ΔH_{rxn}(6h+C1) = -28.1 kcal/mol
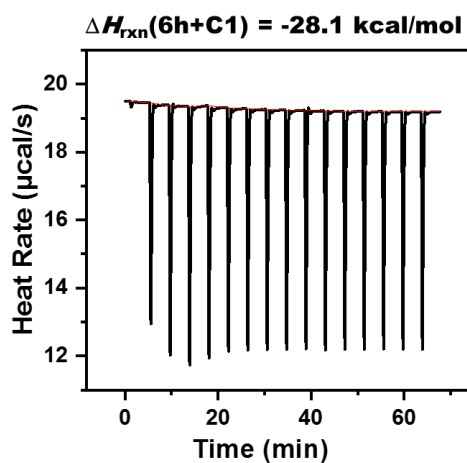
Data S25. Titration graph of hydride transfer reaction between Substrate 6i and hydride acceptor AcNH-TEMPO$^+$ClO$_4^-$, related to Table 1.

ΔH_{rxn}(6i+C1) = -26.6 kcal/mol
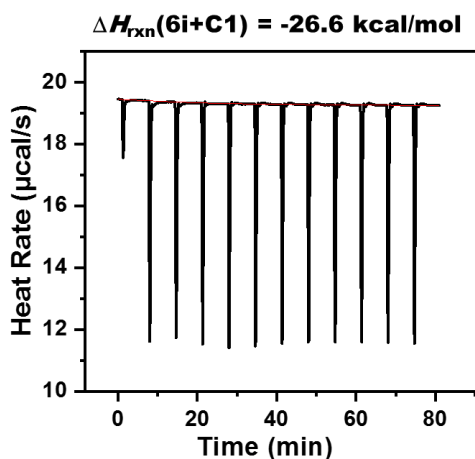
Data S26. Titration graph of hydride transfer reaction between Substrate 7a and hydride acceptor AcNH-TEMPO⁺ClO₄⁻, related to Table 1.

$\Delta H_{rxn}(7a+C1)$ = -32.9 kcal/mol
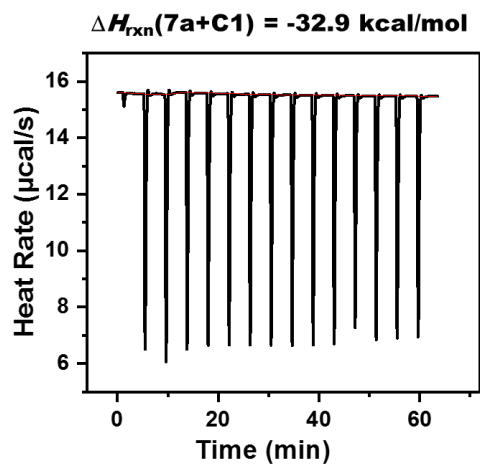
Data S27. Titration graph of hydride transfer reaction between Substrate 7c and hydride acceptor AcNH-TEMPO⁺ClO₄⁻, related to Table 1.

$\Delta H_{rxn}(7c+C1)$ = -26.3 kcal/mol
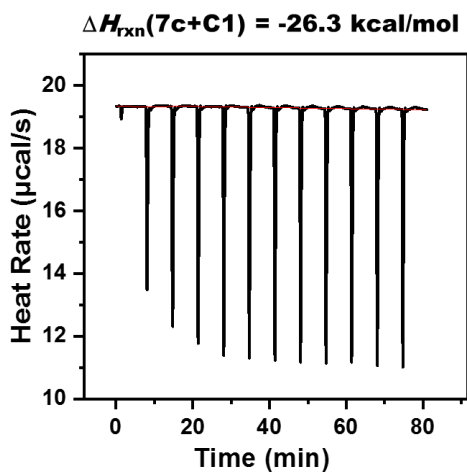
Data S28. Titration graph of hydride transfer reaction between Substrate 7d and hydride acceptor AcNH-TEMPO⁺ClO₄⁻, related to Table 1.

$\Delta H_{rxn}(7d+C1)$ = -32.5 kcal/mol
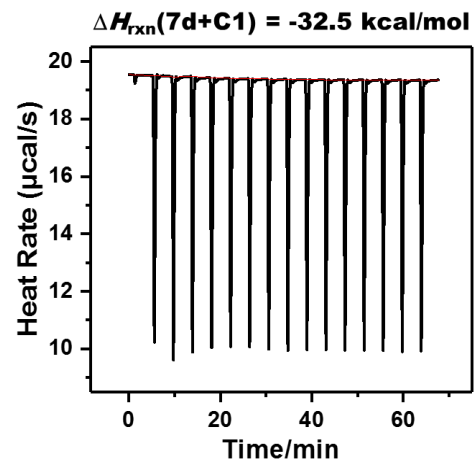
Data S29. Titration graph of hydride transfer reaction between Substrate 7e and hydride acceptor AcNH-TEMPO$^+$ClO$_4^-$, related to Table 1.

ΔH_{rxn}(7e+C1) = -30.5 kcal/mol
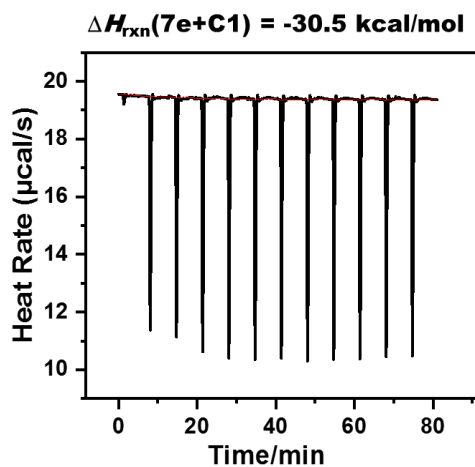
Data S30. Titration graph of hydride transfer reaction between Substrate 7f and hydride acceptor AcNH-TEMPO$^+$ClO$_4^-$, related to Table 1.

ΔH_{rxn}(7f+C1) = -29.1 kcal/mol
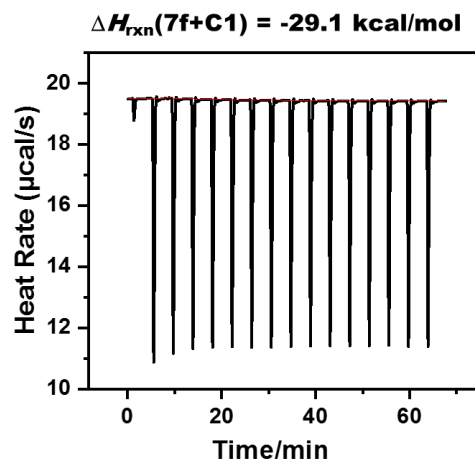
Data S31. Titration graph of hydride transfer reaction between Substrate 7g and hydride acceptor AcNH-TEMPO$^+$ClO$_4^-$, related to Table 1.

ΔH_{rxn}(7g+C2) = -15.0 kcal/mol
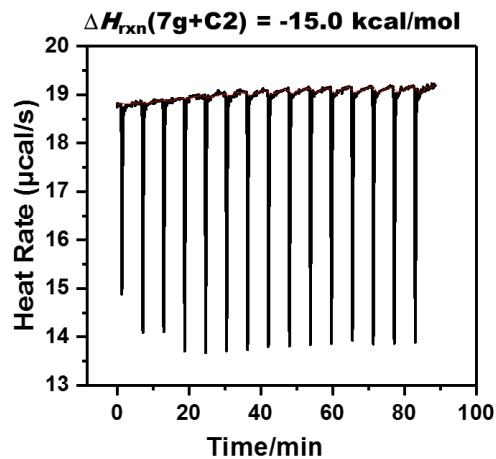
Data S32. Titration graph of hydride transfer reaction between Substrate 7h and hydride acceptor AcNH-TEMPO$^+$ClO$_4^-$, related to Table 1.

ΔH_{rxn}(7h+C1) = -23.5 kcal/mol
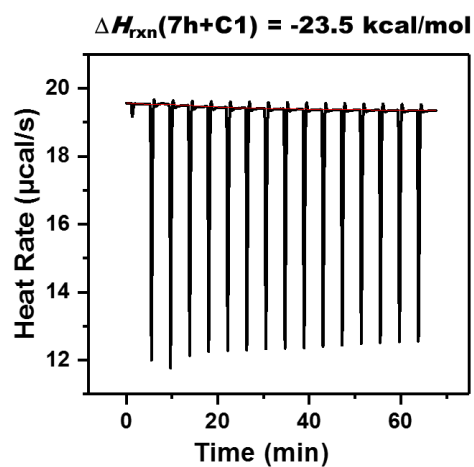
Data S33. Titration graph of hydride transfer reaction between Substrate 7i and hydride acceptor AcNH-TEMPO$^+$ClO$_4^-$, related to Table 1.

ΔH_{rxn}(7i+C1) = -29.5 kcal/mol
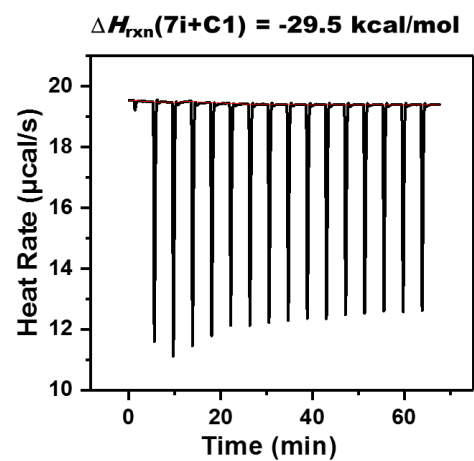
Data S34. Titration graph of hydride transfer reaction between Substrate 8a and hydride acceptor AcNH-TEMPO$^+$ClO$_4^-$, related to Table 1.

ΔH_{rxn}(8a+C1) = -29.9 kcal/mol
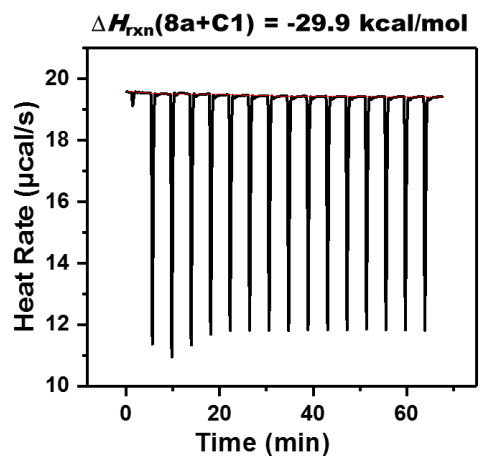
Data S35. Titration graph of hydride transfer reaction between Substrate 8b and hydride acceptor AcNH-TEMPO$^+$ClO$_4^-$, related to Table 1.

$\Delta H_{rxn}(\text{8b+C1}) = -31.4$ kcal/mol
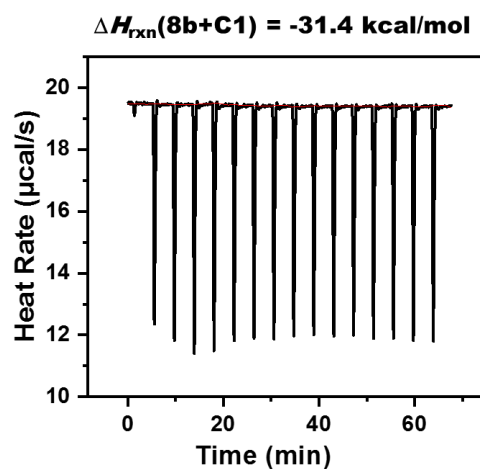
Data S36. Titration graph of hydride transfer reaction between Substrate 9a and hydride acceptor AcNH-TEMPO$^+$ClO$_4^-$, related to Table 1.

$\Delta H_{rxn}(\text{9a+C1}) = -24.2$ kcal/mol

Data S37. Titration graph of hydride transfer reaction between Substrate 9b and hydride acceptor AcNH-TEMPO$^+$ClO$_4^-$, related to Table 1.

$\Delta H_{rxn}(\text{9b+C1}) = -23.7$ kcal/mol

Data S38. Titration graph of hydride transfer reaction between Substrate 9c and hydride acceptor AcNH-TEMPO$^+$ClO$_4^-$, related to Table 1.

ΔH_{rxn}(9c+C1) = -25.3 kcal/mol

Data S39. Titration graph of hydride transfer reaction between Substrate 9d and hydride acceptor AcNH-TEMPO$^+$ClO$_4^-$, related to Table 1.

ΔH_{rxn}(9d+C1) = -28.8 kcal/mol

Data S40. Titration graph of hydride transfer reaction between Substrate 10a and hydride acceptor AcNH-TEMPO$^+$ClO$_4^-$, related to Table 1.

ΔH_{rxn}(10a+C1) = -28.1 kcal/mol
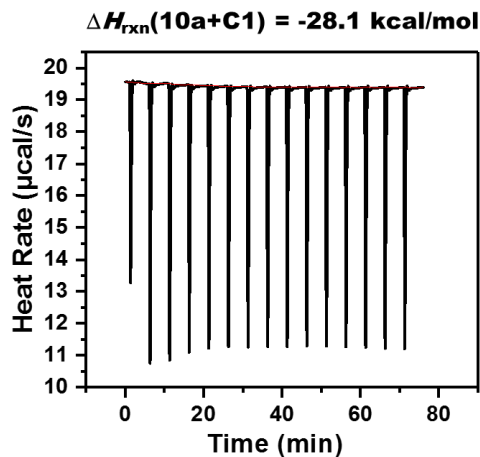
Data S41. Titration graph of hydride transfer reaction between Substrate 10b and hydride acceptor AcNH-TEMPO$^+$ClO$_4^-$, related to Table 1.

$\Delta H_{rxn}(\text{10b+C1}) = -29.9 \text{ kcal/mol}$
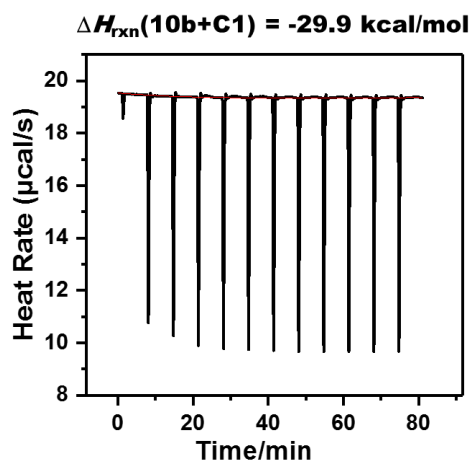
Data S42. Titration graph of hydride transfer reaction between Substrate 1c and hydride acceptor AcNH-TEMPO$^+$ClO$_4^-$, related to Table 1.

$\Delta H_{rxn}(\text{10c+C1}) = -33.6 \text{ kcal/mol}$
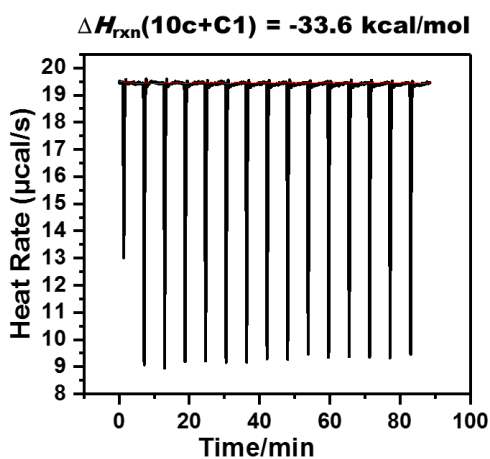
Data S43. Titration graph of hydride transfer reaction between Substrate 11 and hydride acceptor Ph$_3$C$^+$ClO$_4^-$, related to Table 1.

$\Delta H_{rxn}(\text{11+C2}) = -24.4 \text{ kcal/mol}$
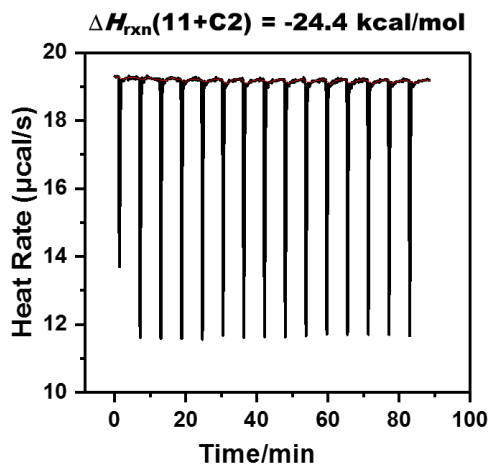
Data S44. Titration graph of hydride transfer reaction between Substrate 12 and hydride acceptor AcNH-TEMPO$^+$ClO$_4^-$, related to Table 1.

ΔH_{rxn}(12+C1) = -34.5 kcal/mol
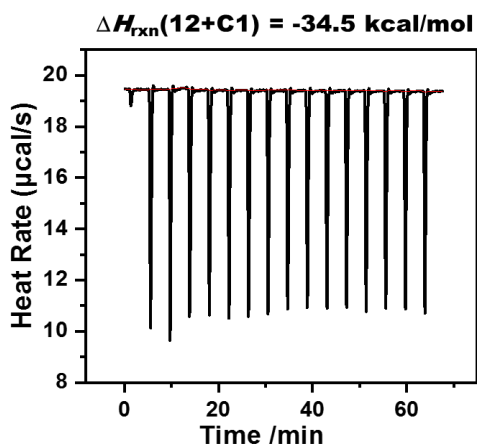
Data S45. Titration graph of hydride transfer reaction between Substrate 13 and hydride acceptor AcNH-TEMPO$^+$ClO$_4^-$, related to Table 1.

ΔH_{rxn}(13+C1) = -27.8 kcal/mol

Data S46. Titration graph of hydride transfer reaction between Substrate 14 and hydride acceptor AcNH-TEMPO$^+$ClO$_4^-$, related to Table 1.

ΔH_{rxn}(14+C1) = -39.0 kcal/mol
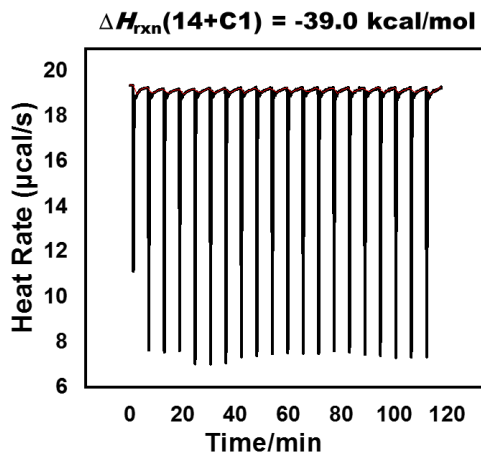
E_{ox}(HD) and E_{red}(D$^+$)-CV graphs of representative tertiary amines and iminium cations

Data S47. CV graph: Oxidation potential E_{ox}(HD) of substrate 2a, related to Table 1.

E_{ox}(2a) = 0.65 V
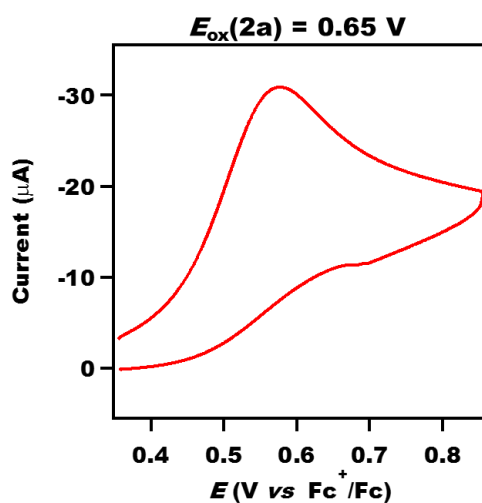
Data S48. CV graph: Oxidation potential E_{ox}(HD) of substrate 2b, related to Table 1.

E_{ox}(2b) = 0.58 V
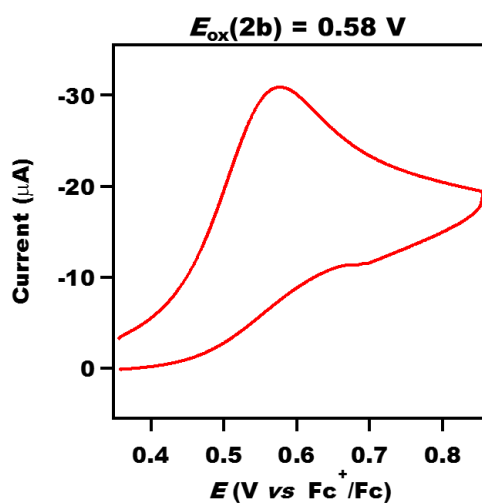
Data S49. CV graph: Oxidation potential E_{ox}(HD) of substrate 2d, related to Table 1.

E_{ox}(2d) = 0.57 V
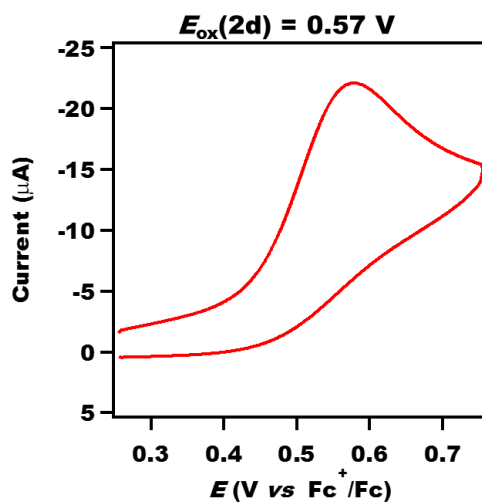
Data S50. CV graph: Oxidation potential E_{ox}(HD) of substrate 2f, related to Table 1.

E_{ox}(2f) = 0.53 V
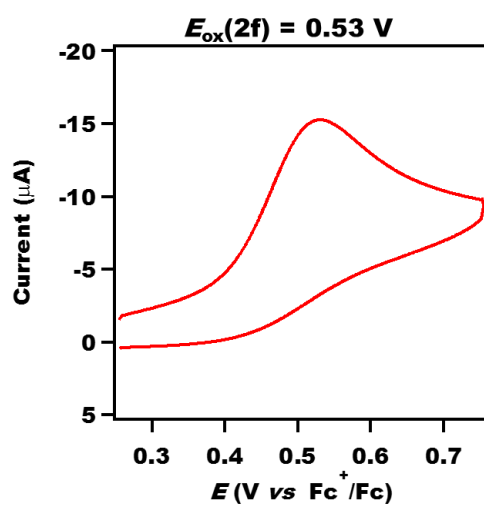
Data S51. CV graph: Oxidation potential E_{ox}(HD) of substrate 2g, related to Table 1.

E_{ox}(2g) = 0.52 V
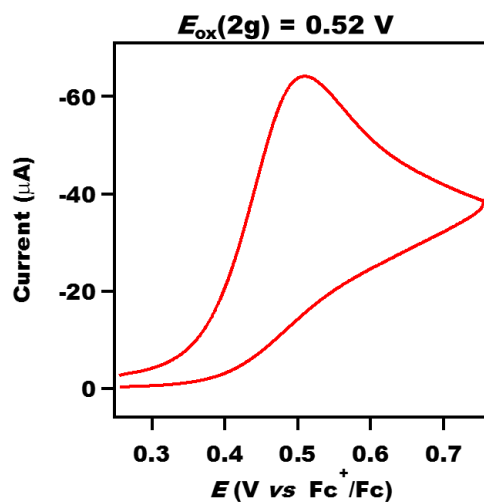
Data S52. CV graph: Oxidation potential E_{ox}(HD) of substrate 2i, related to Table 1.

E_{ox}(2i) = 0.54 V
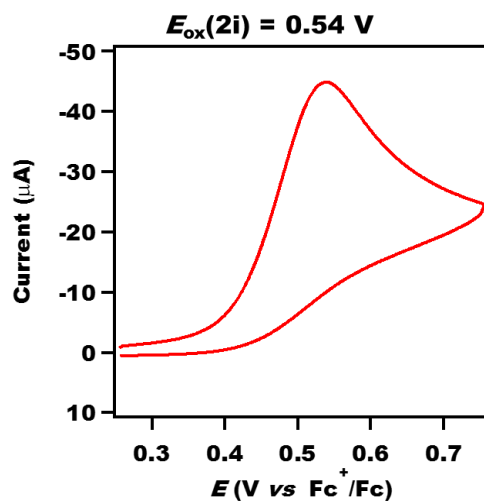
Data S53. CV graph: Oxidation potential E_{ox}(HD) of substrate 3a, related to Table 1.

E_{ox}(3a) = 0.54 V
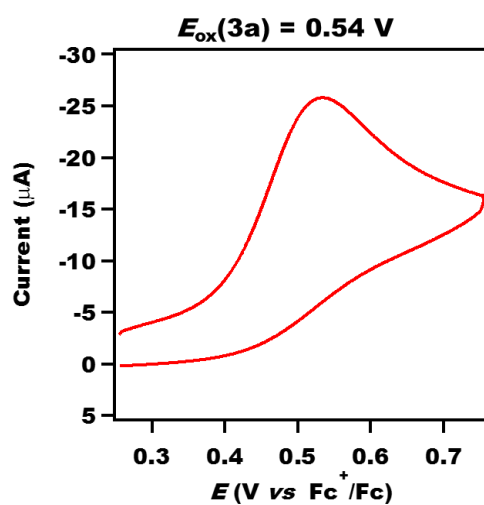
Data S54. CV graph: Oxidation potential E_{ox}(HD) of substrate 3b, related to Table 1.

E_{ox}(3b) = 0.53 V
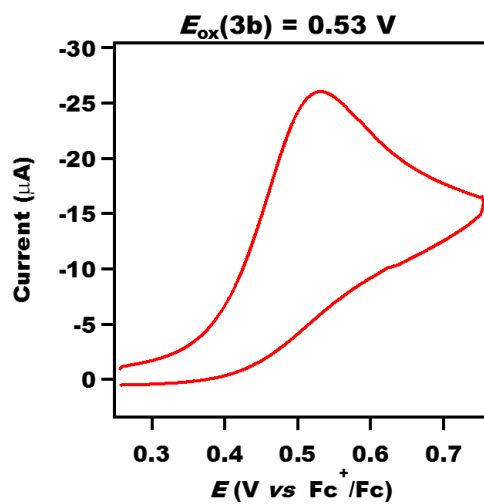
Data S55. CV graph: Oxidation potential E_{ox}(HD) of substrate 4, related to Table 1.

E_{ox}(4) = 0.51 V
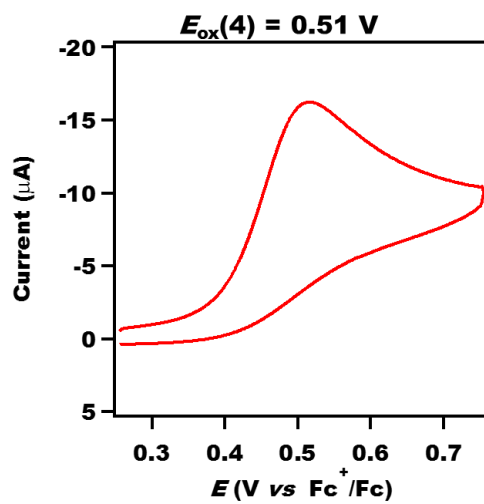
Data S56. CV graph: Oxidation potential E_{ox}(HD) of substrate 5, related to Table 1.

E_{ox}(5) = 0.74 V
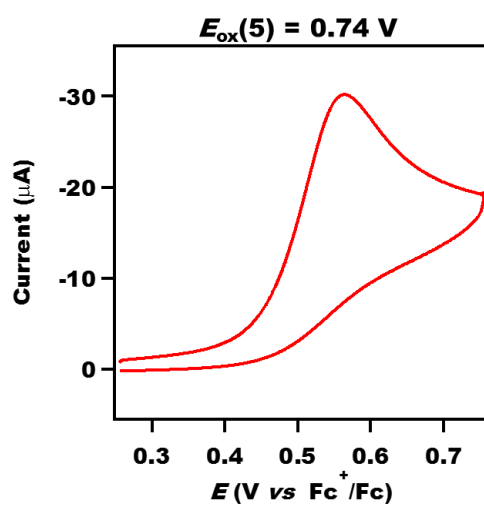
Data S57. CV graph: Oxidation potential E_{ox}(HD) of substrate 6b, related to Table 1.

E_{ox}(6b) = 0.76 V
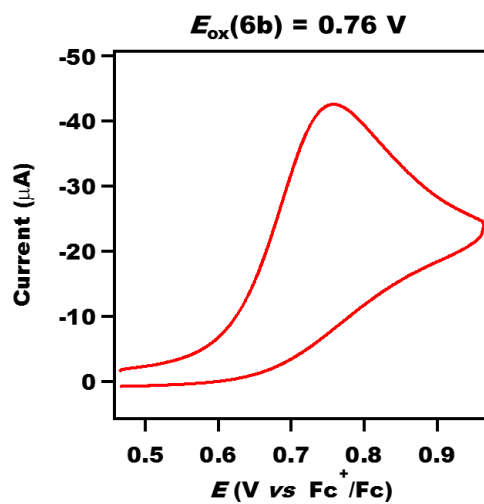
Data S58. CV graph: Oxidation potential E_{ox}(HD) of substrate 6d, related to Table 1.

E_{ox}(6d) = 0.49 V
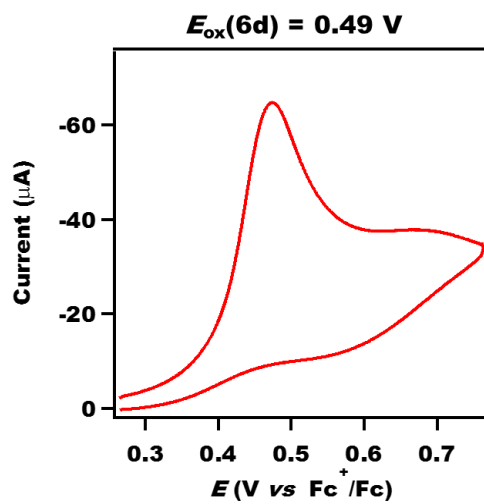
Data S59. CV graph: Oxidation potential E_{ox}(HD) of substrate 6e, related to Table 1.

E_{ox}(6e) = 0.43 V
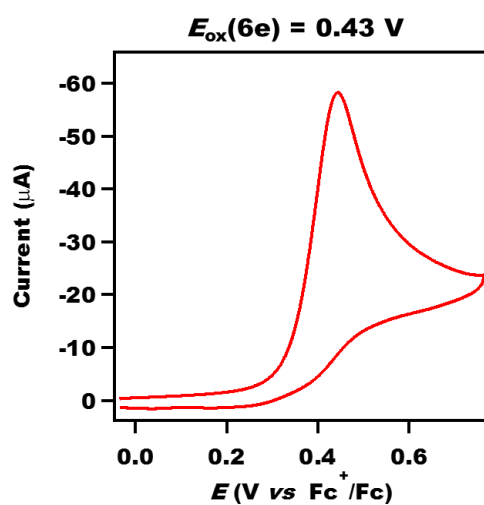
Data S60. CV graph: Oxidation potential E_{ox}(HD) of substrate 6f, related to Table 1.

E_{ox}(6f) = 0.35 V
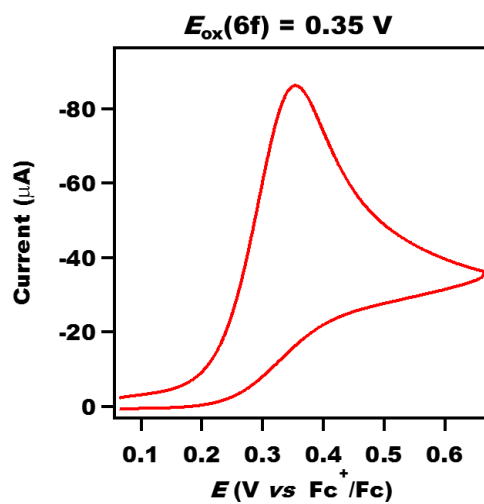
Data S61. CV graph: Oxidation potential E_{ox}(HD) of substrate 6g, related to Table 1.

E_{ox}(6g) = 0.23 V
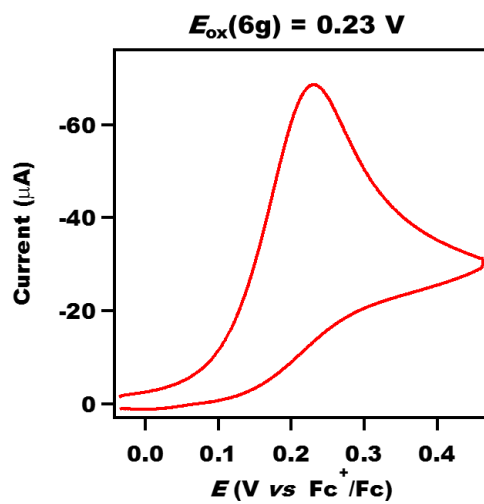
Data S62. CV graph: Oxidation potential E_{ox}(HD) of substrate 6h, related to Table 1.

E_{ox}(6h) = 0.39 V
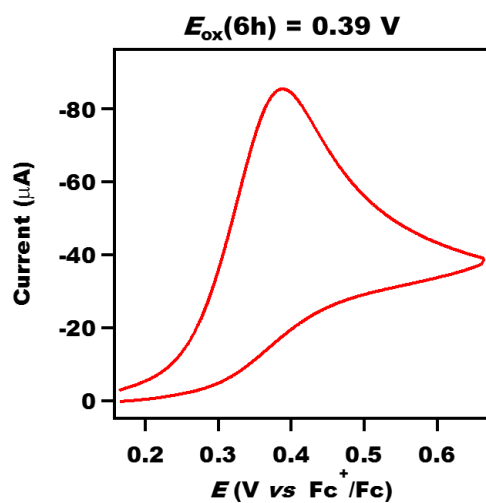
Data S63. CV graph: Oxidation potential E_{ox}(HD) of substrate 6i, related to Table 1.

E_{ox}(6i) = 0.40 V
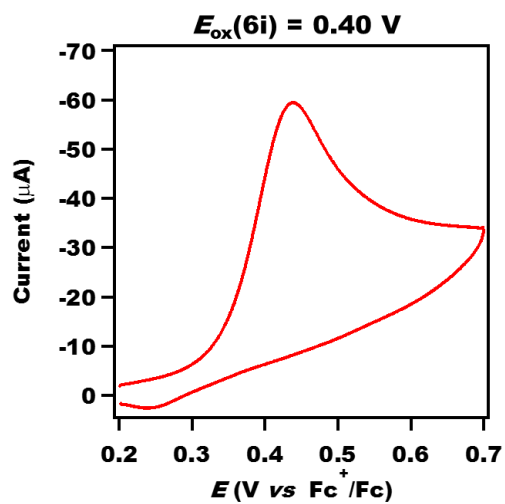
Data S64. CV graph: Oxidation potential E_{ox}(HD) of substrate 7a, related to Table 1.

E_{ox}(7a) = 0.45 V
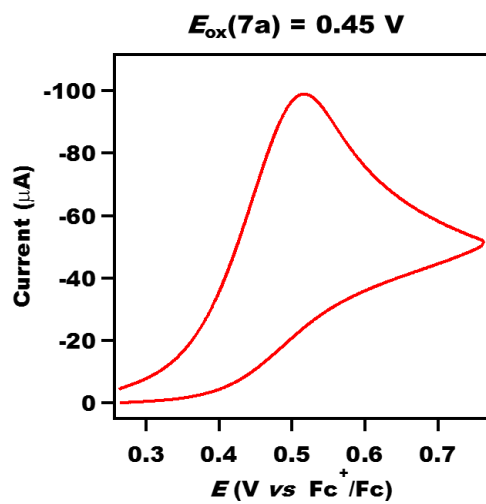
Data S65. CV graph: Oxidation potential E_{ox}(HD) of substrate 7b, related to Table 1.

E_{ox}(7b) = 0.50 V
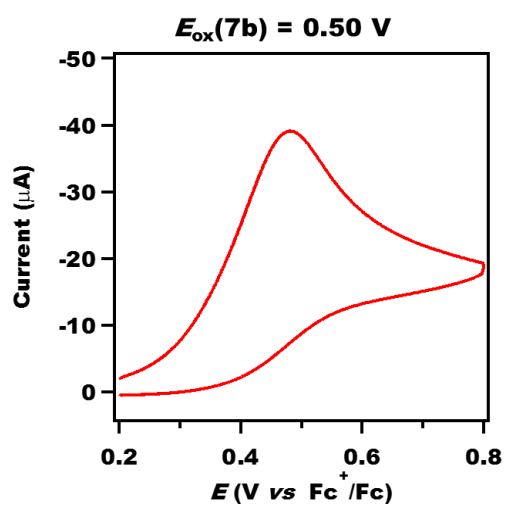
Data S66. CV graph: Oxidation potential E_{ox}(HD) of substrate 7c, related to Table 1.

E_{ox}(7c) = 0.67 V
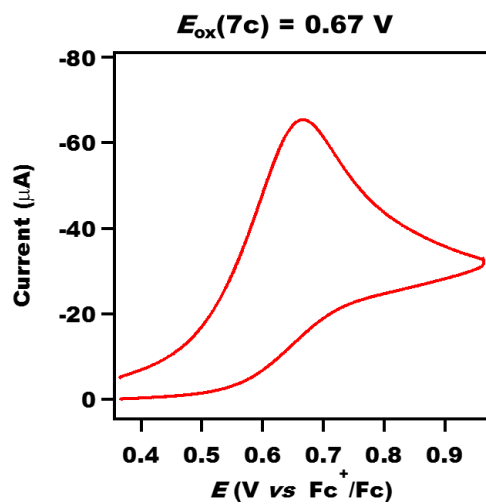
Data S67. CV graph: Oxidation potential E_{ox}(HD) of substrate 7d, related to Table 1.

E_{ox}(7d) = 0.58 V
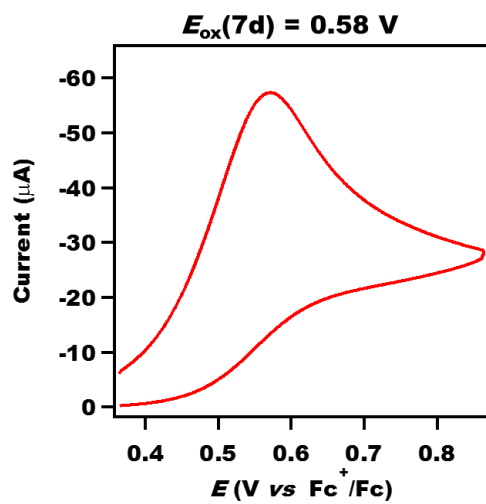
Data S68. CV graph: Oxidation potential E_{ox}(HD) of substrate 7e, related to Table 1.

E_{ox}(7e) = 0.59 V
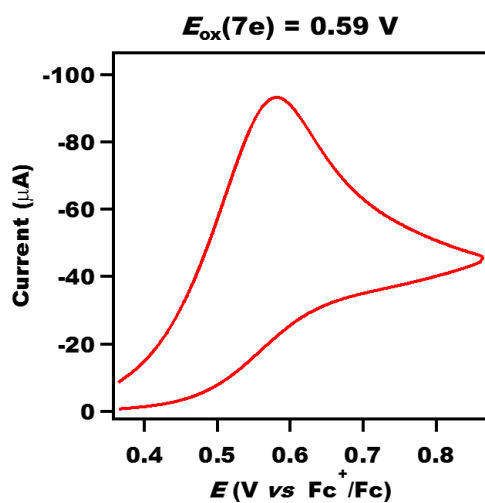
Data S69. CV graph: Oxidation potential E_{ox}(HD) of substrate 7f, related to Table 1.

E_{ox}(7f) = 0.67 V
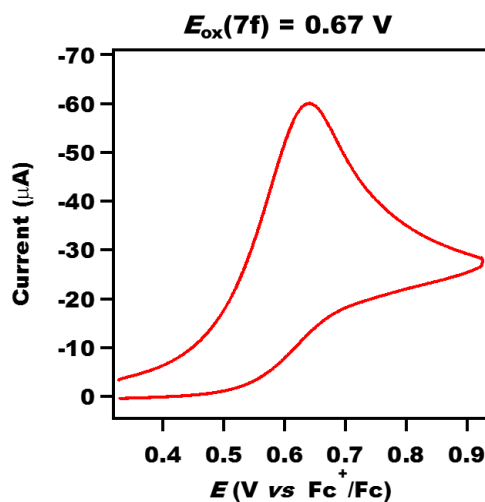
Data S70. CV graph: Oxidation potential E_{ox}(HD) of substrate 7g, related to Table 1.

E_{ox}(7g) = 1.46 V
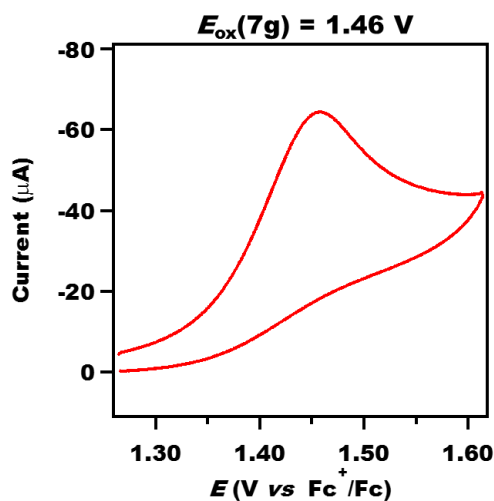
Data S71. CV graph: Oxidation potential E_{ox}(HD) of substrate 7h, related to Table 1.

E_{ox}(7h) = 0.43 V
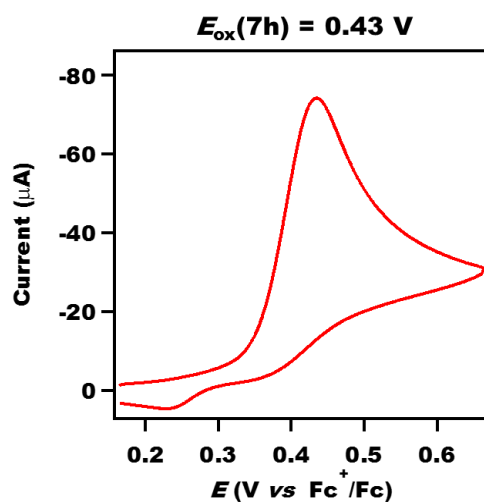
Data S72. CV graph: Oxidation potential E_{ox}(HD) of substrate 7i, related to Table 1.

E_{ox}(7i) = 0.33 V
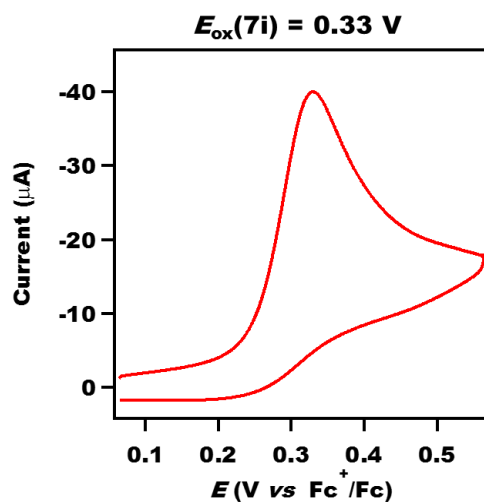
Data S73. CV graph: Oxidation potential E_{ox}(HD) of substrate 8a, related to Table 1.

E_{ox}(8a) = 0.42 V
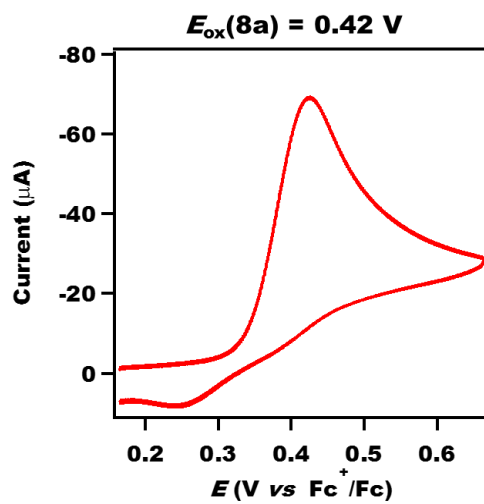
Data S74. CV graph: Oxidation potential E_{ox}(HD) of substrate 8b, related to Table 1.

E_{ox}(8b) = 0.51 V
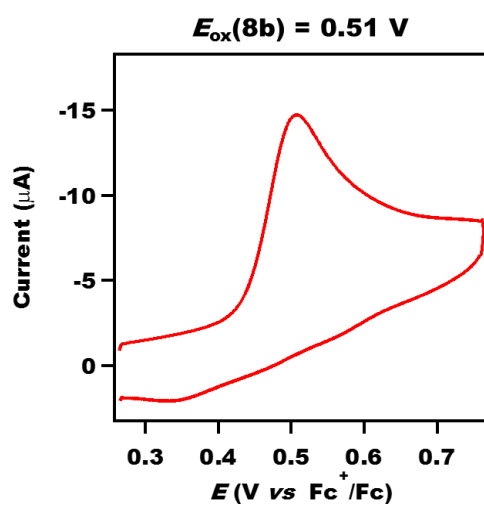
Data S75. CV graph: Oxidation potential E_{ox}(HD) of substrate 9a, related to Table 1.

E_{ox}(9a) = 0.50 V
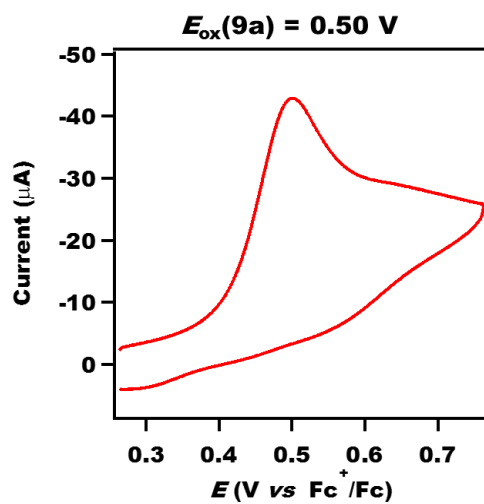
Data S76. CV graph: Oxidation potential E_{ox}(HD) of substrate 9b, related to Table 1.

E_{ox}(9b) = 0.49 V
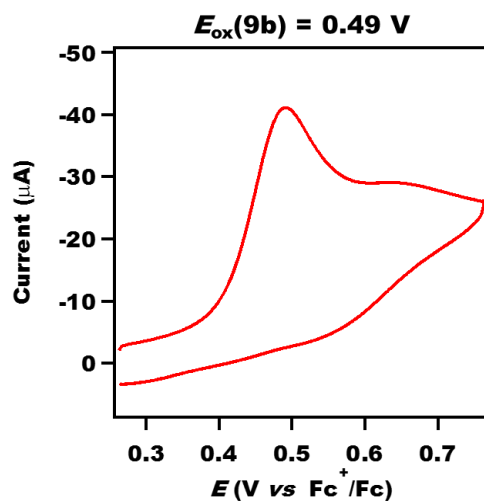
Data S77. CV graph: Oxidation potential E_{ox}(HD) of substrate 9c, related to Table 1.

E_{ox}(9c) = 0.46 V
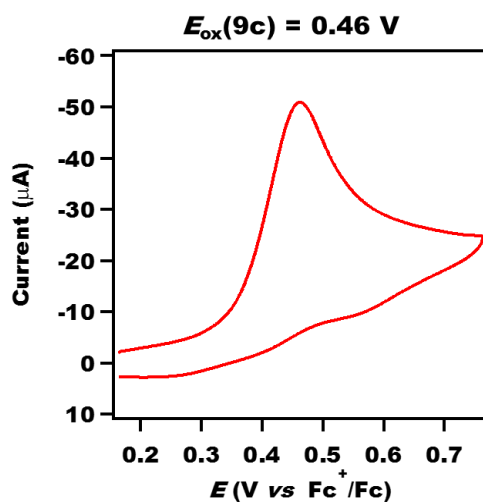
Data S78. CV graph: Oxidation potential E_{ox}(HD) of substrate 9d, related to Table 1.

E_{ox}(9d) = 0.40 V
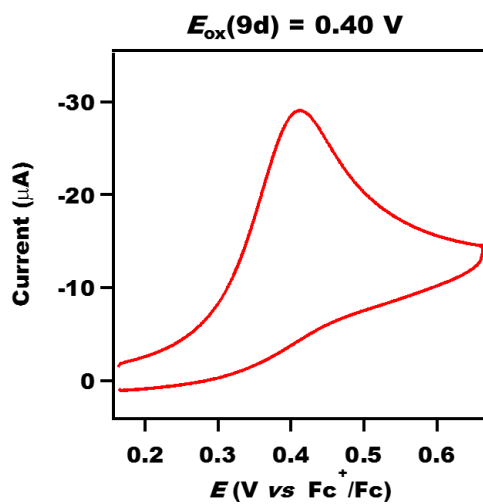
Data S79. CV graph: Oxidation potential E_{ox}(HD) of substrate 10b, related to Table 1.

E_{ox}(10b)=0.40 V
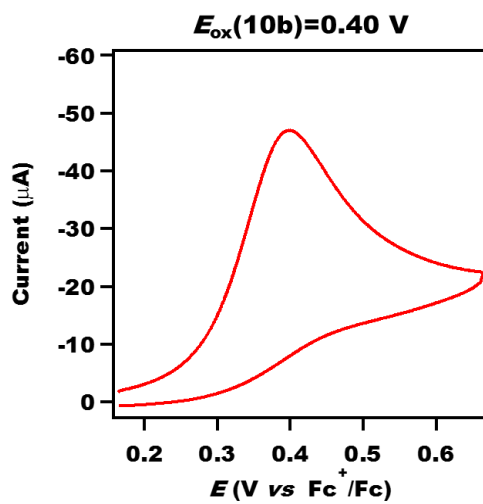
Data S80. CV graph: Oxidation potential E_{ox}(HD) of substrate 10c, related to Table 1.

E_{ox}(10c) = 0.20 V
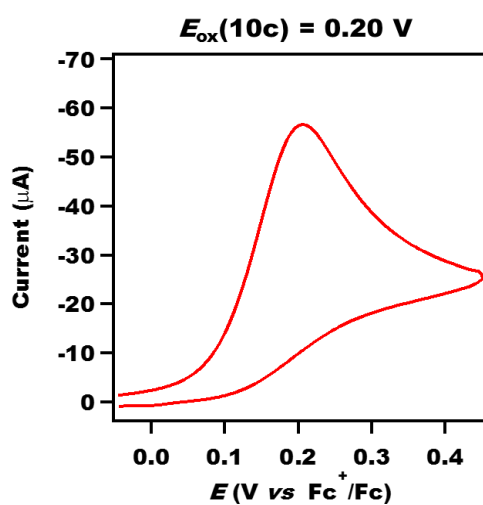
Data S81. CV graph: Oxidation potential E_{ox}(HD) of substrate 11, related to Table 1.

E_{ox}(11) = 0.42 V
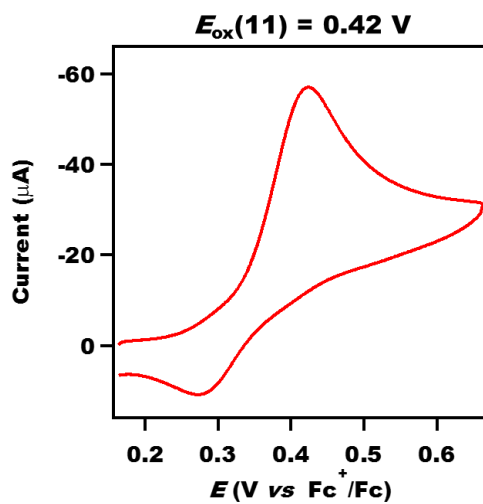
Data S82. CV graph: Oxidation potential E_{ox}(HD) of substrate 14, related to Table 1.

E_{ox}(14) = -0.07V
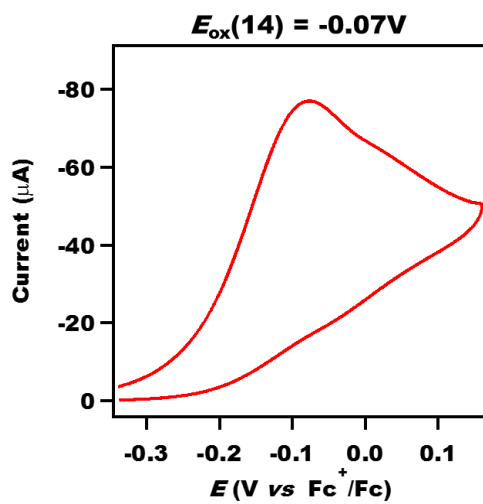
Data S83. CV graph: Oxidation potential $E_{red}(D^+)$ of iminium cation 2a$^+$, related to Table 1.

$E_{red}(2a^+) = -1.05$ V
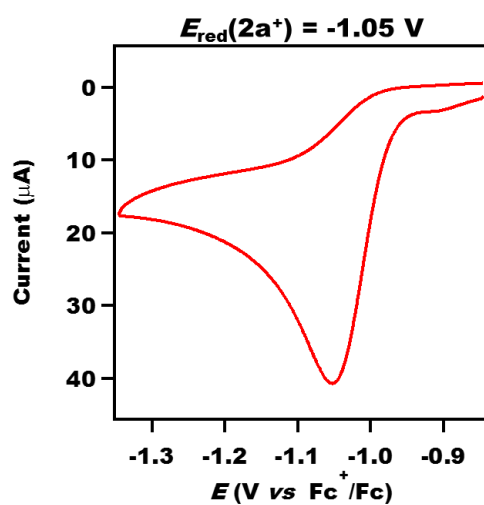
Data S84. CV graph: Oxidation potential $E_{red}(D^+)$ of iminium cation 2b$^+$, related to Table 1.

$E_{red}(2b^+) = -1.27$ V
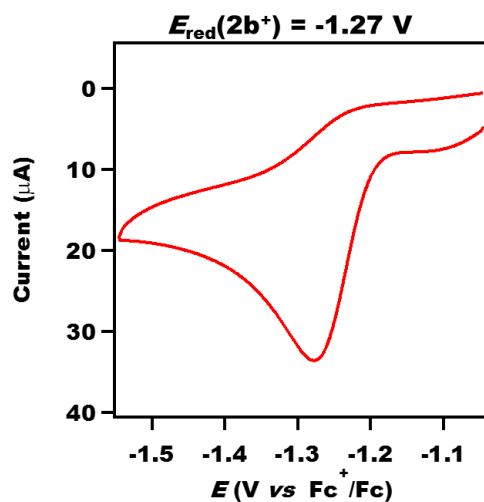
Data S85. CV graph: Oxidation potential $E_{red}(D^+)$ of iminium cation 2d$^+$, related to Table 1.

$E_{red}(2d^+) = -1.37$ V
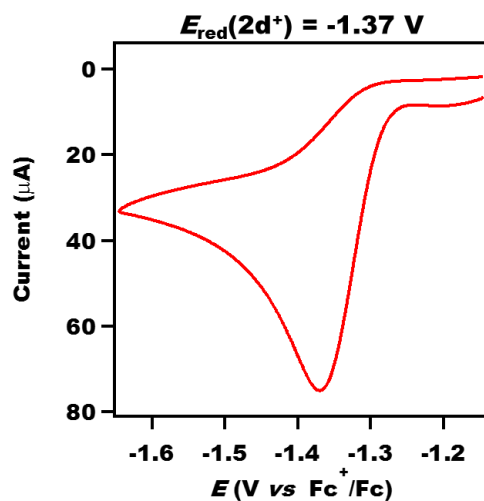
Data S86. CV graph: Oxidation potential $E_{red}(D^+)$ of iminium cation 2f$^+$, related to Table 1.

$E_{red}(2f^+)$ = -1.42 V
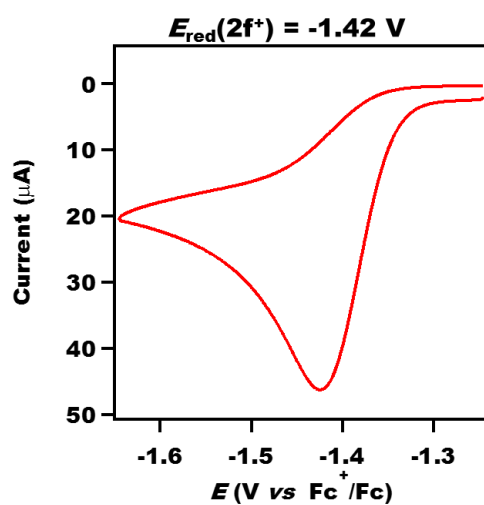
Data S87. CV graph: Oxidation potential $E_{red}(D^+)$ of iminium cation 2g$^+$, related to Table 1.

$E_{red}(2g^+)$ = -1.50 V
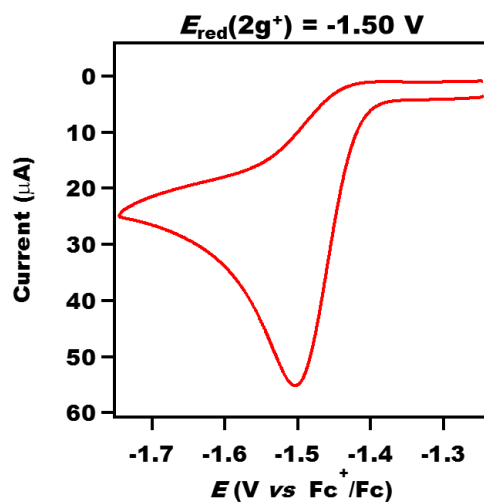
Data S88. CV graph: Oxidation potential $E_{red}(D^+)$ of iminium cation 2h$^+$, related to Table 1.

$E_{red}(2h^+)$ = -1.68 V
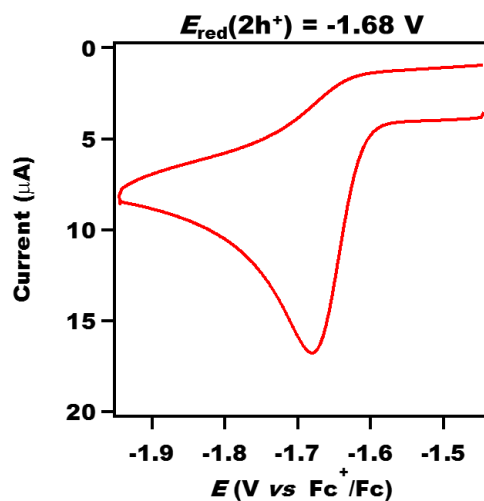
Data S89. CV graph: Oxidation potential $E_{red}(D^+)$ of iminium cation $2i^+$, related to Table 1.
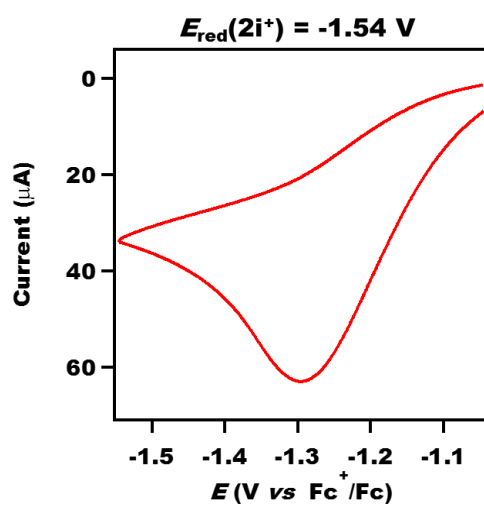
Data S90. CV graph: Oxidation potential $E_{red}(D^+)$ of iminium cation $3a^+$, related to Table 1.
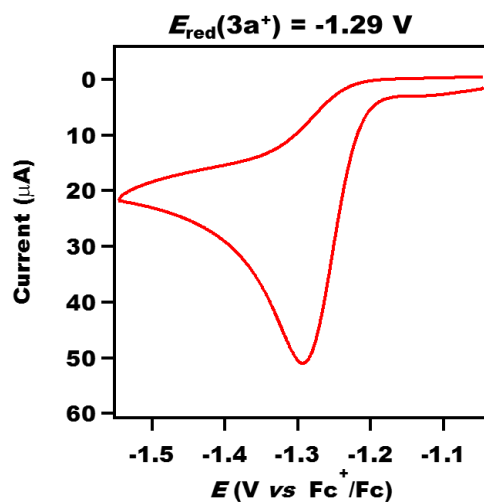
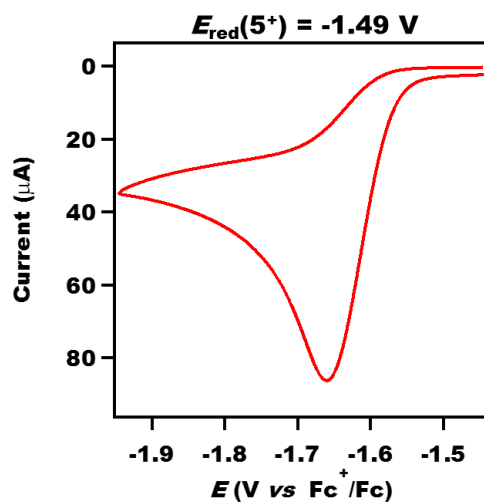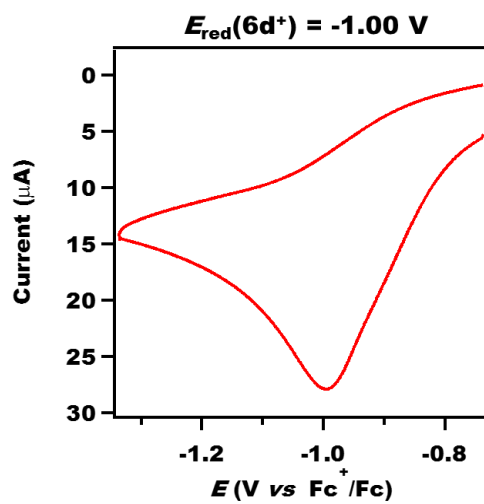Data S91. CV graph: Oxidation potential $E_{red}(D^+)$ of iminium cation $3b^+$, related to Table 1.
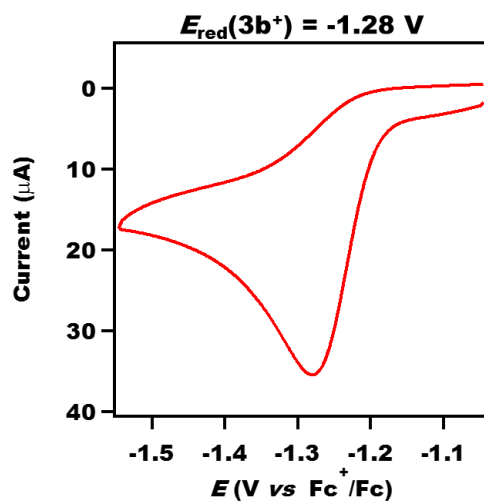
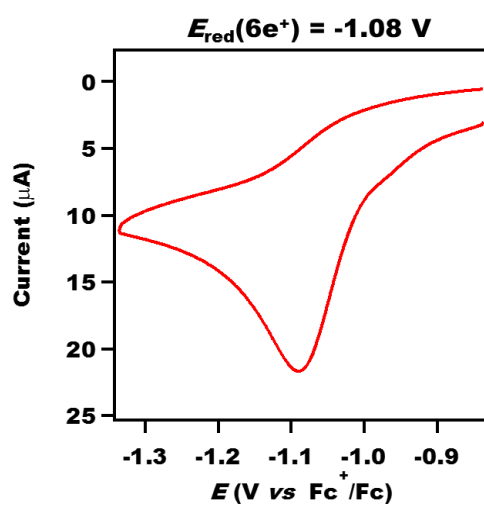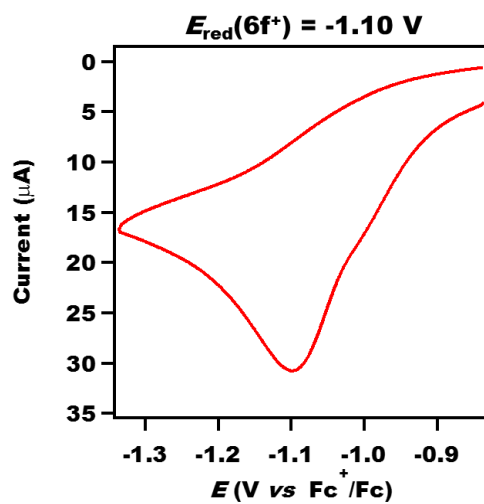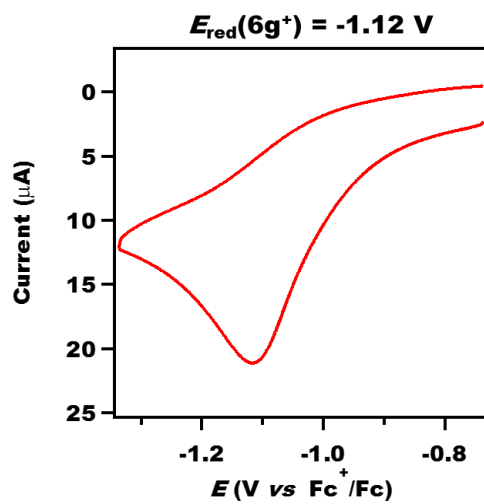Data S92. CV graph: Oxidation potential $E_{red}(D^+)$ of iminium cation 4$^+$, related to Table 1.

$E_{red}(4^+)$ = -1.19 V
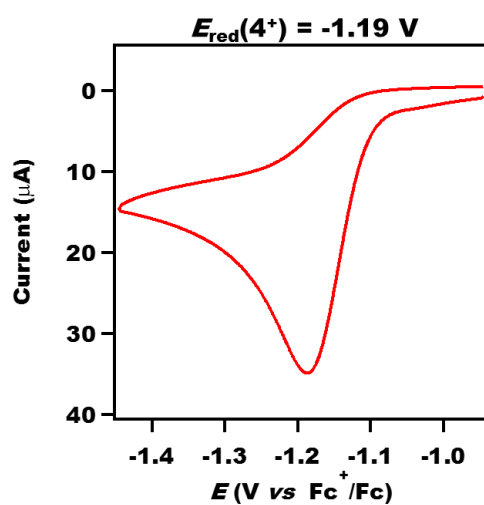
Data S93. CV graph: Oxidation potential $E_{red}(D^+)$ of iminium cation 5$^+$, related to Table 1.

$E_{red}(5^+)$ = -1.49 V

Data S94. CV graph: Oxidation potential $E_{red}(D^+)$ of iminium cation 6d$^+$, related to Table 1.

$E_{red}(6d^+)$ = -1.00 V

Data S95. CV graph: Oxidation potential $E_{red}(D^+)$ of iminium cation 6e$^+$, related to Table 1.

$E_{red}(6e^+) = -1.08$ V

Data S96. CV graph: Oxidation potential $E_{red}(D^+)$ of iminium cation 6f$^+$, related to Table 1.

$E_{red}(6f^+) = -1.10$ V

Data S97. CV graph: Oxidation potential $E_{red}(D^+)$ of iminium cation 6g$^+$, related to Table 1.

$E_{red}(6g^+) = -1.12$ V

Data S98. CV graph: Oxidation potential $E_{red}(D^+)$ of iminium cation 6h⁺, related to Table 1.

$E_{red}(6h^+)$ = -1.19 V
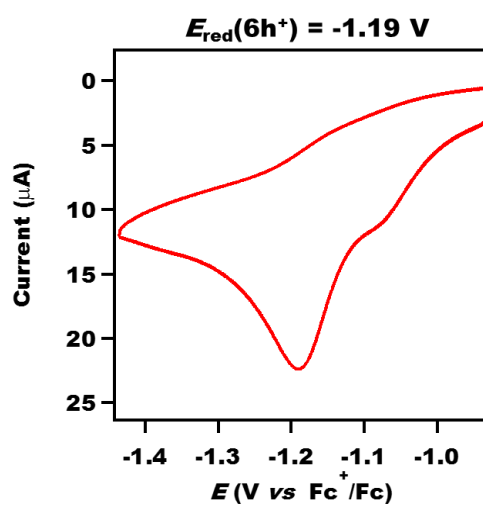
Data S99. CV graph: Oxidation potential $E_{red}(D^+)$ of iminium cation 6i⁺, related to Table 1.

$E_{red}(6i^+)$ = -1.08 V
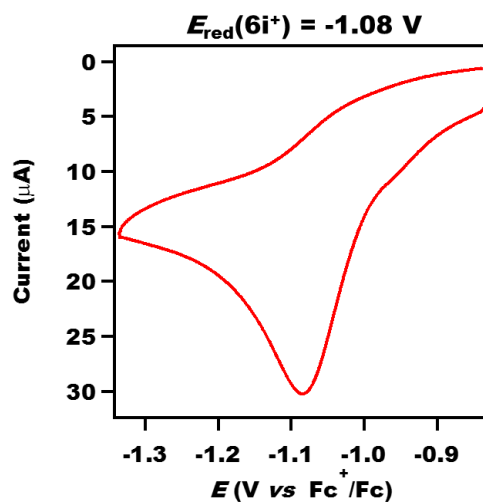
Data S100. CV graph: Oxidation potential $E_{red}(D^+)$ of iminium cation 7e⁺, related to Table 1.

$E_{red}(7e^+)$ = -1.31 V
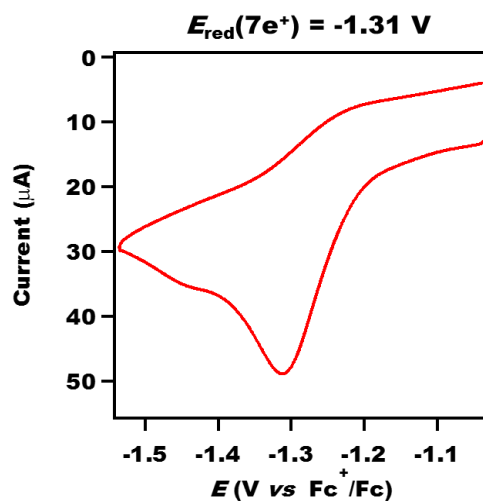
Data S101. CV graph: Oxidation potential $E_{red}(D^+)$ of iminium cation 7f⁺, related to Table 1.

$E_{red}(7f^+) = -1.28$ V
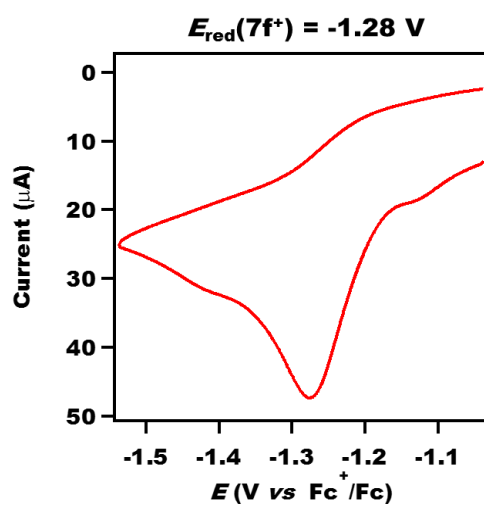
Data S102. CV graph: Oxidation potential $E_{red}(D^+)$ of iminium cation 7i⁺, related to Table 1.

$E_{red}(7i^+) = -1.03$ V
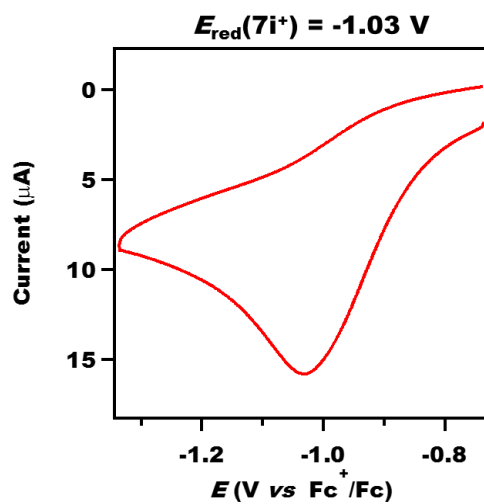
Data S103. CV graph: Oxidation potential $E_{red}(D^+)$ of iminium cation 8b⁺, related to Table 1.

$E_{red}(8b^+) = -1.41$ V
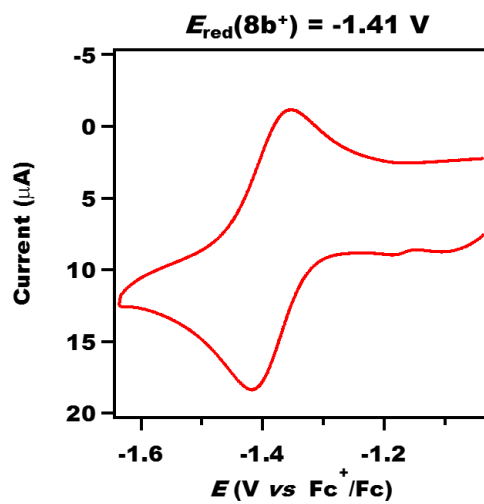
Data S104. CV graph: Oxidation potential $E_{red}(D^+)$ of iminium cation 9a[+], related to Table 1.

$E_{red}(9a^+)$ = -0.88 V
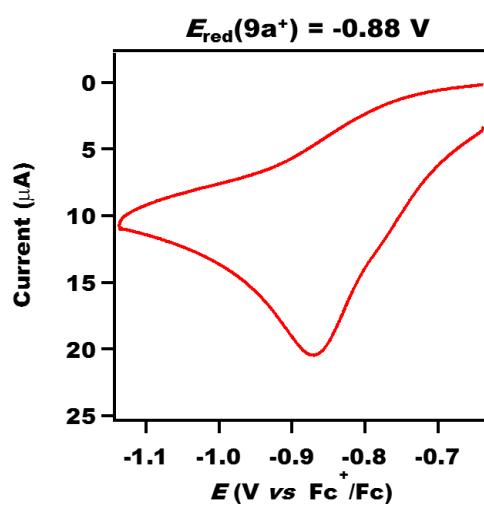
Data S105. CV graph: Oxidation potential $E_{red}(D^+)$ of iminium cation 9b[+], related to Table 1.

$E_{red}(9b^+)$ = -0.80 V
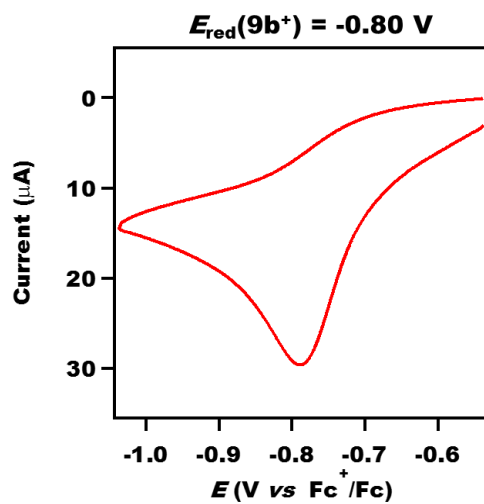
Data S106. CV graph: Oxidation potential $E_{red}(D^+)$ of iminium cation 9c[+], related to Table 1.

$E_{red}(9c^+)$ = -1.00 V
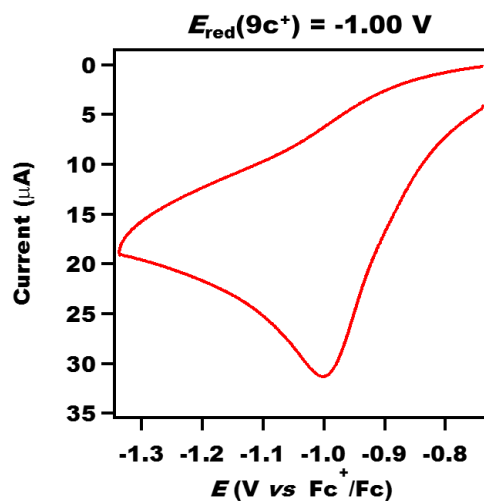
Data S107. CV graph: Oxidation potential $E_{red}(D^+)$ of iminium cation 9d⁺, related to Table 1.

$E_{red}(9d^+)$ = -1.24 V
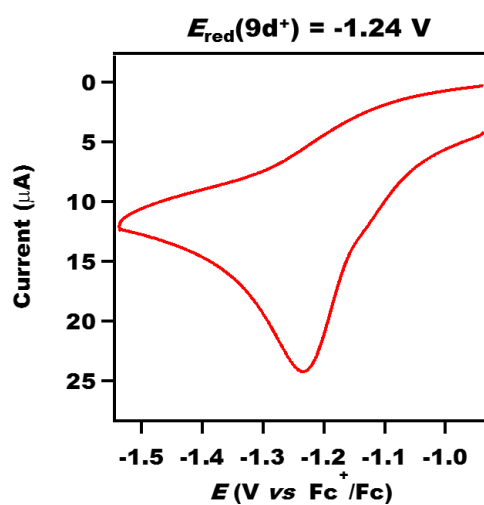
Data S108. CV graph: Oxidation potential $E_{red}(D^+)$ of iminium cation 10b⁺, related to Table 1.

$E_{red}(10b^+)$=-1.21 V
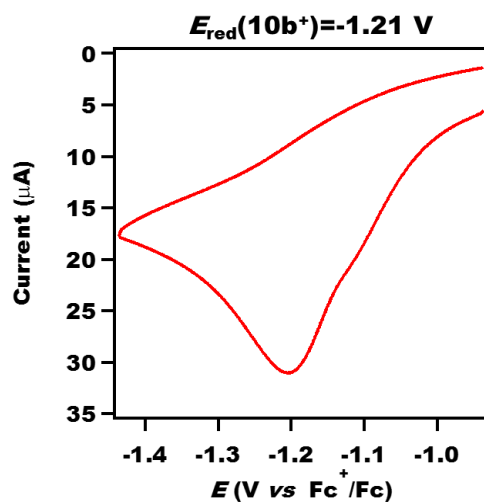
Data S109. CV graph: Oxidation potential $E_{red}(D^+)$ of iminium cation 10c⁺, related to Table 1.

$E_{red}(10c^+)$ = -1.28 V
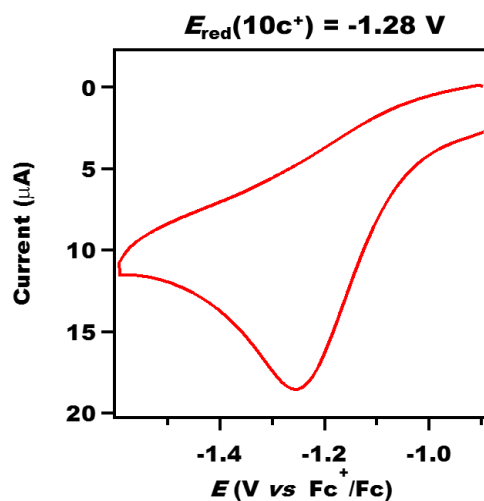
Data S110. CV graph: Oxidation potential $E_{red}(D^+)$ of iminium cation 11^+, related to Table 1.

$$E_{red}(11^+) = -1.06 \text{ V}$$
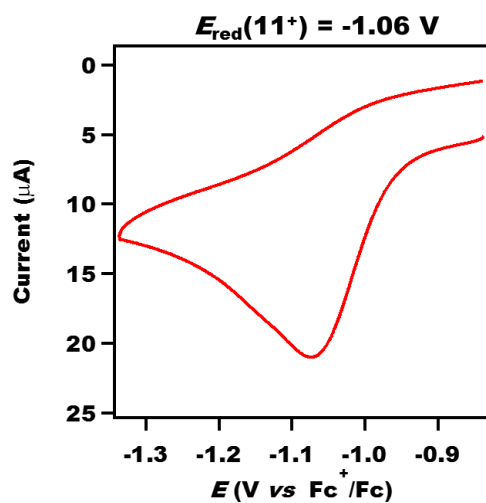
Data S111. CV graph: Oxidation potential $E_{red}(D^+)$ of iminium cation 13^+, related to Table 1.

$$E_{red}(13^+) = -1.12 \text{ V}$$
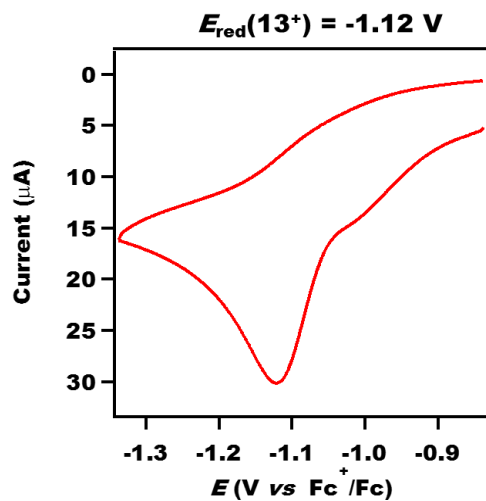
Data S112. CV graph: Oxidation potential $E_{red}(D^+)$ of iminium cation 14^+, related to Table 1.

$$E_{red}(14^+) = -1.48 \text{V}$$
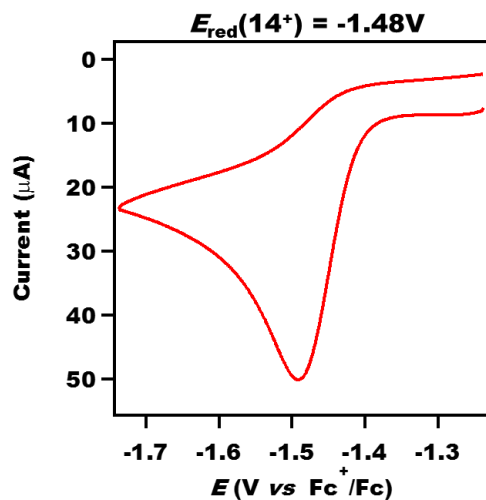
Representative ^{1}H NMR spectra of tertiary amines and iminium salts

Data S113. ^{1}H NMR spectra of substrate 7a, related to Table 1.
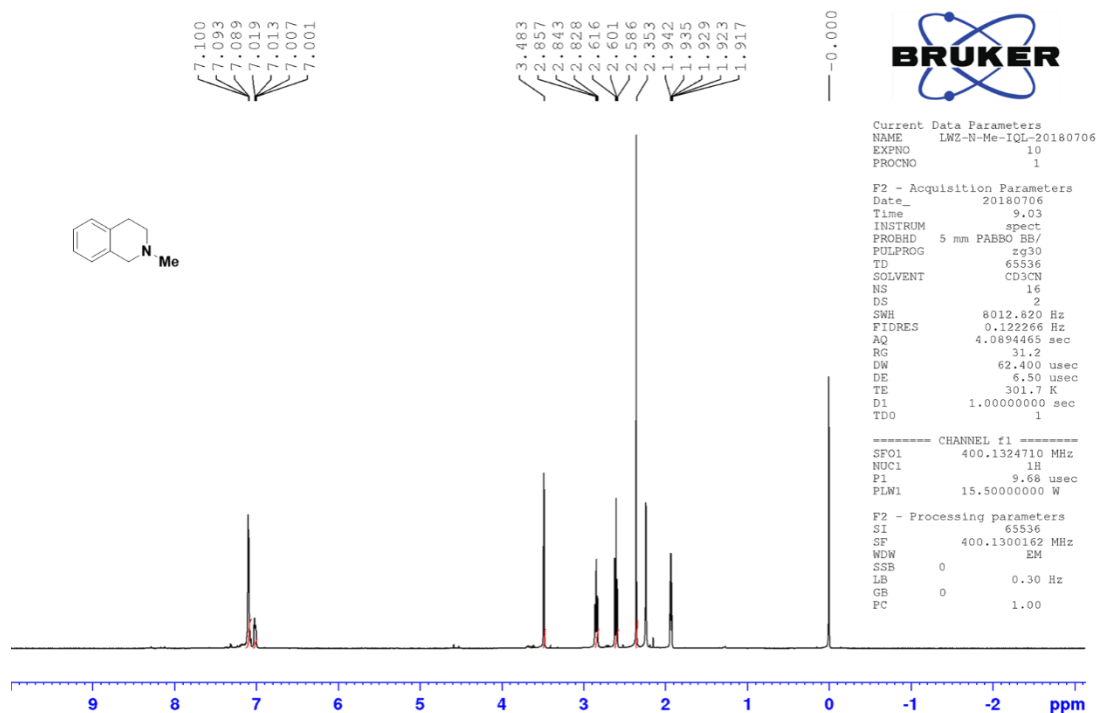
Data S114. ^{1}H NMR spectra of substrate 7d, related to Table 1.
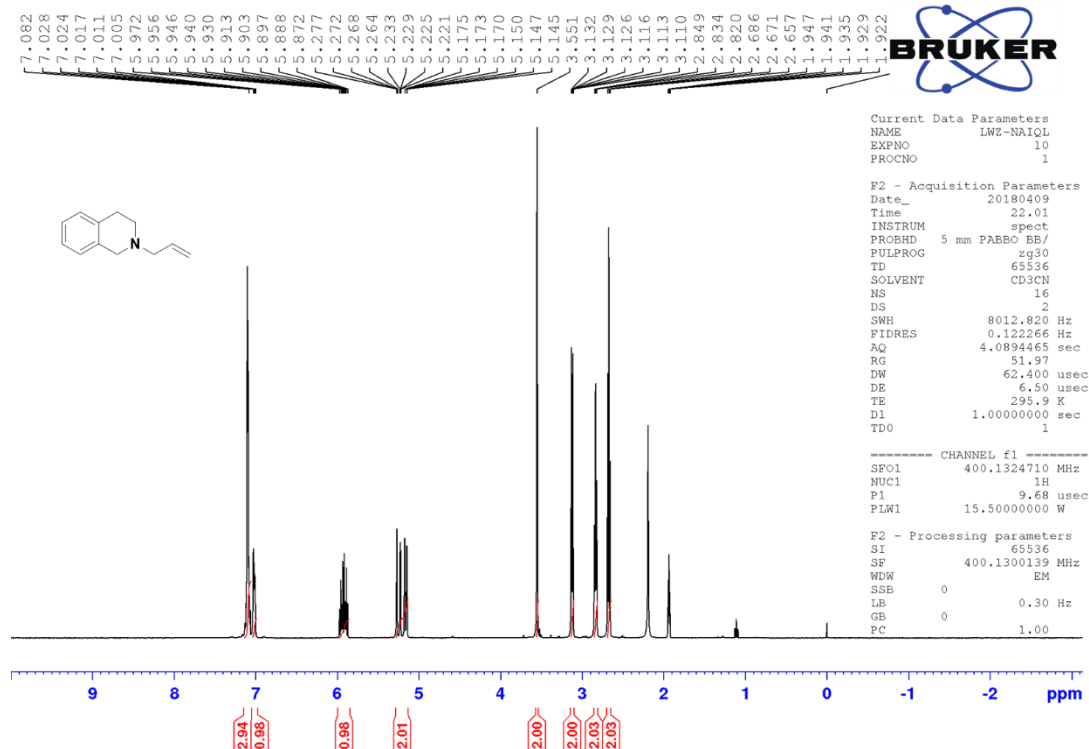
Data S115. ^{1}H NMR spectra of substrate 7e, related to Table 1.
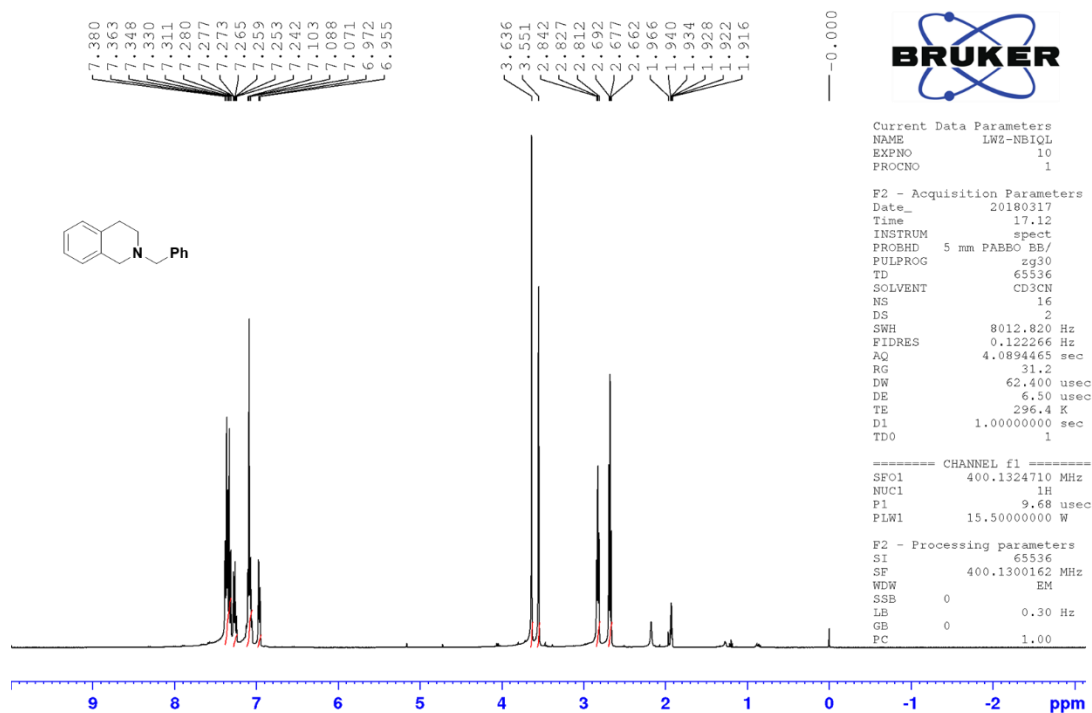
Data S116. ^{1}H NMR spectra of substrate 7f, related to Table 1.
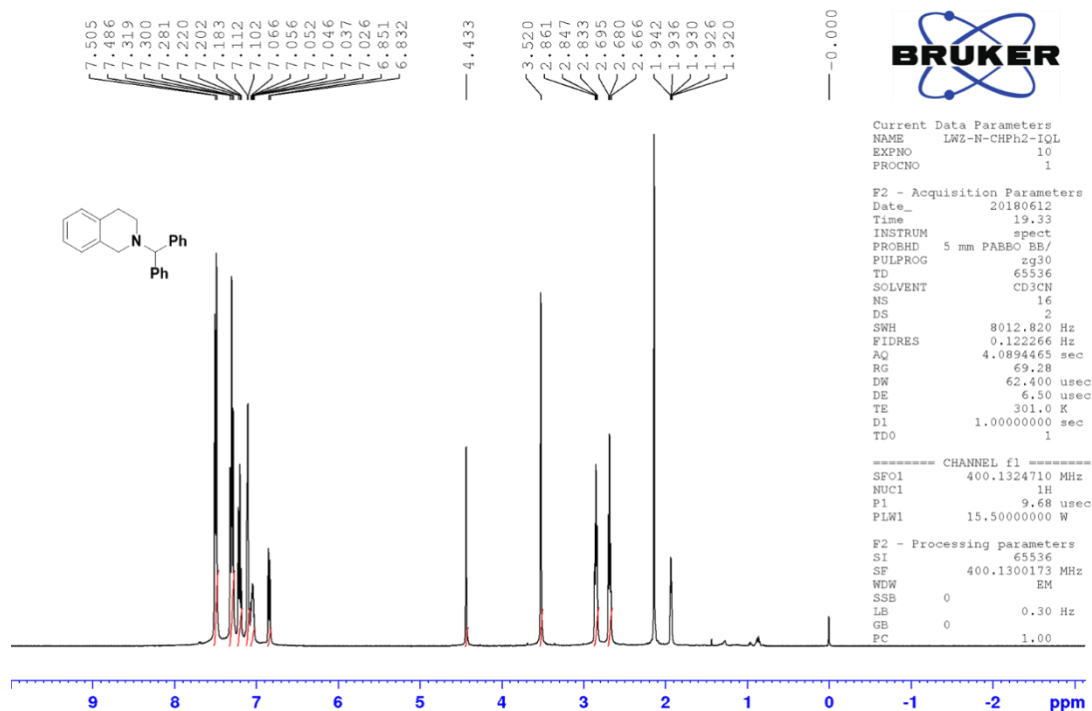
Data S117. ¹H NMR spectra of substrate 6a, related to Table 1.
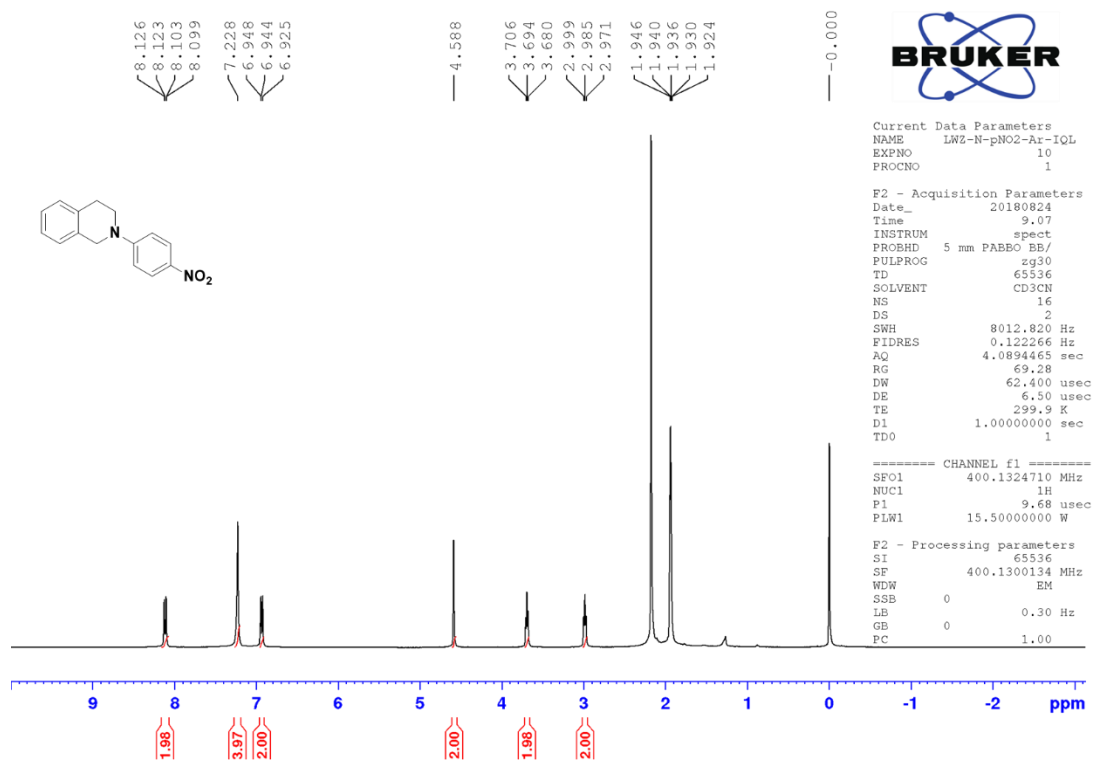
Data S118. ¹H NMR spectra of substrate 6c, related to Table 1.
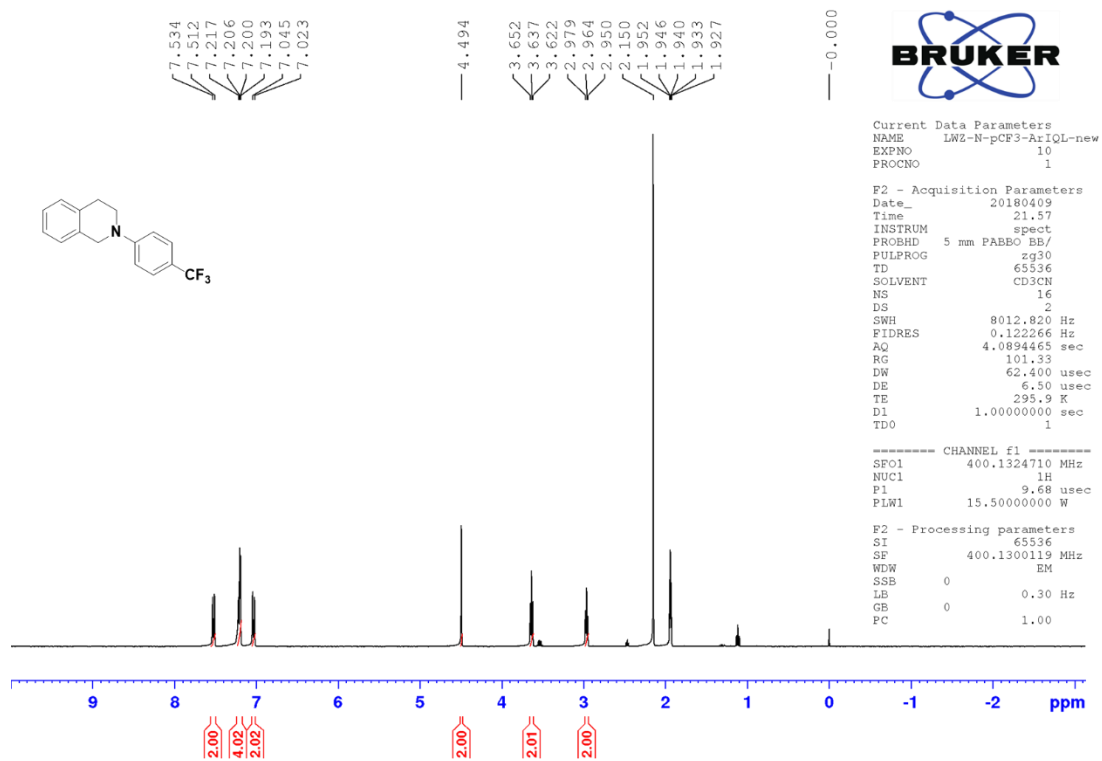
Data S119. ¹H NMR spectra of substrate 6b, related to Table 1.
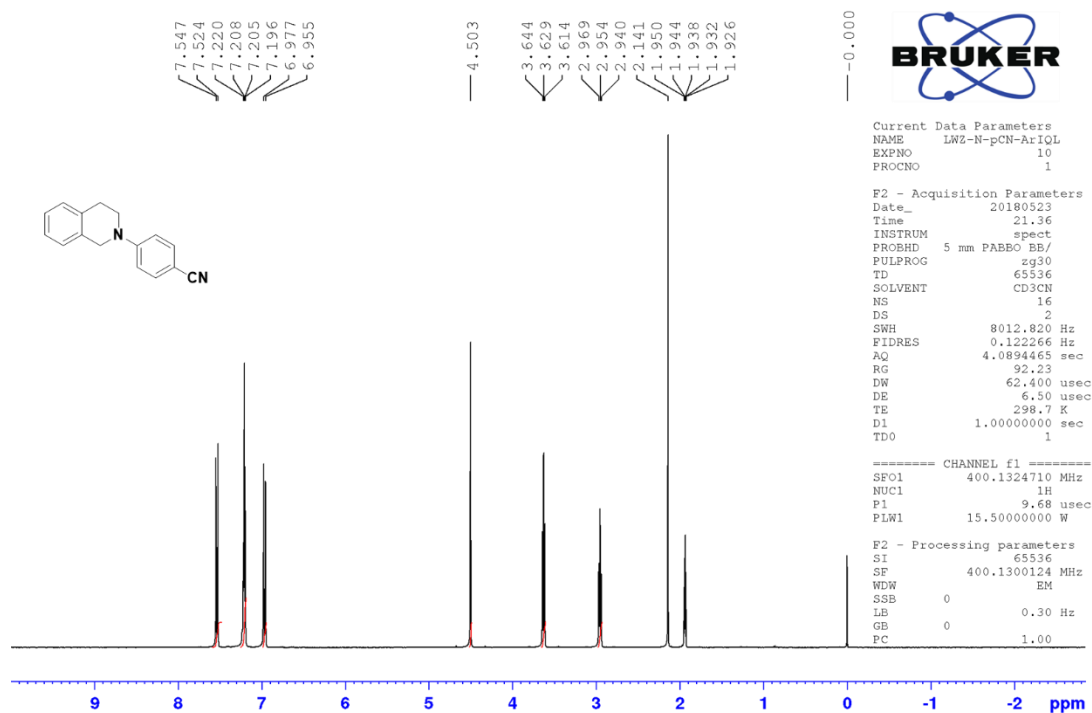
Data S120. ¹H NMR spectra of substrate 6f, related to Table 1.
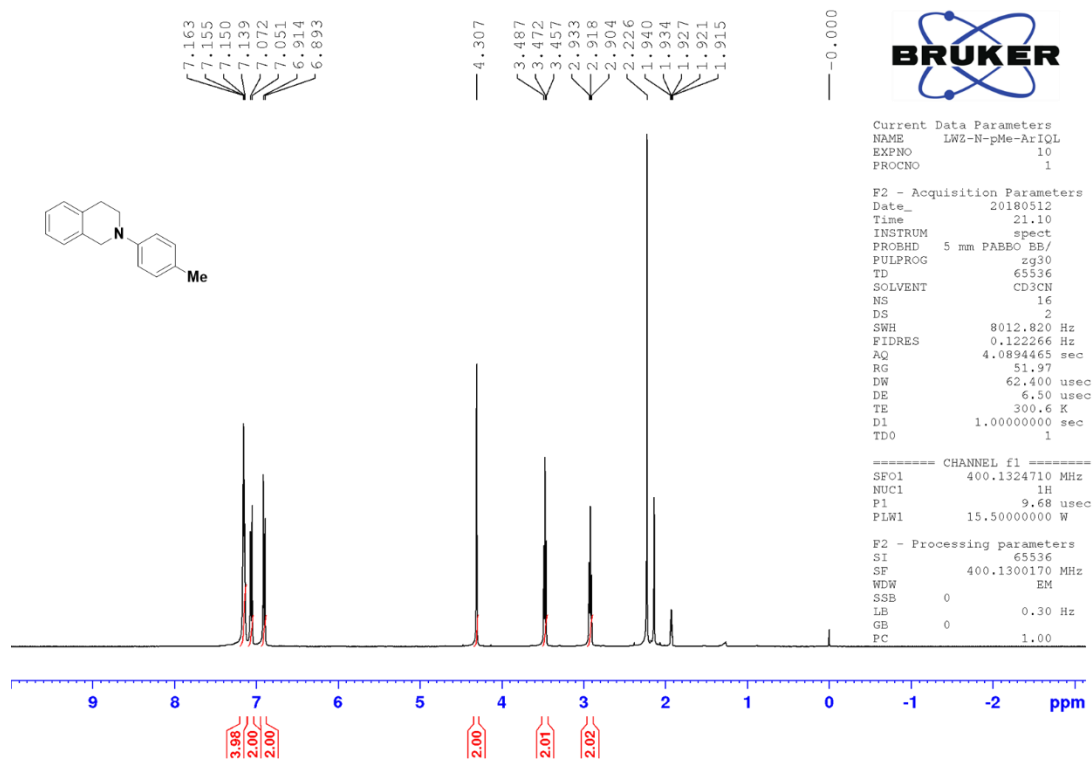
Data S121. ¹H NMR spectra of substrate 6h, related to Table 1.
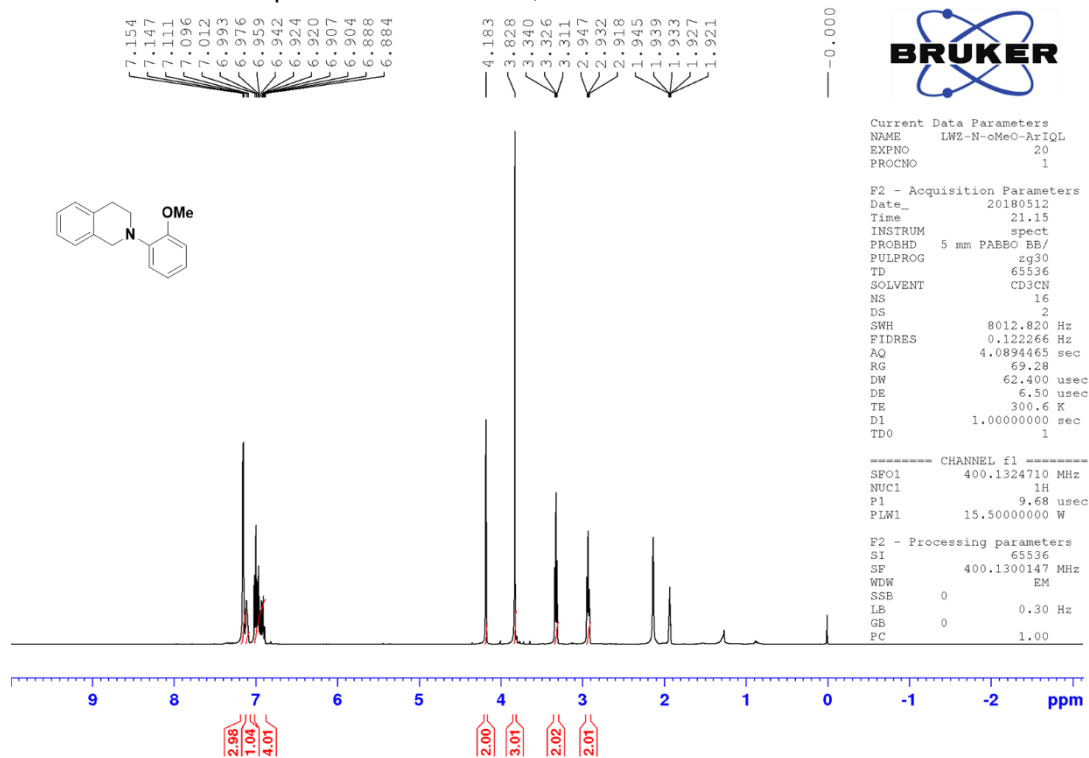
Data S122. ¹H NMR spectra of substrate 9a, related to Table 1.
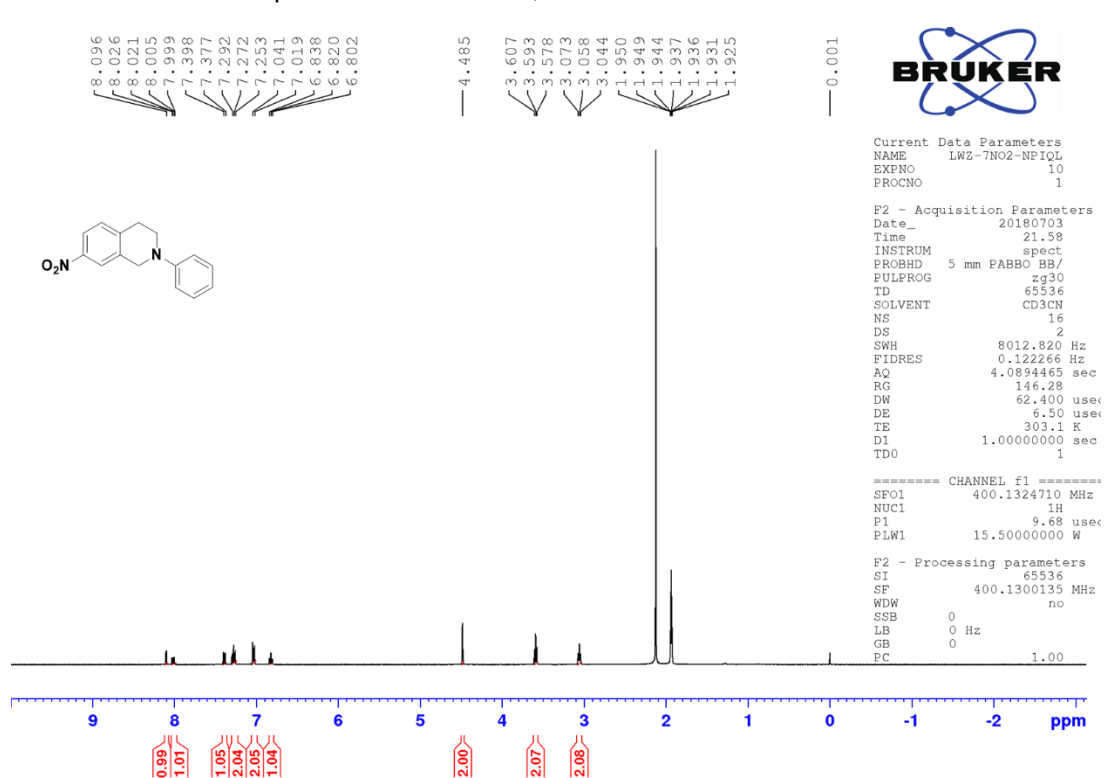
Data S123. ^{1}H NMR spectra of substrate 9b, related to Table 1.
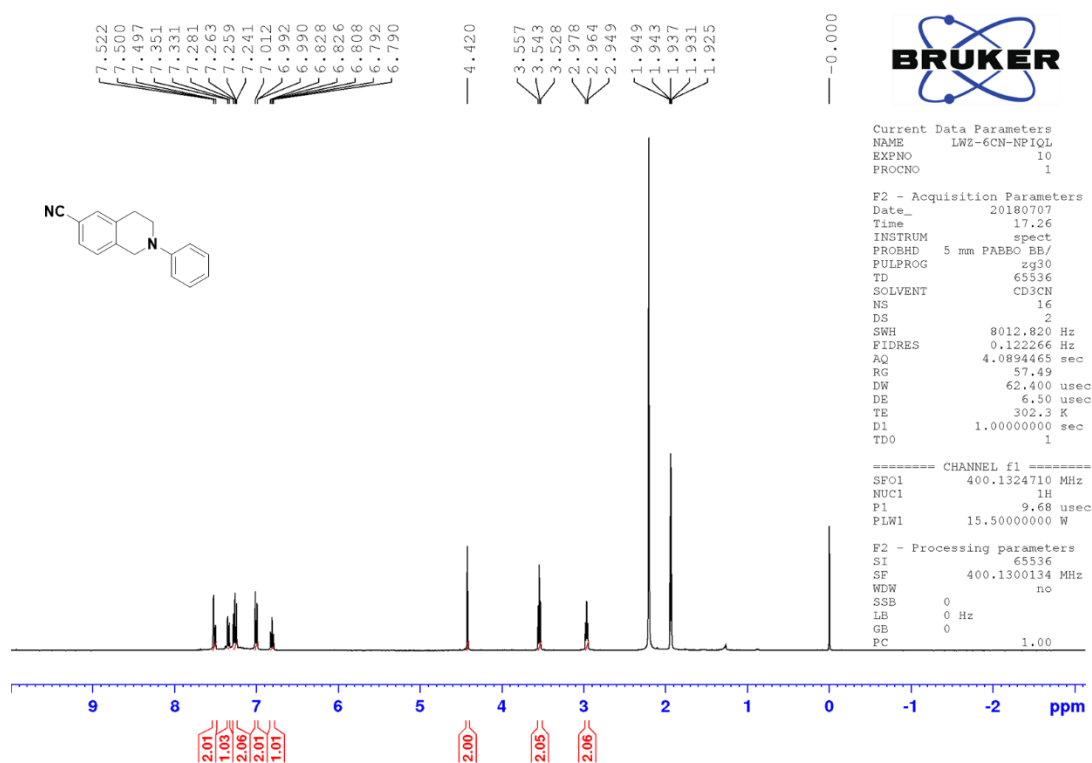
Data S124. ^{1}H NMR spectra of substrate 9d, related to Table 1.
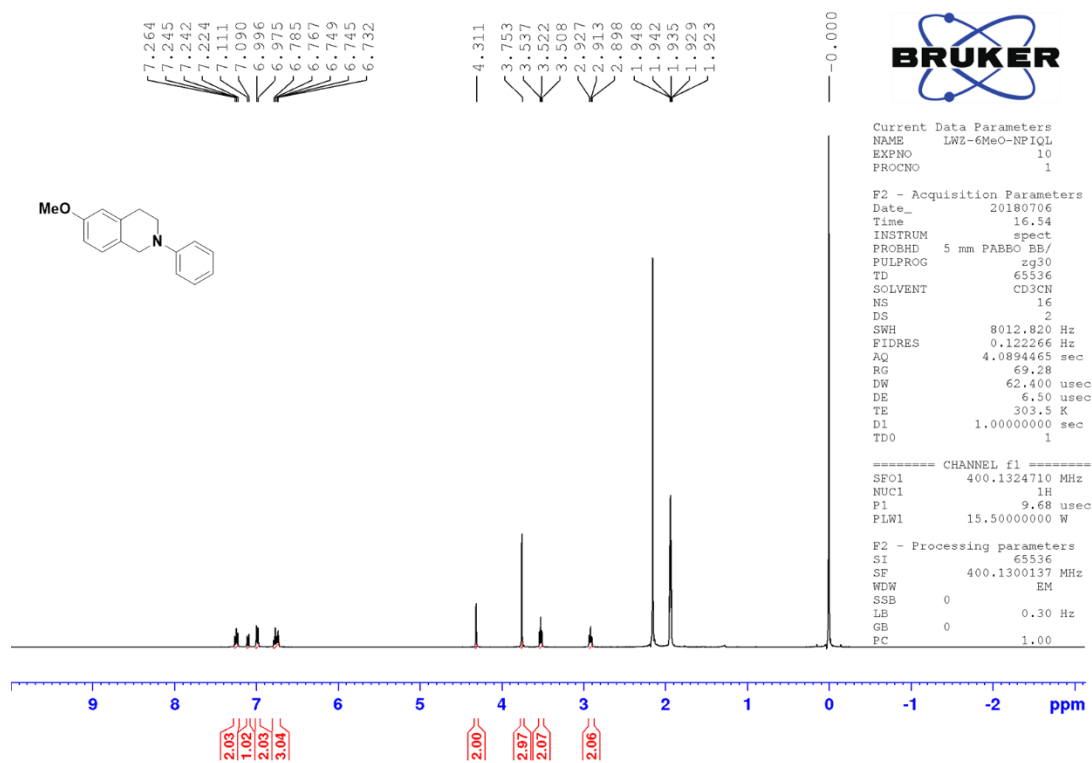
Data S125. ^{1}H NMR spectra of substrate 10b, related to Table 1.
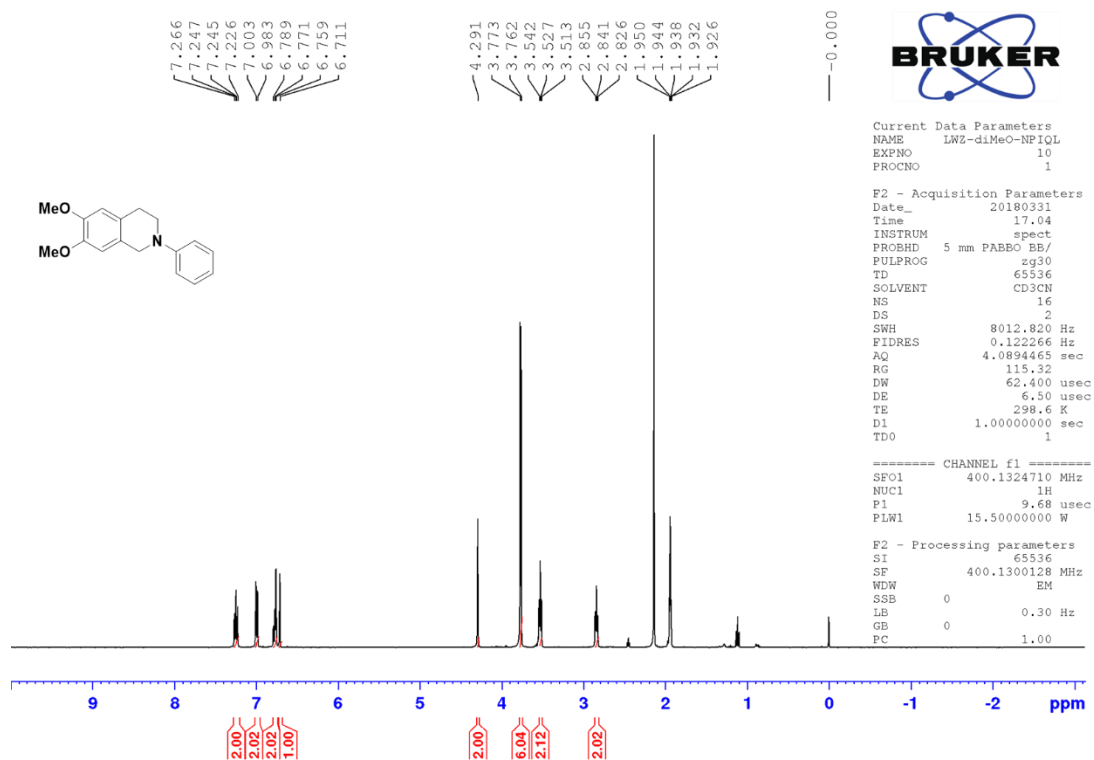
Data S126. ^{1}H NMR spectra of substrate 12, related to Table 1.
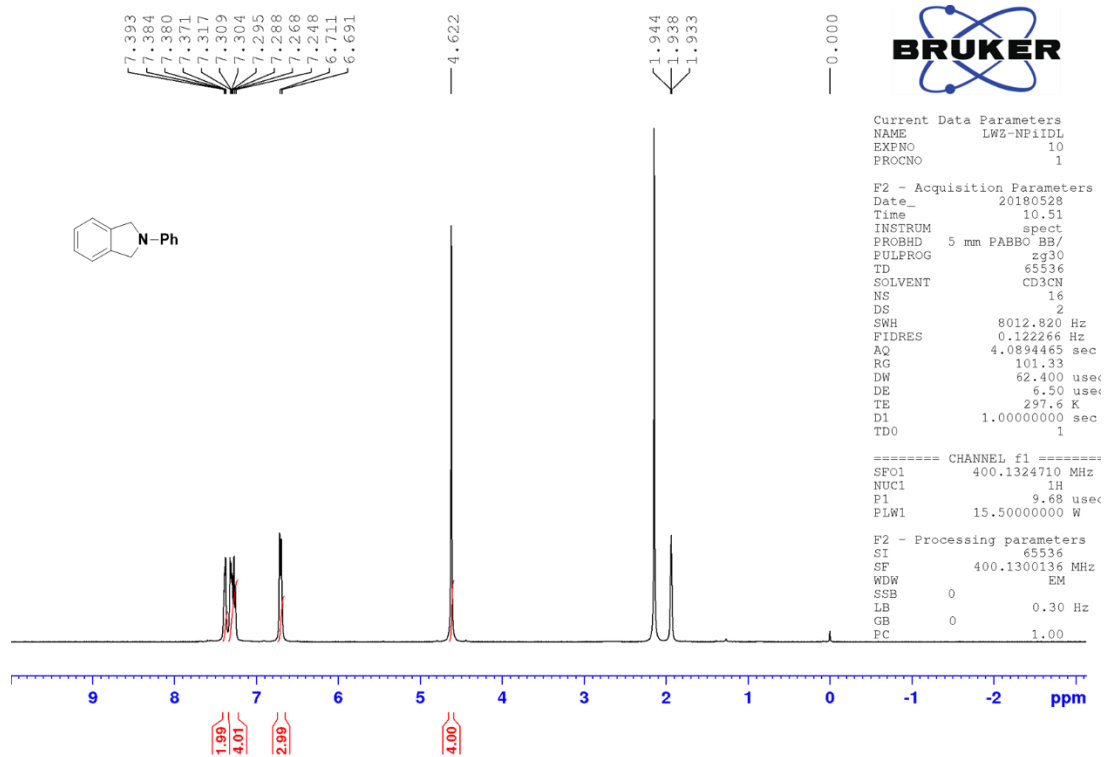
Data S127. ¹H NMR spectra of substrate 11, related to Table 1.
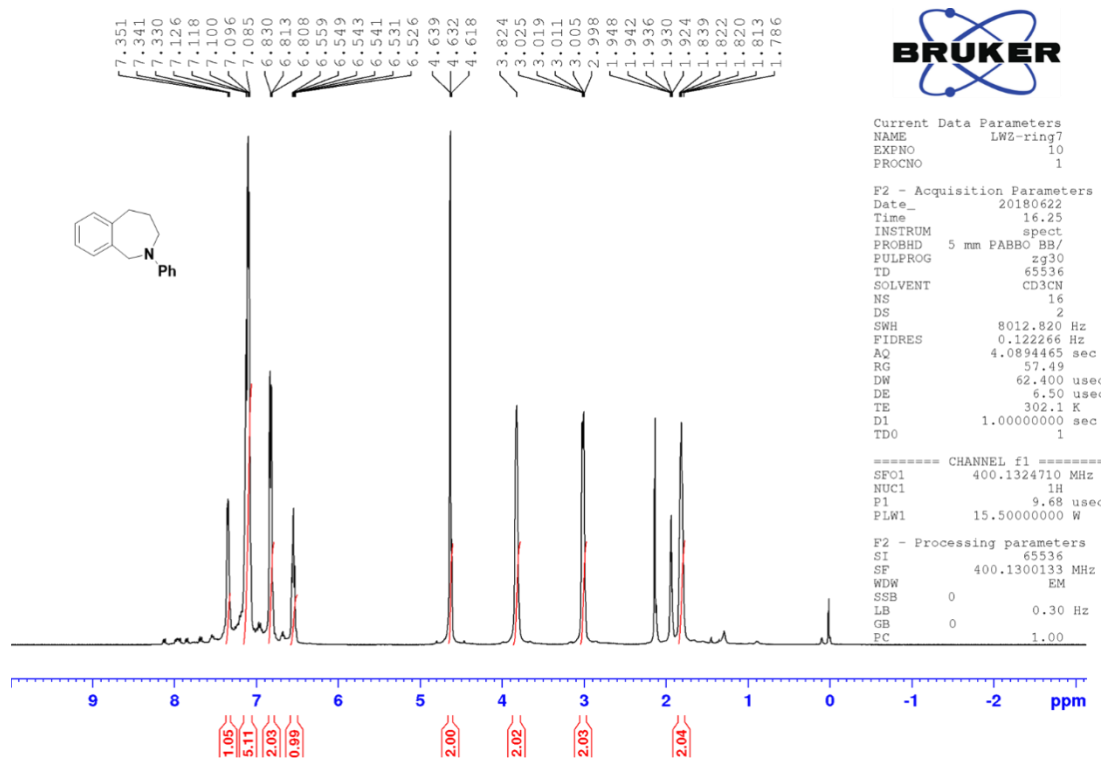
Data S128. ¹H NMR spectra of iminium cation 2e⁺, related to Table 1.
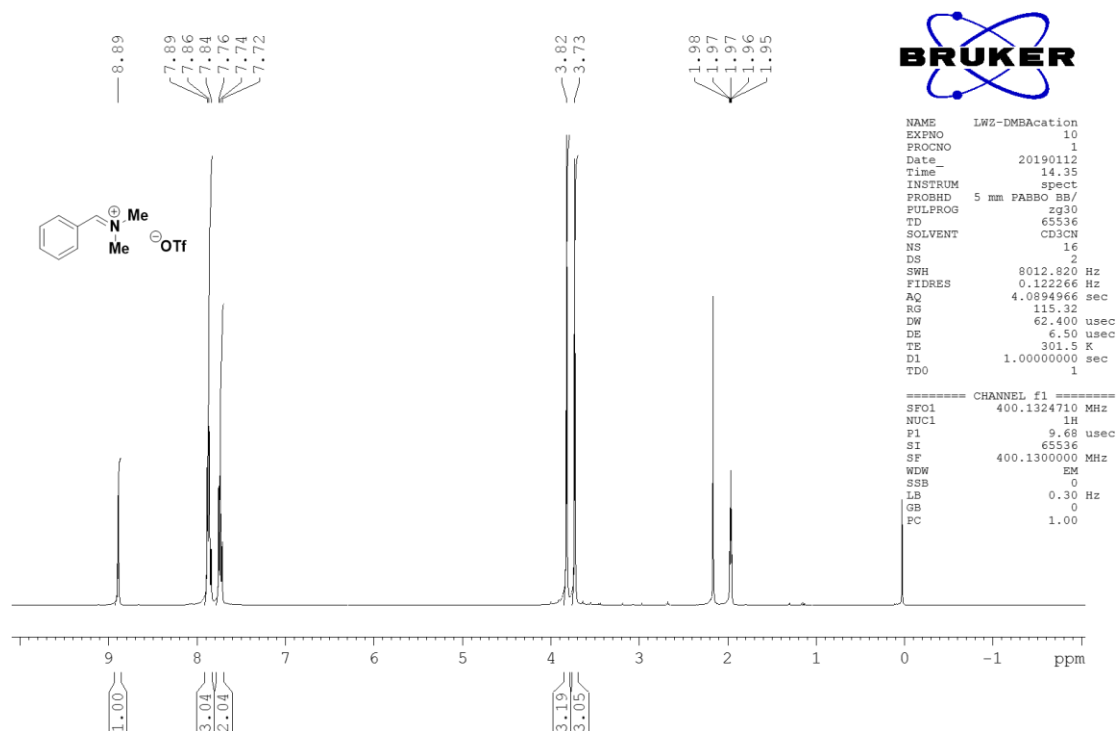
Data S129. ¹H NMR spectra of iminium cation 2b⁺, related to Table 1.

Data S130. ¹H NMR spectra of iminium cation 5⁺, related to Table 1.

Data S131. ¹H NMR spectra of iminium cation 3b⁺, related to Table 1.

Data S132. ¹H NMR spectra of iminium cation 2h⁺, related to Table 1.
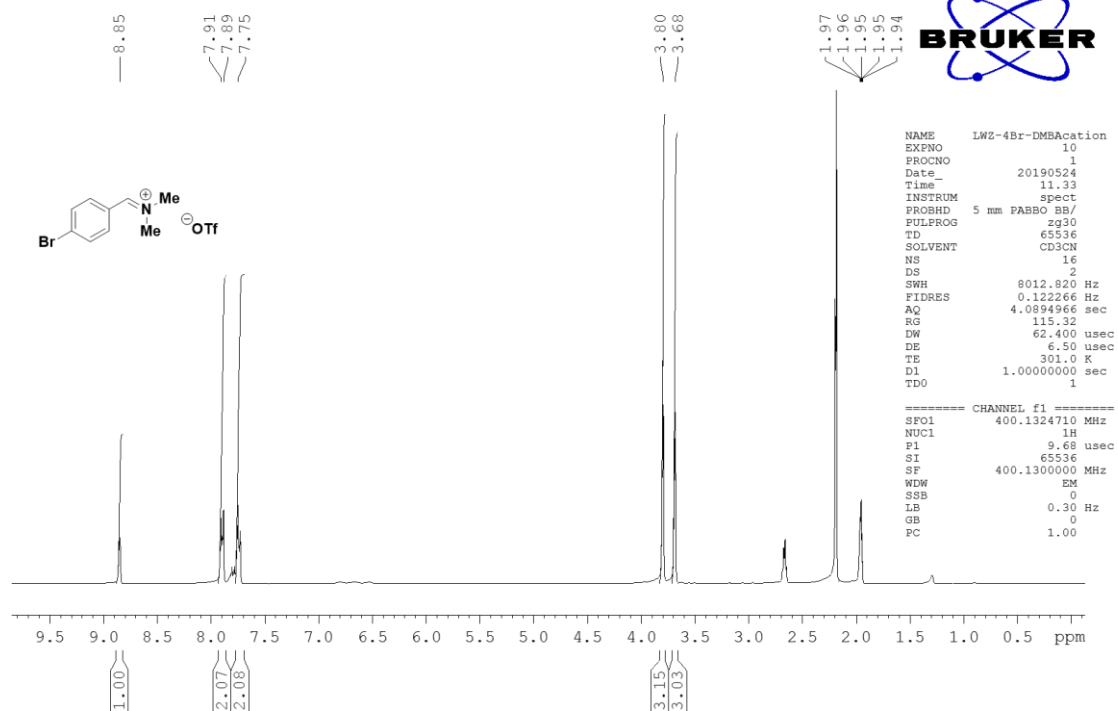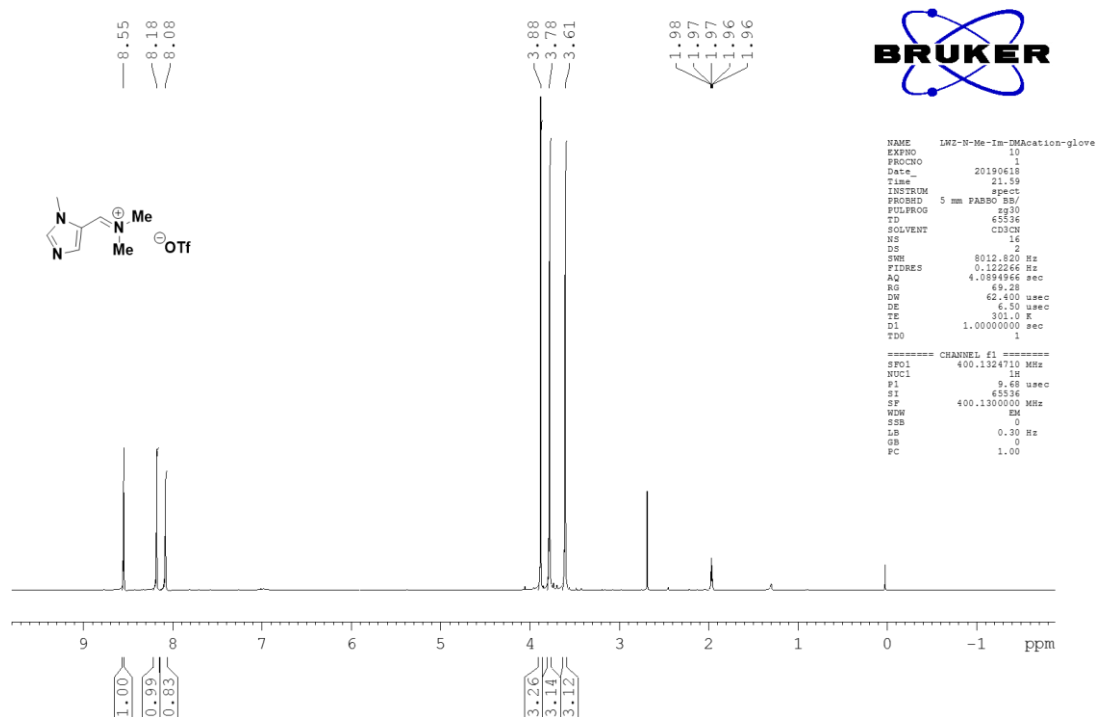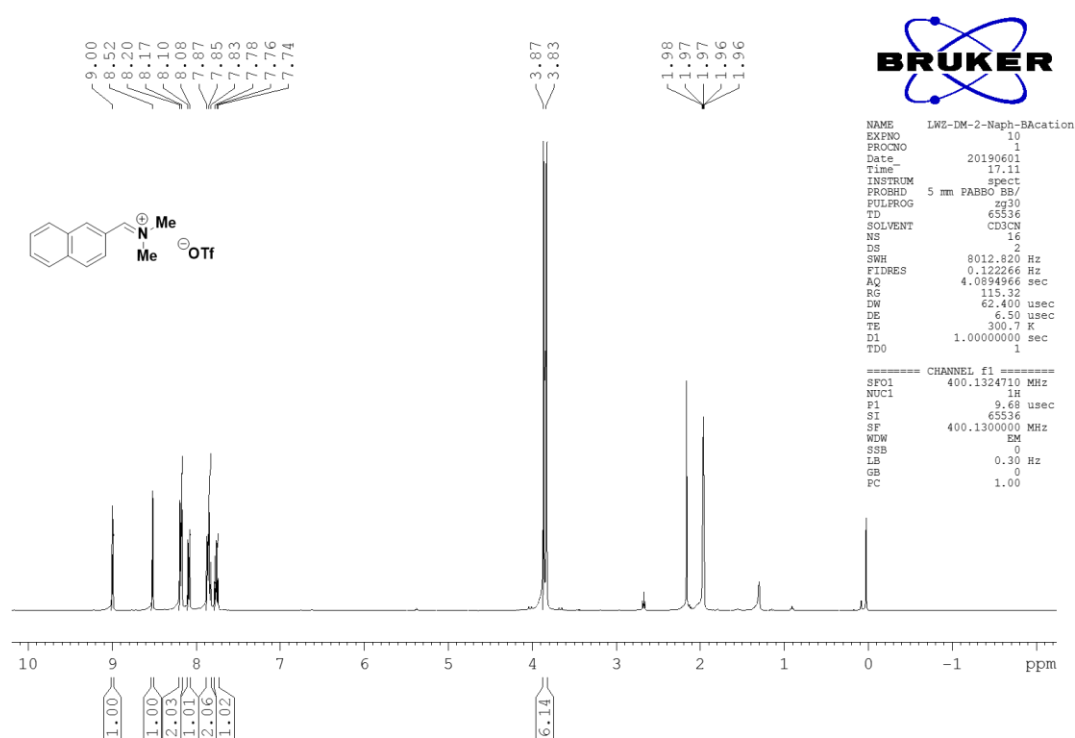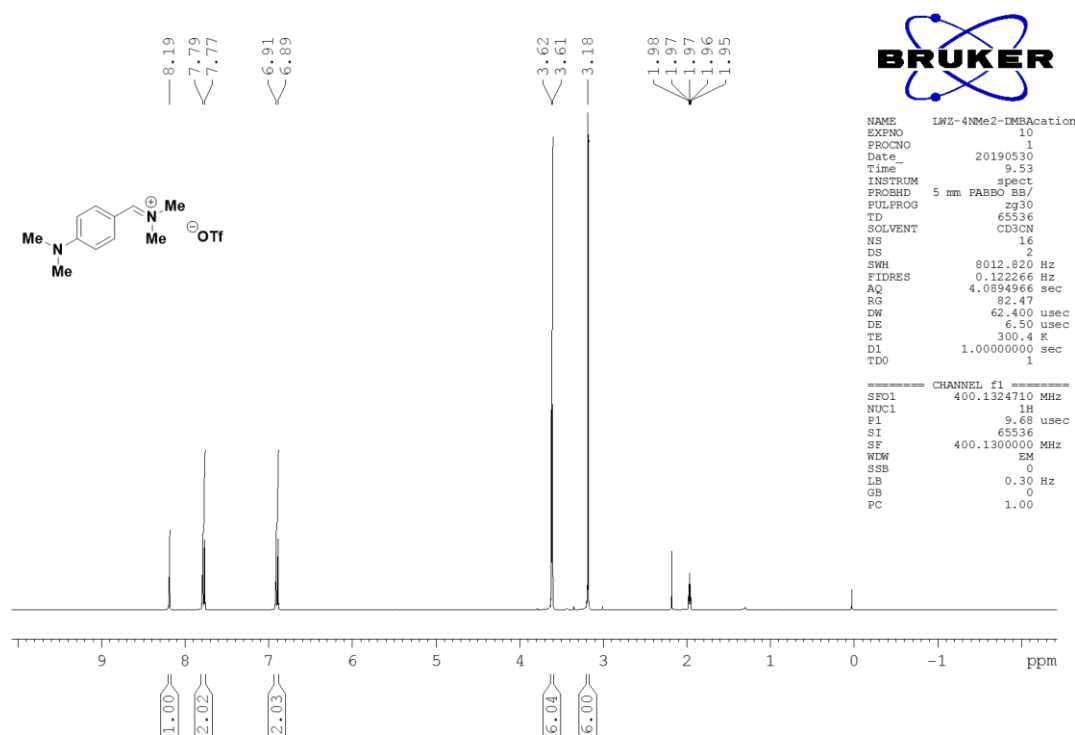
Data S133. ^{1}H NMR spectra of iminium cation 2g$^+$, related to Table 1.
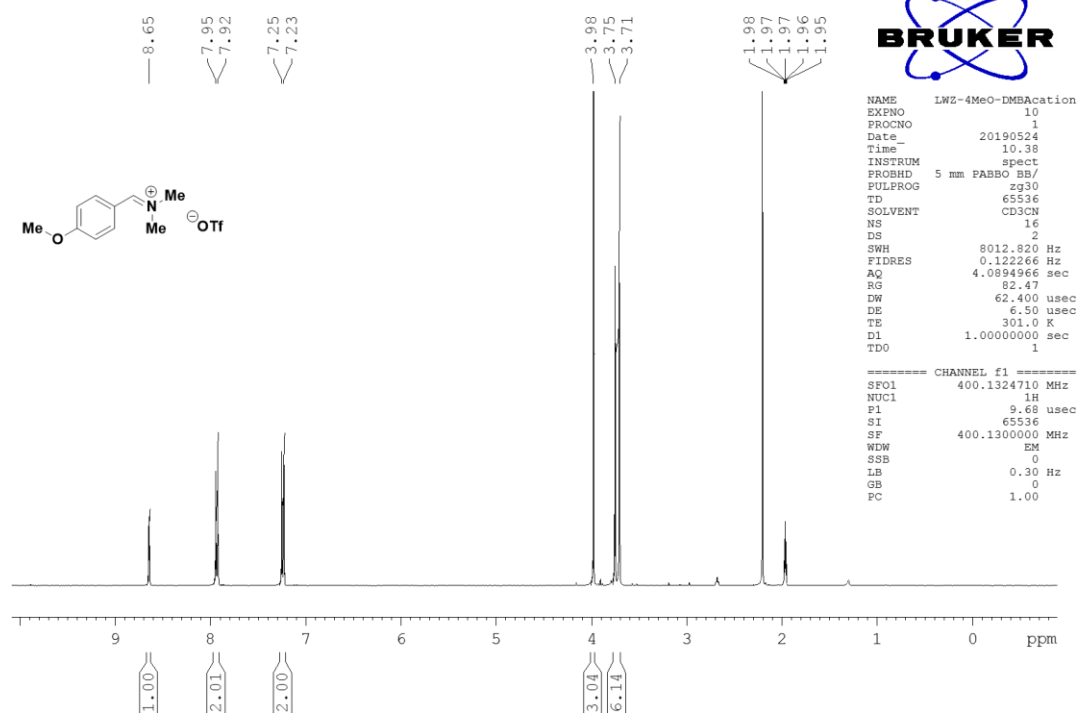
Starting materials were obtained from commercial sources and used without further purification. HPLC acetonitrile used in measurement was treated with dry column with water content <10 ppm. The commercial tetrabutylammonium hexafluorophosphate (nBu_4NPF_6) was recrystallized from CH_2Cl_2/Et_2O, dried under vacuo overnight and stored in glove box.

Reaction heat determination was conducted on MicroCal VP-ITC. ^{1}HNMR spectra were recorded in CD_3CN on Bruker AVANCE III HD (400 MHz) nuclear magnetic resonance spectrometer. Stopped-flow measurement was performed on Hi-Tech Scientific SF-51 stopped-flow set-up and UV-Vis measurements on Hitachi U-3900H UV-Vis spectrophotometer.

Condition optimization for thermodynamic determination

According to Hess' Law, thermodynamic cycles for α-C–H bond scission of tertiary amines and its radical intermediates were established (Scheme 3 in main text). And to identify optimal conditions for the data acquisition, especially for the hydricity $\Delta H_{\text{H-A}}$, we made a lot of explorations, which are shown below.

Determination of hydricity of tertiary amines [$\Delta H_{\text{H-D}}$(HD)]

Strategy 1 We first examined reaction products of tertiary amines with various potential hydride acceptors (Scheme S1). For cation-type acceptors, weakly coordinating counteranion (ClO_4^-) is used to minimize ion-pair effects. Preliminary attempts in stoichiometric reactions demonstrate that weak acceptors tropylium (T^+) and N-methylacridinium ($AcrH^+$) can not efficiently abstract hydrides from N-Ph-THIQ in AN at room temperature (rt). Stronger acceptor phenazinium (PZ^+) reacted with N-Ph-THIQ sluggishly, accompanying with unidentified side reactions. This implies that N-Ph-THIQ's hydricity ($\Delta H_{\text{H-D}}$) is around 80 kcal mol^{-1}. When stronger oxidants 2,3-dichloro-5,6-dicyano-p-benzoquinone (DDQ), di/triphenyl carbocation (Ph_2CH^+ or Ph_3C^+), phenothiazinium (PTZ^+) and 4-acetamido-2,2,6,6-tetramethyl-oxopiperidinium ($AcNH$-$TEMPO^+$) were used, hydride transfer proceeded smoothly. Unfortunately, for Ph_2CH^+, nucleophilic attack by tertiary amine to form Lewis adduct is the dominant pathway, interrupting hydride transfer (Scheme S1). Considering that O-N/N-N bond is much weaker than C-N bond, heteroatom-centred cations $AcNH$-$TEMPO^+$ and PTZ^+ are recommended to minimize the disturbance of Lewis adducts. In order to construct rapid and complete hydride transfer required in thermodynamic determinations, reactions with one of substrates in excess were further examined. However, reactions with excess $AcNH$-$TEMPO^+$ or PTZ^+ are roughly 10 kcal mol^{-1} more exothermic than those with tertiary amine in excess. The absence of thermodynamic self-consistency doubtlessly suggests the disturbance of side reactions. Detailed investigations disclose that when acceptors $AcNH$-$TEMPO^+$ and PTZ^+ are used excessively, residual acceptors would further react with resultant $AcNH$-$TEMPOH$ and PTZH through either comproportionation (Semmelhack et al., 1984) or dimerization (Hanson et al., 1973) (Scheme S1b and c, Fig. S1). Thus we detected the reaction of PTZ^+ and PTZH in NMR experiments (Fig. S1b) and the dimerization of PTZ^+ and PTZH was also verified by former research (Hanson et al., 1973). Such undesired reactions can be well avoided when tertiary amine is used in excess. Eventually, less dosage of $AcNH$-$TEMPO^+ClO_4^-$ or sometimes, excess $Ph_3C^+ClO_4^-$ is selected as optimal acceptors for thermodynamic measurements. Then the heat of the hydride exchange reaction ΔH_{rxn} was measured by isothermal titration

calorimetry.

Strategy 2 When tertiary amines with open chains (e.g. substrates 1-5) were put in the same test condition, unexpected results appeared that complex side reactions were stimulated between neutral amines and oxidants. Then an inverse strategy was adopted: iminium cation was prepared beforehand, which was supposed to be product in previous scheme; and a proper hydride donor was screened out to react with iminium salts. The selected hydride donor is required to possess strong hydride donating ability, guaranteeing the complete and fast hydride transfer process. 1-benzyl-3-methyl-1,4-dihydropyridine displayed more excellent performance among several candidate hydride donors, with hydricity $H_{H-D} = 48.0$ kcal mol^{-1}. Then the heat of the hydride exchange reaction ΔH_{rxn} was measured by isothermal titration calorimetry.

Reaction heat determination was conducted on MicroCal VP-ITC. Acetonitrile used in measurement was treated in the dry column (water ≤ 10 ppm), and the test temperature was kept at 298 K. For substrate2-5, iminium salts were prepared at first and reacted with hydride donor 1-benzyl-3-methyl-1,4-dihydropyridine; For the other substrates, most were reacted with hydride acceptor AcNH-TEMPO$^+$ and a few with Ph$_3$C$^+$ to exclude unexpected side reactions.

1. For hydride donor **H**: Imine salts in AN was titrated into the AN solution of 1-benzyl-3-methyl-1,4-dihydropyridine(**H**, [Imine salt] ≈ 1 mM, [**H**] ≈ 10 mM).

2. For hydride acceptor **C1**: 2,2,6,6-Tetramethylpiperidine N-oxide cation (**C1**, AcNH-T TEMPO$^+$) in AN was titrated into the AN solution of THIQs ([**C1**] ≈ 1 mM, [THIQ] ≈ 3 mM).

3. For hydride acceptor **C2**: THIQs in AN was titrated into the AN solution of trityl cation (**C2**, Ph$_3$C$^+$) ([**C2**] ≈ 3 mM, [THIQ] ≈ 1 mM).

Determination of the redox potentials of tertiary amines [E_{ox}(HD)] and iminium cations [E_{red}(D$^+$)]

The oxidation potentials of neutral tertiary amines and reduction potential of iminium cations were determined by cyclic voltammogram (CV, details seeing below) in anaerobic 0.1 M nBu$_4$NPF$_6$/Acetonitrile solution. The reference electrode, Ag/AgNO$_3$ was calibrated versus Fc$^{+/0}$.

For substrate 1 and 6-14, the reduction potentials of iminium cations were measured when amines were oxidized by AcNH-TEMPO$^+$ClO$_4^-$ or Ph$_3$C$^+$ClO$_4^-$ in the electrolytic cell to in-situ generate iminium cations; For substrate 2-5, the oxidation potentials of neutral amines were measured when iminium salt were reduced by NaBH$_4$ in the electrolytic cell to in-situ generate neutral amines.

Preparation of substrates

S1-14   **2a$^+$-j$^+$, 3a$^+$-b$^+$, 4$^+$, 5$^+$**
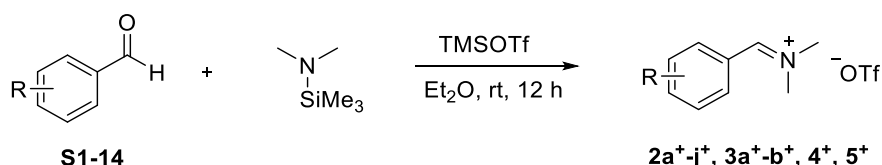
A 50 mL schlenk-tube was evacuated and back filled with argon for 3 times. Anhydrous Et$_2$O (25 mL) and benzaldehydes (5 mmol) were added. Then pentamethylsilanamine (5 mmol) and TMSOTf (5 mmol) were dropwise added successively. The solution was stirred at rt for 12 h. The precipitated salt was washed by Et$_2$O for several times (Schroth et al., 1994).

2a⁺ ¹H NMR (400 MHz, Acetonitrile-d_3) δ 9.05 (s, 1H), 8.04 (d, J = 8.5 Hz, 2H), 7.94 (d, J = 8.5 Hz, 2H), 3.87 (d, J = 1.3 Hz, 3H), 3.69 (d, J = 1.3 Hz, 3H) ppm.

2b⁺ ¹H NMR (400 MHz, Acetonitrile-d_3) δ 8.85 (s, 1H), 7.90 (d, J = 8.7 Hz, 2H), 7.74 (d, J = 8.7 Hz, 2H), 3.79 (d, J = 1.4 Hz, 2H), 3.68 (d, J = 1.4 Hz, 2H) ppm.

2c⁺ ¹H NMR (400 MHz, Acetonitrile-d_3) δ 8.89 (s, 1H), 7.85 (d, J = 8.7 Hz, 2H), 7.74 (d, J = 8.7 Hz, 2H), 3.82 (d, J = 1.3 Hz, 3H), 3.71 (d, J = 1.3 Hz, 3H) ppm.

2d⁺ ¹H NMR (400 MHz, Acetonitrile-d_3) δ 8.89 (s, 1H), 8.02 – 7.91 (m, 2H), 7.52 – 7.41 (m, 2H), 3.82 (d, J = 1.2 Hz, 3H), 3.72 (d, J = 1.2 Hz, 3H) ppm.

2e⁺ ¹H NMR (400 MHz, Acetonitrile-d_3) δ 8.86 (s, 1H), 7.89 – 7.79 (m, 3H), 7.71 (t, J = 7.8 Hz, 2H), 3.79 (d, J = 1.4 Hz, 3H), 3.70 (d, J = 1.4 Hz, 3H) ppm.

2f⁺ ¹H NMR (400 MHz, Acetonitrile-d_3) δ 8.79 (s, 1H), 7.81 (d, J = 8.1 Hz, 2H), 7.56 (d, J = 8.1 Hz, 2H), 3.80 (d, J = 1.2 Hz, 3H), 3.73 (d, J = 1.2 Hz, 3H), 2.21 (s, 3H) ppm.

2g⁺ ¹H NMR (400 MHz, Acetonitrile-d_3) δ 8.65 (s, 1H), 7.94 (d, J = 9.0 Hz, 2H), 7.24 (d, J = 9.0 Hz, 2H), 3.98 (s, 3H), 3.75 (d, J = 1.2 Hz, 3H), 3.71 (d, J = 1.2 Hz, 3H) ppm.

2h⁺ ¹H NMR (400 MHz, Acetonitrile-d_3) δ 8.19 (s, 1H), 7.78 (d, J = 9.4 Hz, 2H), 6.90 (d, J = 9.4 Hz, 2H), 3.63 (d, J = 0.9 Hz, 3H), 3.61 (d, J = 0.9 Hz, 3H), 3.18 (s, 6H) ppm.

2i⁺ ¹H NMR (400 MHz, Acetonitrile-d_3) δ 9.17 (s, 1H), 7.40 (t, J = 7.7 Hz, 1H), 7.18 (d, J = 7.7 Hz, 2H), 3.83 (d, J = 1.4 Hz, 3H), 3.34 (d, J = 1.4 Hz, 3H), 2.20 (s, 6H) ppm.

3a⁺ ¹H NMR (400 MHz, Acetonitrile-d_3) δ 9.57 (s, 1H), 8.35 (d, J = 8.3 Hz, 1H), 8.15 – 8.12 (m, 1H), 8.08 – 8.03 (m, 1H), 7.94 – 7.91 (m, 1H), 7.84 – 7.72 (m, 3H), 3.96 (d, J = 1.3 Hz, 3H), 3.71 (d, J = 1.3 Hz, 3H) ppm.

3b⁺ ¹H NMR (400 MHz, Acetonitrile-d_3) δ 9.00 (s, 1H), 8.52 (s, 1H), 8.19 (d, J = 9.2 Hz, 2H), 8.09 (d, J = 8.3 Hz, 1H), 7.89 – 7.81 (m, 2H), 7.76 (t, J = 7.6 Hz, 1H), 3.87 (s, 3H), 3.83 (s, 3H).

4⁺ ¹H NMR (400 MHz, Acetonitrile-d_3) δ 8.37 (d, J = 10.5 Hz, 1H), 7.92 (d, J = 15.3 Hz, 1H), 7.89 – 7.84 (m, 2H), 7.68 – 7.61 (m, 1H), 7.61 – 7.53 (m, 2H), 7.30 (dd, J = 15.3, 10.5 Hz, 1H), 3.64 (d, J = 1.1 Hz, 3H), 3.57 (d, J = 1.1 Hz, 3H) ppm.

5⁺ ¹H NMR (400 MHz, Acetonitrile-d_3) δ 8.55 (s, 1H), 8.18 (s, 1H), 8.08 (s, 1H), 3.88 (s, 3H), 3.78 (s, 3H), 3.61 (s, 3H) ppm.
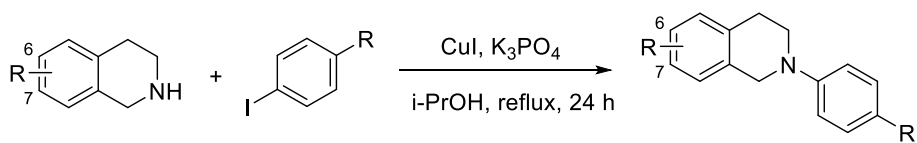
S15-22   **6a-i, 7h-i, 8a-b,9a-d, 10a-c**

CuI (1mmol) and K_3PO_4 (20 mmol) were added into a Schlenk-tube. The tube was evacuated and back filled with argon for 3 times. *i*-PrOH (10 mL), ethyleneglycol (20 mmol), 1,2,3,4-tetrahydroisoquinoline and its analogues (15 mmol), and *p*-substituted iodobenzene (10 mmol) were added at rt. The reaction mixture was refluxed for 24 h. After cooling to rt, diethyl ether (20 mL) and water (20 mL) were added to the reaction. The resulted mixture was extracted with diethyl ether 3 times. The combined organic extracts were washed with brine, dried over anhydrous $MgSO_4$, filtered, and concentrated under reduced pressure. The crude product was purified by column chromatography on silica gel using EtOAc/PE (Pandey et al., 2016).

6a ¹H NMR (400 MHz, Acetonitrile-d_3) δ 8.15 (d, J = 9.4 Hz, 2H), 7.29 – 7.25 (m, 4H), 6.97 (d, J = 9.4 Hz, 1H), 4.62 (s, 2H), 3.73 (t, J = 6.0 Hz, 2H), 3.02 (t, J = 6.0 Hz, 2H) ppm.

6b ^{1}H NMR (400 MHz, Acetonitrile-d_3) δ 7.59 – 7.54 (m, 2H), 7.26 – 7.21 (m, 4H), 7.02 – 6.97 (m, 2H), 4.53 (s, 2H), 3.66 (t, J = 5.9 Hz, 2H), 2.99 (t, J = 5.9 Hz, 2H) ppm.

6c ^{1}H NMR (400 MHz, Acetonitrile-d_3) δ 7.55 (d, J = 8.8 Hz, 2H), 7.27 – 7.21 (m, 4H), 7.06 (d, J = 8.8 Hz, 2H), 4.52 (s, 2H), 3.67 (t, J = 5.9 Hz, 2H), 2.99 (t, J = 5.9 Hz, 2H) ppm.

6d ^{1}H NMR (400 MHz, Chloroform-d) δ 7.30 – 7.15 (m, 6H), 6.95 – 6.88 (m, 2H), 4.41 (s, 2H), 3.56 (t, J = 5.9 Hz, 2H), 3.01 (t, J = 5.9 Hz, 2H) ppm.

6e ^{1}H NMR (400 MHz, Acetonitrile-d_3) δ 7.29 (t, J = 7.8 Hz, 2H), 7.24 – 7.17 (m, 4H), 7.04 (d, J = 8.1 Hz, 2H), 6.81 (t, J = 7.3 Hz, 1H), 4.41 (s, 2H), 3.58 (t, J = 5.9 Hz, 2H), 2.98 (t, J = 5.9 Hz, 2H) ppm.

6f ^{1}H NMR (400 MHz, Acetonitrile-d_3) δ 7.21 – 7.18 (m, 4H), 7.10 (d, J = 8.3 Hz, 2H), 6.98 – 6.92 (m, 2H), 4.35 (s, 2H), 3.51 (t, J = 5.9 Hz, 2H), 2.96 (t, J = 5.9 Hz, 2H), 2.27 (s, 3H) ppm.

6g ^{1}H NMR (400 MHz, Acetonitrile-d_3) δ 7.21 – 7.11 (m, 4H), 7.03 – 6.93 (m, 2H), 6.89 – 6.82 (m, 2H), 4.26 (s, 2H), 3.73 (s, 3H), 3.43 (t, J = 5.9 Hz, 2H), 2.94 (t, J = 5.9 Hz, 2H) ppm.

6h ^{1}H NMR (400 MHz, Acetonitrile-d_3) δ 7.19 (d, J = 3.3 Hz, 3H), 7.16 – 7.12 (m, 1H), 7.06 – 6.91 (m, 4H), 4.22 (s, 2H), 3.87 (s, 3H), 3.36 (t, J = 5.8 Hz, 2H), 2.97 (t, J = 5.8 Hz, 2H) ppm.

6i ^{1}H NMR (400 MHz, Acetonitrile-d_3) δ 7.26 – 7.09 (m, 5H), 6.59 (dd, J = 8.3, 2.4 Hz, 1H), 6.52 (t, J = 2.4 Hz, 1H), 6.36 (dd, J = 8.1, 2.4 Hz, 1H), 4.37 (s, 2H), 3.76 (s, 3H), 3.54 (t, J = 5.9 Hz, 2H), 2.93 (t, J = 5.9 Hz, 2H) ppm.

7h ^{1}H NMR (400 MHz, Acetonitrile-d_3) δ 8.29 – 8.21 (m, 1H), 7.95 – 7.88 (m, 1H), 7.63 (d, J = 8.2 Hz, 1H), 7.57 – 7.43 (m, 3H), 7.30 – 7.14 (m, 5H), 4.31 (s, 2H), 3.41 (t, J = 6.1 Hz, 2H), 3.16 (t, J = 6.1 Hz, 2H) ppm.

7i ^{1}H NMR (400 MHz, Acetonitrile-d_3) δ 7.79 – 7.68 (m, 3H), 7.44 – 7.36 (m, 2H), 7.29 – 7.17 (m, 6H), 4.51 (s, 2H), 3.67 (t, J = 5.9 Hz, 2H), 3.01 (t, J = 5.9 Hz, 2H) ppm.

8a ^{1}H NMR (400 MHz, Acetonitrile-d_3) δ 7.34 – 7.13 (m, 6H), 6.99 (d, J = 8.2 Hz, 2H), 6.79 – 6.71 (m, 1H), 5.00 (q, J = 6.7 Hz, 1H), 3.72 – 3.62 (m, 1H), 3.55 – 3.45 (m, 1H), 3.07 – 2.95 (m, 1H), 2.95 – 2.84 (m, 1H), 1.40 (d, J = 6.7, 3H) ppm.

8b ^{1}H NMR (400 MHz, Acetonitrile-d_3) δ 7.40 – 7.18 (m, 11H), 6.92 – 6.86 (m, 2H), 6.76 – 6.68 (m, 1H), 5.94 (s, 1H), 3.84 – 3.75 (m, 1H), 3.55 – 3.43 (m, 1H), 3.03 – 2.97 (m, 2H) ppm.

9a ^{1}H NMR (400 MHz, Acetonitrile-d_3) δ 8.13 (d, J = 2.4 Hz, 1H), 8.05 (dd, J = 8.4, 2.4 Hz, 1H), 7.42 (d, J = 8.4 Hz, 1H), 7.37 – 7.24 (m, 2H), 7.10 – 7.00 (m, 2H), 6.85 (td, J = 7.3, 1.0 Hz, 1H), 4.52 (s, 2H), 3.63 (t, J = 5.9 Hz, 2H), 3.09 (t, J = 5.9 Hz, 2H) ppm.

9b ^{1}H NMR (400 MHz, Acetonitrile-d_3) δ 7.62 – 7.48 (m, 2H), 7.37 (d, J = 7.8 Hz, 1H), 7.32 – 7.26 (m, 2H), 7.06 – 7.00 (m, 2H), 6.87 – 6.81 (m, 1H), 4.45 (s, 2H), 3.58 (t, J = 5.9 Hz, 2H), 3.00 (t, J = 5.9 Hz, 2H) ppm.

9c ^{1}H NMR (400 MHz, Acetonitrile-d_3) δ 7.43 – 7.34 (m, 2H), 7.33 – 7.25 (m, 2H), 7.15 (d, J = 7.8 Hz, 1H), 7.06 – 6.99 (m, 2H), 6.83 (t, J = 7.3 Hz, 1H), 4.36 (s, 2H), 3.55 (t, J = 6.2, 2H), 2.96 (t, J = 6.2 Hz, 3H) ppm.

9d ^{1}H NMR (400 MHz, Acetonitrile-d_3) δ 7.27 – 7.21 (m, 2H), 7.10 (d, J = 8.3 Hz, 1H), 7.01 – 6.96 (m, 2H), 6.80 – 6.71 (m, 3H), 4.31 (s, 2H), 3.75 (s, 3H), 3.52 (t, J = 5.9 Hz, 2H), 2.91 (t, J = 5.9 Hz, 2H) ppm.

10a ^{1}H NMR (400 MHz, Chloroform-d) δ 7.28 – 7.22 (m, 2H), 6.94 (d, J = 8.4 Hz, 2H), 6.67 (s, 2H), 4.34 (s, 2H), 3.90 (s, 3H), 3.89 (s, 3H), 3.55 (t, J = 5.8 Hz, 2H), 2.92 (t, J = 5.8 Hz, 2H) ppm.

10b ^{1}H NMR (400 MHz, Acetonitrile-d_3) δ 7.36 – 7.19 (m, 2H), 7.06 – 7.00 (m, 2H), 6.83 –

6.77 (m, 2H), 6.74 (s, 1H), 4.32 (s, 2H), 3.81 (s, 3H), 3.79 (s, 3H), 3.56 (t, J = 5.8 Hz, 2H), 2.87 (t, J = 5.8 Hz, 2H) ppm.

10c ^{1}H NMR (400 MHz, Chloroform-d) δ 7.03 – 6.98 (m, 2H), 6.92 – 6.86 (m, 2H), 6.66 (d, J = 3.5 Hz, 2H), 4.25 (s, 2H), 3.90 (s, 3H), 3.89 (s, 3H), 3.81 (s, 3H), 3.46 (t, J = 5.8 Hz, 2H), 2.92 (t, J = 5.8 Hz, 2H) ppm.
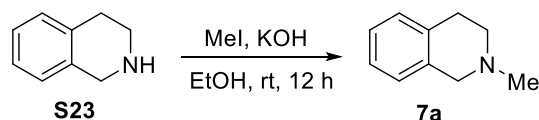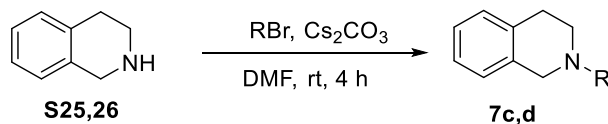

KOH (22 mmol) was added into a Schlenk-tube. The tube was evacuated and back filled with argon for 3 times. EtOH (40 mL), 1,2,3,4-tetrahydroisoquinoline(20 mmol), and methyl iodide (30 mmol) were added at rt. The mixture was stirred at rt for 12 h. The solvent was removed at reduced pressure and the crude was extracted with CHCl$_3$ three times. Combined extracts were dried over anhydrous Na$_2$SO$_4$ and concentrated under reduced pressure. The crude product was purified by column chromatography using EtOAc/PE (Kumar et al., 2018).

7a ^{1}H NMR (400 MHz, Acetonitrile-d_3) δ 7.13 – 7.06 (m, 3H), 7.04 – 6.98 (m, 1H), 3.48 (s, 2H), 2.84 (t, J = 6.0 Hz, 2H), 2.60 (t, J = 6.0 Hz, 2H), 2.35 (s, 3H) ppm.
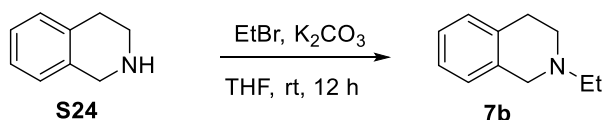
K$_2$CO$_3$ (22 mmol) was added into a Schlenk-tube. The tube was evacuated and back filled with argon for 3 times. THF (15 mL), 1,2,3,4-tetrahydroisoquinoline (20 mmol), and ethyl bromide (22 mmol) were added at rt. The reaction mixture was heated at reflux for 12 h. After cooling to rt, the resulted mixture was filtered, concentrated and purified by column chromatography on silica gel using EtOAc/PE (Huang et al., 2013).

7b ^{1}H NMR (400 MHz, Acetonitrile-d_3) δ 7.17 – 7.09 (m, 3H), 7.09 – 7.04 (m, 1H), 3.58 (s, 2H), 2.87 (t, J = 5.9 Hz, 2H), 2.69 (t, J = 5.9 Hz, 2H), 2.54 (q, J = 7.2 Hz, 2H), 1.16 (t, J = 7.2 Hz, 3H) ppm.

Cs$_2$CO$_3$ (22 mmol) was added into a Schlenk-tube. The tube was evacuated and back filled with argon for 3 times. DMF (23 mL), 1,2,3,4-tetrahydroisoquinoline (20 mmol), and ethyl 2-bromoacetate or allyl bromide (22 mmol) were added successively. The reaction mixture was stirred at rt for 4 h. The resulted mixture was concentrated, washed with brine and extracted with diethyl ether three times. The combined organic layers were concentrated and purified by column chromatography on silica gel using EtOAc/PE.

7c ^{1}H NMR (400 MHz, Acetonitrile-d_3) δ 7.23 – 7.10 (m, 3H), 7.06 – 7.04 (m, 1H), 4.18 (q, J = 7.1 Hz, 2H), 3.74 (s, 2H), 3.38 (s, 2H), 2.91 – 2.83 (m, 4H), 1.27 (t, J = 7.2 Hz, 3H) ppm.

7d ¹H NMR (400 MHz, Acetonitrile-d_3) δ 7.17 – 7.09 (m, 3H), 7.08 – 7.03 (m, 1H), 5.96 (ddt, J = 16.7, 10.2, 6.4 Hz, 1H), 5.28 (dq, J = 16.7, 1.7 Hz, 1H), 5.19 (ddt, J = 10.2, 1.7, 1.4 Hz, 1H), 3.58 (s, 1H), 3.16 (dt, J = 6.4, 1.4 Hz, 2H), 2.87 (t, J = 6.0 Hz, 2H), 2.71 (t, J = 6.0 Hz, 2H) ppm.

S27 → **7e**
BnBr, K₂CO₃ / MeCN, reflux, 12 h

K₂CO₃ (20 mmol) was added into a Schlenk-tube. The tube was evacuated and back filled with argon for 3 times. AN (15 mL), 1,2,3,4-tetrahydroisoquinoline (10 mmol), and benzyl bromide (10 mmol) were added at rt. The reaction mixture was refluxed for 12 h. After cooling to rt, the resulted mixture was filtered, concentrated and purified by column chromatography on silica gel using EtOAc/PE .
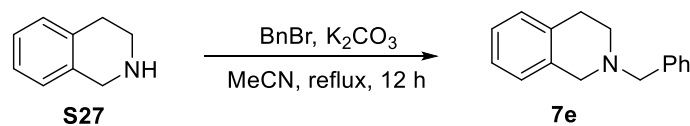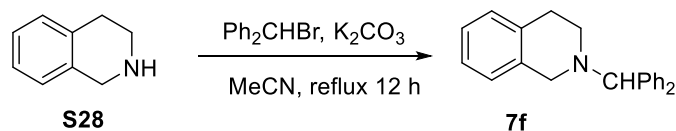
7e ¹H NMR (400 MHz, Acetonitrile-d_3) δ 7.44 – 7.34 (m, 4H), 7.33 – 7.27 (m, 1H), 7.17 – 7.08 (m, 3H), 7.00 (d, J = 6.7 Hz, 1H), 3.68 (s, 2H), 3.59 (s, 2H), 2.87 (t, J = 6.0 Hz, 2H), 2.72 (t, J = 6.0 Hz, 2H) ppm.


S28 → **7f**
Ph₂CHBr, K₂CO₃ / MeCN, reflux 12 h

K₂CO₃ (20 mmol) was added into a Schlenk-tube. The tube was evacuated and back filled with argon for 3 times. AN (15 mL), 1,2,3,4-tetrahydroisoquinoline (10 mmol), and diphenylbromomethane (10 mmol) were added at rt. The reaction mixture was refluxed for 12 h. After cooling to rt, the resulted mixture was filtered, concentrated and purified by column chromatography on silica gel using EtOAc/PE .

7f ¹H NMR (400 MHz, Acetonitrile-d_3) δ 7.53 – 7.45 (m, 4H), 7.34 – 7.26 (m, 4H), 7.24 – 7.16 (m, 2H), 7.13 – 7.08 (m, 2H), 7.08 – 7.02 (m, 1H), 6.84 (d, J = 7.5 Hz, 1H), 4.43 (s, 1H), 3.52 (s, 2H), 2.85 (t, J = 6.0 Hz, 2H), 2.68 (t, J = 6.0 Hz, 1H) ppm.

S29 → **7g**
triethylamine / MeCN, rt, 2 h
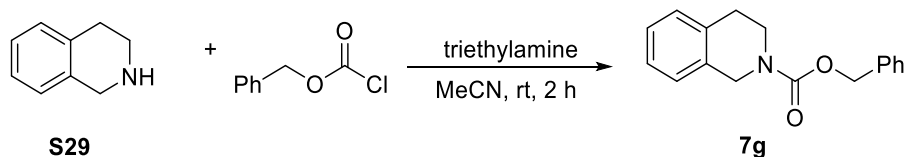
1,2,3,4-Tetrahydroisoquinoline was dissolved in 10 mL of acetonitrile, triethylamine was added dropwise. After 10 min, benzyl chloroformate was added dropwise and the temperature was kept at 0 °C for another 10 min. The reaction mixture stirred at rt for 2 h. The reaction mixture was washed with water (3 × 20 mL) and dried with anhydrous sodium sulfate. The organic solution was concentrated under reduced pressure and purified with flash chromatography .

7g ¹H NMR (400 MHz, Acetonitrile-d_3) δ 7.46 – 7.33 (m, 5H), 7.23 – 7.14 (m, 4H), 5.17 (s, 2H), 4.63 (s, 2H), 3.70 (t, J = 6.0 Hz, 2H), 2.86 (t, J = 6.0 Hz, 2H) ppm.
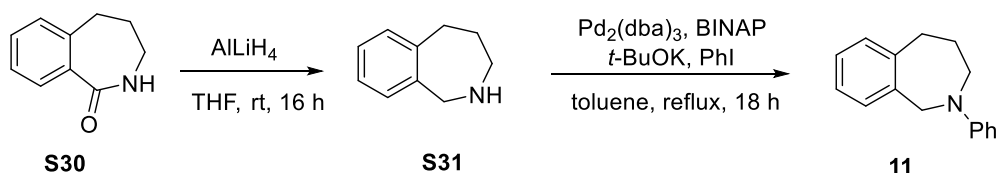
Lithium aluminum hydride (18 mmol) was added into a Schlenk-tube and dry THF (10 mL) was injected. 2,3,4,5-tetrahydro-1H-benzo[c]azepin-1-one (6 mmol) in dry THF (20 mL) was slowly added under argon at 0 °C. The solution was stirred at rt for 30 min, then heated to reflux. After 16 h, the mixture was cooled, and water (20 mL) was slowly added. The solids were filtered through a plug of Celite and then washed with ethyl ether (20 mL). The mixture was then further extracted with ethyl ether three times, and the combined extracts were dried and concentrated to give the 2,3,4,5-tetrahydro-1Hbenzo[c]azepine without further purification (Shonberg et al., 2015).

Bis(dibenzylideneacetone)palladium(0) (0.15 mmol), BINAP (0.3 mmol) were added into dry toluene (10 mL) under argon. The mixture was heated to 110 °C for 15 min. Then the solution was cooled to rt and sodium tert-butoxide (6 mmol), 2,3,4,5-tetrahydro-1Hbenzo[c]azepine (S31, 3 mmol), and iodobenzene (3 mmol) were added. The solution was refluxed for 18 h. After cooling to rt, the resulted mixture was filtered through a short plug of Celite and washed with toluene. The solvent was removed under vacuum and the residue was purified by chromatography using EtOAc/PE (Min et al., 2014).

11 ^{1}H NMR (400 MHz, Acetonitrile-d_3) δ 7.39 – 7.35 (m, 1H), 7.18 – 7.09 (m, 5H), 6.85 (d, J = 8.3 Hz, 2H), 6.57 (t, J = 7.2 Hz, 1H), 4.67 (s, 2H), 3.86 (t, J = 5.2 Hz, 2H), 3.09 – 3.00 (m, 2H), 1.84 (p, J = 5.6 Hz, 2H) ppm.

A solution of 2-phenylisoindoline-1,3-dione (3.75 mmol) in dry THF (30 mL) under argon was cooled to 0 °C., and a solution of borane in THF (1.0 M, 25 mL) was slowly added. The reaction mixture was then refluxed for 12 h. After cooled to rt, the mixture was poured into ice water (500 mL) and filtered. The precipitate was further purified by filtration over silica as a white powder using EtOAc/PE (Kelber et al., 2015).

12 ^{1}H NMR (400 MHz, Acetonitrile-d_3) δ 7.45 – 7.39 (m, 2H), 7.38 – 7.26 (m, 4H), 6.77 – 6.69 (m, 3H), 4.66 (s, 4H) ppm.
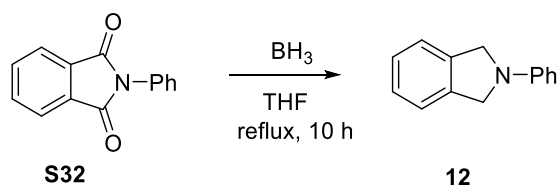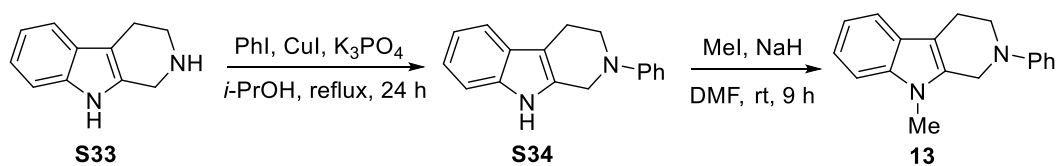

CuI (1mmol) and K_3PO_4 (20 mmol) were added into a Schlenk-tube. The tube was evacuated and back filled with argon for 3 times. i-PrOH (10 mL), ethylene glycol (20 mmol),

1,2,3,4-tetrahydroisoquinoline (15 mmol), and iodobenzene (10 mmol) were added at rt. The reaction mixture was refluxed for 24 h. After cooling to rt, diethyl ether (20 mL) and water (20 mL) were added to the reaction. The resulted mixture was extracted with diethyl ether three times. The combined organic extracts were washed with brine, dried over anhydrous $MgSO_4$, filtered, and concentrated under reduced pressure. The crude product was purified by column chromatography on silica gel using toluene/PE (Pandey et al., 2016).

To a stirred solution of N-phenyltetrahydro-β-carboline (S34, 1.21 mmol) in DMF were added MeI (1.45 mmol), and NaH (1.81 mmol, 60% dispersion in mineral oil) at 0 °C. Then the reaction temperature was increased to rt. After 9 h, the reaction mixture was poured into saturated aqueous NH_4Cl, and the resulting mixture was extracted with EtOAc three times. The combined organic extracts were washed with brine, dried over anhydrous Na_2SO_4, filtered, and concentrated under reduced pressure. The residue was purified by column chromatography on silica gel .

13 ^{1}H NMR (400 MHz, Acetonitrile-d_3) δ 7.46 (d, J = 7.8 Hz, 1H), 7.37 – 7.23 (m, 1H), 7.30 – 7.24 (m, 2H), 7.17 – 7.13 (m, 1H), 7.12 – 7.07 (m, 2H), 7.06 – 7.01 (m, 1H), 6.81 (tt, J = 7.3, 1.1 Hz, 1H), 4.42 (s, 2H), 3.68 (s, 3H), 3.65 (t, J = 5.7 Hz, 2H), 2.86 (t, J = 5.7 Hz, 2H) ppm.
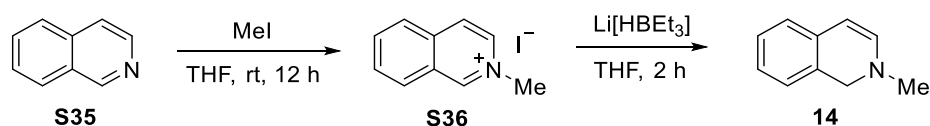
A 50 mL schlenk-tube was evacuated and back filled with argon for 3 times. THF (25 mL), 1,2,3,4-tetrahydroisoquinoline (20 mmol), and iodomethane (10 mmol) were added. The solution was stirred at rt for 12 h. The precipitated quinolinium salt was collected by filtration without further purification (Xu et al., 2016).

The quinolinium salt (S6) was dissolved in THF under argon. And then a solution of LiHBEt$_3$ in THF (1 M, 7.5 mL) was added slowly at -25 °C.. The temperature was increased to 25 °C. and kept for 2 h. The solvent was removed under reduced pressure and the residue was extracted with dry pentane three times. Combined extracts were concentrated to give the product (Chernyshov et al., 2010).

14 ^{1}H NMR (400 MHz, Acetonitrile-d_3) δ 7.06 – 7.02 (m, 2H), 6.98 – 6.93 (m, 1H), 6.86 – 6.81 (m, 1H), 6.15 (d, J = 7.4 Hz, 1H), 5.28 (d, J = 7.4 Hz, 1H), 4.15 (s, 2H), 2.74 (s, 3H) ppm.

C1
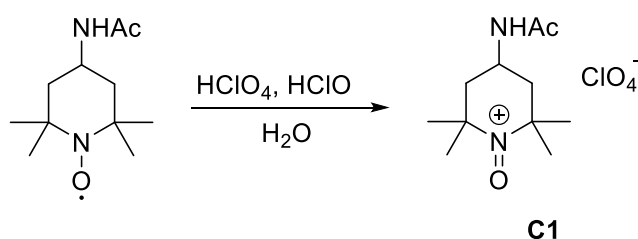
2,2,6,6-Tetramethylpiperidine nitroxide radical (9.2 mmol) was mixed with water (10 mL). 50% Perchloric acid (9.2 mmol) was added dropwise in 15 min. And then fresh 10% sodium hypochlorite (4.6 mmol) was added dropwise in 30 min. The resulted mixture was cooled in ice and yellow solid precipitated. The solid was washed with 5% $NaHCO_3$, icy water, and icy CH_2Cl_2 successively. Then the crude product was recrystallized in water (Bobbitt, 1998).

C1 ¹H NMR (400 MHz, DMSO-d_6) δ 8.23 (d, J = 5.9 Hz, 1H), 4.47 – 4.22 (m, 2H), 3.78 – 3.61 (m, 1H), 2.60 (S, 3H), 2.39 (s, 3H), 2.35 – 2.28 (m, 1H), 2.11 – 2.02 (m, 1H), 1.86 (s, 3H), 1.66 (s, 3H), 1.55 (s, 3H) ppm.
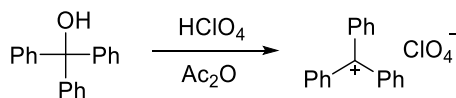
C2

Triphenylmethanol (3.85 mmol) was dissolved in acetic anhydride (15 mL). 50% Perchloric (15 mmol) acid was added dropwise at 10-20 °C. The mixture was stirred at 0 °C. for 1 h. The solvent was removed by pipet, and the yellow residue was washed by anhydrous ethyl ether until the washing was colorless. The solid was placed under high vacuum for 24 h to rid of the solvent. The final yellow product was stored in a seal bottle at 2 °C (Lambert et al., 1988).

C2 ¹H NMR (400 MHz, Acetonitrile-d_3) δ 8.32 (t, J = 7.5 Hz, 3H), 7.91 (t, J = 7.7 Hz, 6H), 7.75 (d, J = 7.7 Hz, 6H) ppm.
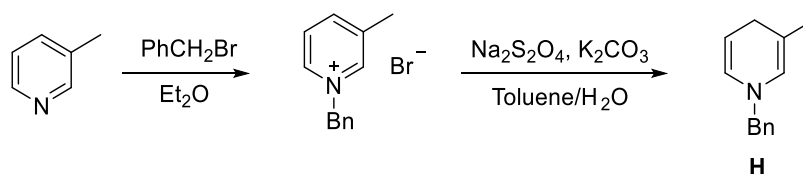
H

3-methylpyridine (30 mmol) was dissolved in Et₂O and Benzyl bromide (30mmol) was added. The mixture was stirred at rt until white solid precipitates in the bottom of flask. The precipitated pyridinium salt was washed by Et₂O for several times.

Pyridinium salt (28 mmol) was dissolved in water (20 mL) and added into the two-phase solution of toluene (150 mL) and water (170 mL) containing Sodium ditbionite (30g) and potassium carbonate (24 g). The mixture was heated up to 100 °C during 0.2h under vigorous stirring. Then the organic phase was separated , washed with an aqueous solution of Na₂CO₃ and dried over anhydrous Na₂SO₄. Evaporation of the solvent under reduced pressure and filtration over alumina (30 g) with pentane-EtOAc (1:l) as eluant gave the product (Wong et al., 1994).

H ¹H NMR (400 MHz, Acetonitrile-d_3) δ 7.41 – 7.24 (m, 5H), 5.89 (d, J = 8.1, 1H), 5.67 (d, J = 2.3 Hz, 1H), 4.36 (dt, J = 8.1, 3.2 Hz, 1H), 4.14 (s, 2H), 2.85 – 2.80 (m, 2H), 1.48 (s, 3H) ppm.

Supplemental references

Bobbitt, J. M. (1998). Oxoammonium Salts. 6.[1] 4-Acetylamino-2,2,6,6-tetramethylpiperidine-1-oxoammonium Perchlorate: A Stable and Convenient Reagent for the Oxidation of Alcohols. Silica Gel Catalysis. J. Org. Chem. *63*, 9367-9374.

Braïda, B., Hiberty, P. C. and Savin, A. (1998). A Systematic Failing of Current Density Functionals: Overestimation of Two-Center Three-Electron Bonding Energies. J. Phys. Chem. A *102*, 7872-7877.

Chernyshov, I. Y., Levin, V. V., Dilman, A. D., Belyakov, P. A., Struchkova, M. I. and Tartakovsky, V. A. (2010). Synthesis of CF_3-Substituted 1,2,3,4-Tetrahydroisoquinolines and 1,2,3,6-Tetrahydropyridines. Russ. Chem. Bull. *59*, 2102-2107.

Grüning, M., Gritsenko, O., Van Gisbergen, S. and Baerends, E. (2001). The Failure of Generalized Gradient Approximations (GGAs) and Meta-GGAs for the Two-Center Three-Electron Bonds in He^{2+}, $(H_2O)_2^{+}$, and $(NH_3)_2^{+}$. J. Phys. Chem. A *105*, 9211-9218.

Hanson, P. and Norman, R. O. C. (1973). Heterocyclic Free Radicals. Part IV. Some Reactions of Phenothiazine, Two Derived Radicals, and Phenothiazin-5-ium Ion. J. Chem. Soc., Perkin Trans. 2 264-271.

Huang, L. and Zhao, J. (2013). C_{60}-Bodipy Dyad Triplet Photosensitizers as Organic Photocatalysts for Photocatalytic Tandem Oxidation/[3+2] Cycloaddition Reactions to Prepare Pyrrolo[2,1-*a*]isoquinoline. Chem. Commun. *49*, 3751-3753.

Kelber, J. B., Panjwani, N. A., Wu, D., G´omez-Bombarelli, R., Lovett, B. W., Morton, J. J. L. and Anderson, H. L. (2015). Synthesis and Investigation of Donor-Porphyrin-Acceptor Triads with Long-lived Photo-induced Charge-separate States. Chem. Sci. *6*, 6468-6481.

Kumar, P. and Venkatakrishnan, P. (2018). Coumarin[4]arene: A Fluorescent Macrocycle. Org. Lett. *20*, 1295-1299.

Lambert, J. B., Schulz, W. J. and McConnell, J. A. (1988). The First Silylenium Ions in Solution. J. Am. Chem. Soc. *110*, 2201-2210.

Min, C., Sanchawala, A. and Seidel, D. (2014). Dual C-H Functionalization of *N*-Aryl Amines: Synthesis of Polycyclic Amines via an Oxidative Povarov Approach. Org. Lett. *16*, 2756-2759.

Pandey, G., Tiwari, S. K. and Singh, B. (2016). a-Alkylation of Tertiary Amines by $C(sp^3)$-$C(sp^3)$ Cross-coupling under Redox Neutral Photocatalysis. Tetrahedron Lett. *57*, 4480-4483.

Schroth, W., Jahn, U. and Ströhl, D. (1994). Neue Synthesen von Methyleniminium-Salzen aus Carbonylverbindungen und aus α-Chlorethern; ein Zugang zu vinylogen Viehe-Salzen. Chem. Ber. *127*, 2013-2022.

Semmelhack, M. F., Schmid, C. R., Cortes, D. A. and Chou, C. S. (1984). Oxidation of Alcohols to Aldehydes with Oxygen and Cupric Ion, Mediated by Nitrosonium Ion. J. Am. Chem. Soc. *106*, 3374-3376.

Shonberg, J., Draper-Joyce, C., Mistry, S. N., Christopoulos, A., Scammells, P. J., Lane, J. R. and Capuano, B. (2015). Structure-Activity Study of *N*-((trans)-4-(2-(7-Cyano-3,4-dihydroisoquinolin-2(1*H*)-yl)ethyl)cyclohexyl)-1*H*-indole-2-carboxamide (SB269652), a Bitopic Ligand That Acts as a Negative

Allosteric Modulator of the Dopamine D$_2$ Receptor. J. Med. Chem. *58*, 5287-5307.

Wong, Y.-S., Marazano, C., Gnecco, D. and Das, B. C. (1994). 1,4-Dihydropyridines from Dithionite Reduction of Pyridinium Salts without Electron-withdrawing Groups as Substituents. Tetrahedron Lett. *35*, 707-710.

Xu, J.-H., Zheng, S.-C., Zhang, J.-W., Liu, X.-Y. and Tan, B. (2016). Construction of Tropane Derivatives by the Organocatalytic Asymmetric Dearomatization of Isoquinolines. Angew. Chem. Int. Ed. *55*, 11834-11839.